Doctoral Dissertation
Doctoral Program in Materials Science and Technology (30th Cycle)

# Joining of Ceramics and Ceramic Matrix Composites (CMC) for Aerospace and Energy Applications

By
**Pardeep Kumar Gianchandani**

******

**Supervisor(s):**
Prof. Monica Ferraris
Dr. Valentina Casalegno

**Doctoral Examination Committee:**
Prof. Walter Krenkel, University of Bayreuth, Germany
Prof. Antonio Rinaldi, ENEA, Italy
Prof. Milena Salvo, Politecnico di Torino
Prof. Federico Smeacetto, Politecnico di Torino
Prof. Alberto Ortona, University of Applied Sciences and Arts of Southern Switzerland

Politecnico di Torino
20 July 2018

# Declaration

I hereby declare that, the contents and organization of this dissertation constitute my own original work and does not compromise in any way the rights of third parties, including those relating to the security of personal data.

Pardeep Kumar Gianchandani

Turin, July 20, 2018

* This dissertation is presented in partial fulfillment of the requirements for **Ph.D. degree** in the Graduate School of Politecnico di Torino (ScuDo).

*I would like to dedicate this thesis to my loving Parents, my mother KAVEETA and my father ASHOK KUMAR GIANCHANDANI*

For their endless love, support and encouragement

# Acknowledgment

Foremost, I would like to express my deepest gratitude to **Prof. Monica Ferraris**, for providing me the opportunity to pursue this Ph.D. under her supervision. Under her guidance, I was given the freedom to pursue my research in my own way and I greatly appreciated that freedom and continuous support. I gained invaluable knowledge and experience in the joining of ceramics and ceramics matrix composites.

Secondly, I would like to express my deep appreciation to my co-supervisor **Dr. Valentina Casalegno** for her support in all the research activities. It was an immense pleasure to work and discuss with her. Thanks for supporting and encouraging me through these years.

Thirdly, I would like to express gratitude to all the colleagues of GLANCE (Glasses Ceramics and Composites) research group at DISAT, for their assistance in laboratories at Politecnico di Torino, Italy.

Many thanks to **Prof. Ivo Dlouhý** from Institute of Physics of Materials (IPM), Academy of Sciences of the Czech Republic, for hosting me at IPM. I am grateful to KMM VIN for providing me a research grant to perform high temperature tests at IPM and to the **American Ceramic Society** for providing me the travel grants to attend the International Conference and Exposition on Advanced Ceramics and Composites on 2017 and 2018.

Further, acknowledgment to the Higher Education Commission, **(HEC**) Pakistan for providing me a scholarship to pursue Masters and Doctorate. Sincere thanks to Mehran University of Engineering & Technology, Jamshoro, Sindh Pakistan for permitting me to peruse higher studies at Politecnico di Torino, Italy.

Sincere thanks to all the colleagues, friends and teachers from Italy and Pakistan, for their everlasting love and support, during stay in Italy.

Finally, I would like to thank my family for standing by me unconditionally.

# Abstract

SiC-based ceramics and composites (SiC, C/SiC & SiC/SiC) are more and more extensively used as advanced materials for aerospace and energy applications. Existing applications are expanding continuously and require advanced materials, design and joining technologies.

The objective of this thesis was to join SiC-based ceramic matrix composites (CMC), ceramics (SiC, Mullite, Alumina) and SiC-based ceramic foams for aerospace and energy applications.

The research was aimed to develop strong, oxidation resistant and high temperature stable joints.

A novel joining technique defined "RM-Wrap" (RM=Mo, Nb, Ta, W Refractory Metals) has been developed within this thesis. The developed technique is a novel brazing technology named RM-Wrap after the metal used as a wrap to contain one or more silicon foils (e.g. Mo-Wrap when a Mo wrap is used to contain a Si foil).
It is a pressure-less joining technology performed at 1450 $^{o}$C, under an inert environment (Argon flow).

Joining materials are in-situ formed composites made of refractory metals silicides ($MoSi_2$, $NbSi_2$, $TaSi_2$ and $WSi_2$) embedded in a silicon matrix.

RM-Wrap is a highly tailorable joining technique: the quantity of each phase can be modified and more than one refractory metals can be used together. RM-Wrap has been very effective in joining both coated and uncoated CMC, porous and non-porous materials: ceramics (oxide and non-oxide), CMC (SiC-based) and highly porous substrates (SiC foams) having porosity higher than 80% have been soundly joined.

The joint morphology (interphase and interface) and elemental composition of the joining material was investigated in detail using FESEM and EDS which showed uniform, continuous and crack free joints. XRD investigation confirms the formation of metal silicides. Oxidation resistance of joints was carried out at 1100 $^{o}$C for 30 minutes (for CMC joints) and 6 hours (for monolithic ceramic joints) in the air; prior and post oxidation examination of joint morphology showed no morphological change and joints remained firmly joined.

Sandwich structures have been developed by Mo-wrap joining two C/SiC as “skins” to the “core” SiC foam. Sandwich structures were tested for thermal shock resistance from RT to 1100 $^{o}$C in the air for 2 minutes. Three cycles on a single sandwich structure were performed, which remained joined and the joining material composition unchanged.

Joints were mechanically tested in three different modes (i) compression, (ii) tensile and (iii) torsion. Joint strength was higher than the interlaminar shear strength of composites as the fracture was always observed in composites.

In case of monolithic ceramic (SiC) a mixed failure (cohesive and adhesive) was found, which suggest that the joint strength is comparable to ceramic one.

Micro- and nanoindentation tests were also carried out on joining materials.

# Thesis Overview

## Abstract

## Chapter 1

This chapter highlights the need for joining of ceramic and ceramics matrix composites (CMC) for aerospace and energy applications, and defines the objective of this study.

## Chapter 2

This chapter is a brief overview of joining techniques, of the state of the art of the most commonly used joining materials specifically for SiC based ceramics.

## Chapter 3

This chapter describes the Experimental Part of this study: (i) development of RM-Wrap joining (ii) materials joined in this study and (iii) characterizations performed.

## Chapter 4

All the results of thesis are presented and discussed in this chapter. The results are grouped separately for each joining technique such as Mo-Wrap, followed by Nb, Ta, Mo/W-wrap joining.

## Conclusion and future insights

# Contents

# List of Figures

# List of Tables

# Acronyms

| | |
|---|---|
| **Al** | Aluminium |
| **BDTT** | Brittle To Ductile Transition Temperature |
| **C** | Carbon |
| **C/C** | Carbon Fiber Reinforced Carbon |
| **C/SiC** | Carbon Fiber Reinforced Silicon Carbide |
| **CA** | Calcia-Alumina Glass-Ceramic |
| **CMC** | Ceramic Matrix Composites |
| **CT** | Computer Tomography |
| **CTE** | Coefficients of Thermal Expansion |
| **CVD** | Chemical Vapor Deposition |
| **CVI** | Chemical Vapor Infiltration |
| **EDS** | Energy Dispersion Spectroscopy |
| **G-CVI** | Gradient-Chemical Vapor Infiltration |
| **GE** | General Electric |
| **GPa** | Giga Pascal |
| **HPT** | High Pressure Turbine |
| **IM** | Ingot Metallurgy |
| **Keraman®** | CMC materials (CVI) produced by MT Aerospace |
| **LAS** | Lithium Aluminum Silicate |
| **LEAP** | High-Bypass Turbofan Engine |
| **LPI** | Liquid Polymer Infiltration |
| **LSI** | Liquid Silicon Infiltration |
| **MAS** | Magnesium Aluminum Silicate |
| **Mo** | Molybdenum |
| **MPa** | Mega Pascal |

| | |
|---|---|
| **MT** | MT Aerospace, Augsburg, Germany |
| **NASA** | National Aeronautics and Space Administration |
| **Nb** | Niobium |
| **NITE** | Nano-Infiltration and Transient Eutectic Phase |
| **PIP** | Polymer Infiltration and Pyrolysis |
| **PM** | Powder Metallurgy |
| **RM** | Refractory Metals |
| **RT** | Room Temperature |
| **SAMg** | Magnesium Alumino-Silicate Glass |
| **SAY** | Silica alumina yttria based glass |
| **SEM** | Scanning Electron Microscopy |
| **SHS** | Self-Propagating High-Temperature Synthesis |
| **Si** | Silicon |
| **SiC** | Silicon Carbide |
| **SiC/SiC** | Silicon Carbide fiber reinforced Silicon Carbide matrix composites |
| **SICARBON®** | C/SiC composites (PIP) |
| **SiCN** | Silicon Carbon Nitride |
| **SiSiC** | Silicon Infiltrated Silicon Carbide |
| **SPS** | Spark Plasma Sintering |
| **SSDR** | Solid State Displacement Reactions |
| **Ta** | Tantalum |
| **TLPB** | Transient-Liquid-Phase Bonding |
| **TPS** | Thermal Protection Systems |
| **W** | Tungsten |
| **Zr** | Zirconium |

# Chapter 1

# Aim of work

This chapter briefly describes the objectives of the thesis in the field of joining of engineering materials for various high-performance applications.

Parts of the experimental activity have been carried out within the following EU projects:

- Project **"ADMACOM"** "Advanced manufacturing routes for metal/composite components for aerospace", funded with 7th EU Framework Programme (grant agreement 609188 - www.admacomproject.eu).

- Project "**NEXTOWER**" "Advanced materials solutions for next-generation high efficiency concentrated solar power (CSP) tower systems" funded by the European Commission H2020 (NMBP-17-2016- www.h2020-nextower.eu).

# 1 Introduction

SiC-based composites (C/SiC and SiC/SiC) are extensively used as advanced materials for aerospace and energy applications. Existing applications are expanding continuously and requires advanced materials, design and joining technologies [1].

Ceramics are very hard and high-temperature stable materials, lacking in ductility compared to ceramic matrix composites (CMC). CMC offers a unique combination of properties such as lightweight, high temperature stability and chemical inertness and are more and more being used in heat engines, turbines, defense, energy production, space and many other high-performance applications. These materials have great potential to replace conventional metals and super alloys in many applications.

However, joining CMC to themselves, to ceramics and metals remains a critical point. Manufacturing of net-shape/ready to use ceramic (monolithic and composites) components is impossible because of their brittleness and difficult machining. Advance design solutions require large and complex parts which can be built by joining and integrating discrete units. Manufacturing technology (joining and integration) remains a critical tool for efficient use of these materials in order to reduce fuel consumption, air pollution and optimization of existing components [2, 3].

## 1.1 Applications of SiC-based CMC

CMCs have a wide range of applications in aerospace, gas turbines, nuclear and friction applications, each application area with specific requirements depending on service conditions (time and temperature), as shown in Figure 1. Among CMC, the C/SiC (carbon fibre reinforced silicon carbide matrix) and SiC/SiC (silicon carbide fibre reinforced silicon carbide matrix) are the most widely used composites.

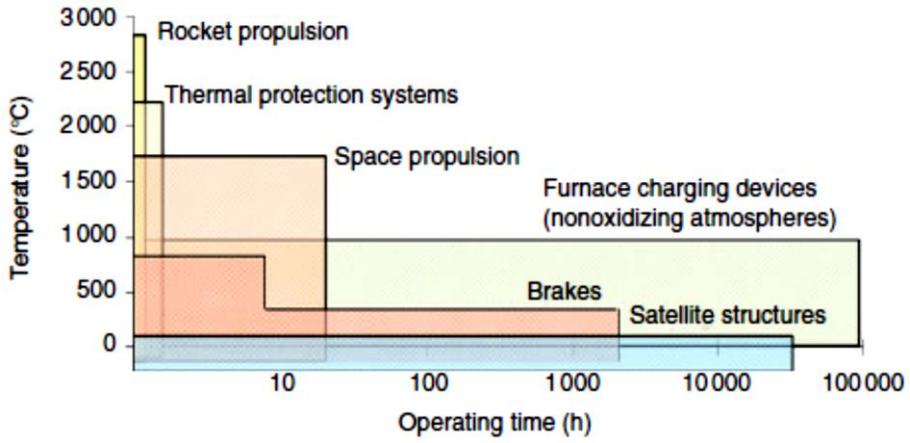


**Figure 1 Ceramics and CMC application areas dependent on service time and temperature [1]**

C/SiC composites have found their main application in the **thermal protection systems in spacecraft** all over the world and specifically in Europe, Japan and USA. The NASA's X-38 hot structure was made from C/SiC (Figure 2). C/SiC has been used in many other parts such as a nose cap, nose skirt, body flaps for steering the vehicle (Figure 3) [1, 4-6]. Jet-vanes for rocket motors must have high thermal shock resistance, low coefficient of thermal expansion and resistance to corrosion: C/SiC is one of the most suitable material which can be used in rocket motors. Chemical Vapour Deposition-SiC (CVD-SiC) coating improves the performance of C/SiC composites at high temperature in the oxidative environment. CVD-SiC coated C/SiC has a high potential to be employed in many parts of rocket and jet combustion engines where the temperature reaches up to 1500 $^{o}$C. Flame-holders, exhaust cones and engine flaps for military jet engines are made of C/SiC composites. SNECMA M 88-2 engine has been made from C/SiC composites using the CVI process (Figure 4 and Figure 5).

C/SiC composites are suitable below 500 $^{o}$C in oxidative environment or can be used at a higher temperature for short duration; the carbon oxidation over 500 $^{o}$C is a foremost limitation.


Figure 2 C/SiC and C/C-SiC application in X-38 spacecraft [1]

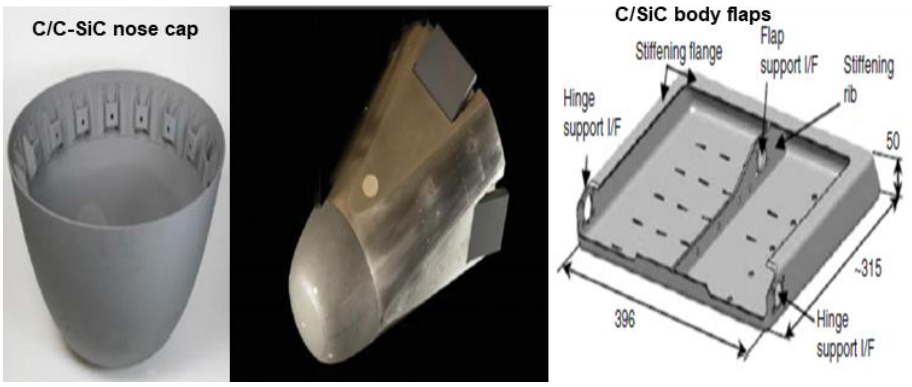


Figure 3 Re-entry capsule, C/SiC body flaps and C/C-SiC nose cap with in situ flanges[1]

Figure 4 C/SiC (CVI) combustion chambers [1]

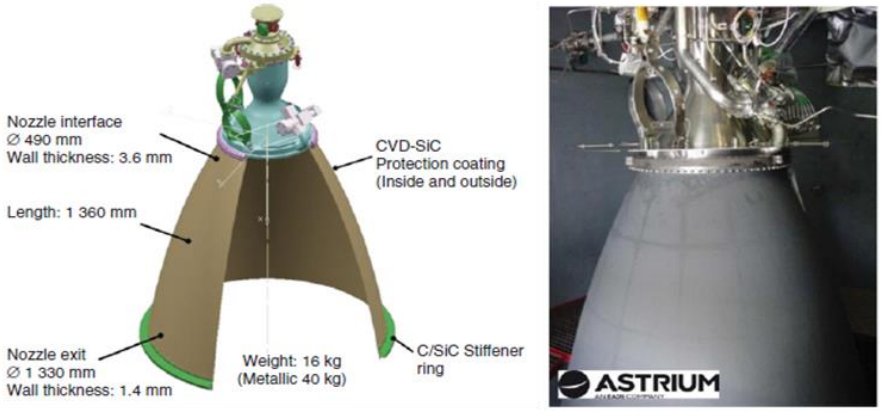


Figure 5 C/SiC nozzle extension technology demonstrator for the upper stage engine AESTUS [1]

Another field of application for C/SiC is as **brakes**: with the development of an economic manufacturing route such as liquid silicon infiltration (LSI), C/SiC and C/C can be transformed in Si-SiC (1). Since 1999, CMC based commercial brakes were adopted by DaimlerChrysler (now Daimler Benz), Porsche and Mercedes.

Figure 6 C/SiC Porsche Ceramic Brake (PCCB) manufactured via LSI [1]

Soon after the invention of SiC fiber in the mid-1970s, the race has begun to develop the ceramic composites reinforced with these ceramics fibers to replace C/C and C/SiC composites in many applications.

SiC/SiC overcomes the drawbacks of C/SiC composites offering the outstanding high-temperature strength, creep resistance, oxidation resistance, radiation stability [7]. SiC/SiC offers advanced applications for a long duration under extreme conditions. Recently SiC/SiC composite has been used in **commercial aircraft engines** ("LEAP", developed by a joint venture of General Electric-USA and SAFRAN-France), as shown in Figure 7 for Airbus A320 Neo (LEAP-1A version) and in Figure 8 for Boeing 737 max (LEAP-1B, Version) .

The CMC used in the Leap engine is a SiC+Si matrix and Hi-Nicalon SiC fibers composite made by LSI [2, 8]. The future LEAP (High-Bypass Turbofan Engine) engines (GE90x for Boeing 777X will start in 2019-20) consist of the combustor, High Pressure Turbine (HPT) nozzle and HPT shrouds made of these CMC [8].

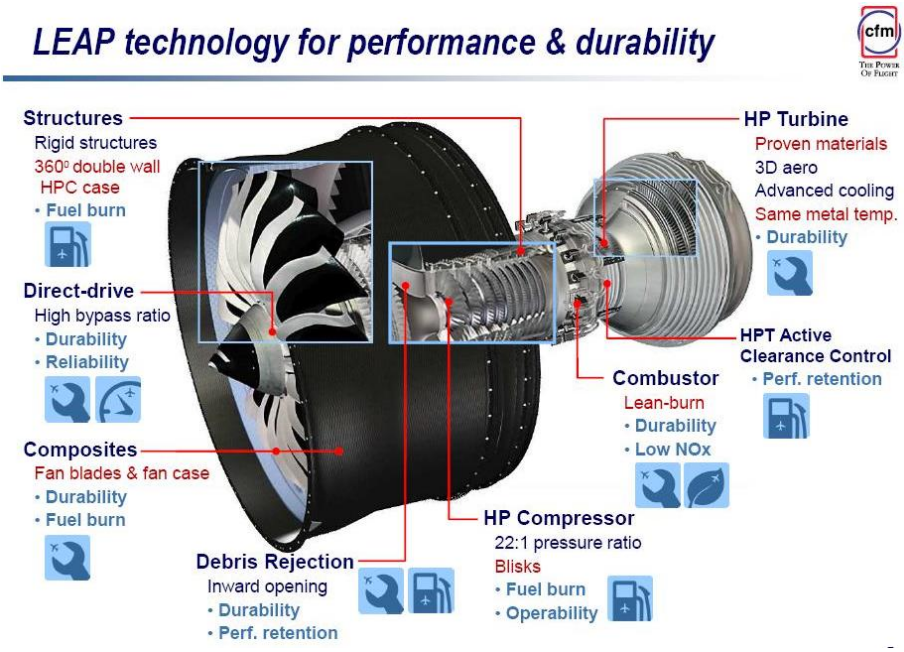


Figure 7 Typical LEAP engine [9]


Figure 8 Prepreg melt infiltrated (prepreg-MI) ceramic matrix composite (CMC) shrouds used in LEAP engine [8]

CMC allows a significant increase in temperature (over 150 $^{o}$C) compared to superalloys. CMC have replaced the nickel-based superalloys providing significant lightweight components, roughly 1/3 of their density. The "LEAP" engines are highly demanded because of lightweight and efficient fuel consumption (yield 1.5% cut off). More than 10000 LEAP engines (worth 140 billion dollars) and 700 orders of GE9x (29 billion dollars) were placed in 2016 [10-12].

Finally, SiC based composites get much attraction for **light water reactors** after the Fukushima Dai-ichi accident in Japan, 2011. SiC/SiC composites have low activation/decay properties, thus offering good opportunities for applications in some fission reactors such as accident tolerant light water reactors [13].

## 1.2 Objectives of thesis

The objective of this thesis was to join SiC-based (i) ceramic matrix composites (CMC), (ii) monolithic ceramics and (ii) ceramic foams with innovative joining methods and materials, for aerospace and energy applications. The research aimed to obtain a joint having following requirements:

- **Oxidation resistance (up to 1100 $^{o}$C)**
- **High temperature stability up to 1100 $^{o}$C in air**
- **Adequate mechanical strength**
- **Thermal shock resistance**
- **Pressure-less joining**
- **Cost-effective process**

Silicides of refractory metals are among the few materials which can satisfy the oxidation resistance and high temperature stability. All the Refractory metals (RM) have a higher melting temperature over 2400 $^{o}$C. Despite of having high melting point none of them is good in oxidation resistance at elevated temperature and are being used in alloying with nickel-based superalloys due to their better creep resistance [14]. This research work has exploited the potential use of refractory metal silicides for the first time ever in joining and explored the key strengths and weaknesses.

Advance materials and designs require special attention in carefully selection of joining procedure and process parameters. General rules are: (1) select a joining process that minimally alters or disrupts the material's inherent microstructure (including chemistry), while still achieving required or desired functionality; and (2) consider the effect of joining process on the material being joined and structure [2, 15-17]. Several joining techniques have been developed so far for CMC. Most of the joining processes require high temperature, high pressure, and long thermal treatment, thus resulting in expensive procedures.

A novel joining technique called **"RM-Wrap"** (Refractory Metal – RM) has been developed within this thesis; it consists of wrapping Si foils inside a refractory metal (Mo, Nb, Ta and W) wrap. Wrapping was done to prevent molten silicon to leak from the joined area during the joining process and infiltrate porous materials. RM-Wrap brazing is a tailorable cost-effective pressure-less joining technique which requires an inert atmosphere (i.e. vacuum/inert) [18].

This technique (RM-Wrap) provides the new insights in joining ceramics, ceramics matrix composites and ceramic foams. The study presented in this thesis is the first (to the best of author's knowledge) investigation to use the silicides ($MoSi_2$, $NbSi_2$, $TaSi_2$, and $WSi_2$) in joining. Silicides are among few materials have higher melting temperature and excellent oxidation resistance at elevated temperature. Conventional manufacturing routes of silicides are lengthy and prone to contamination and oxidation. On the contrary, RM-Wrap is quick, free from undesired phases and has excellent reproducibility and versatility.

# Chapter 2

# Joining of SiC-based CMC: state of the art

This chapter provides an overview of joining techniques and the state of the art of joining materials used for SiC based ceramics and composites.

There has been very intense research on joining of SiC based ceramics and composites in past decade all over the world, but mainly in USA (Pacific Northwest National Laboratory and NASA Glenn Research Center), Japan (Joining and Welding Research Institute) and Europe (TWI-UK, Fraunhofer Institute-Germany).

Many joining techniques have been developed so for to join similar and dissimilar materials, as shown in Figure 9.

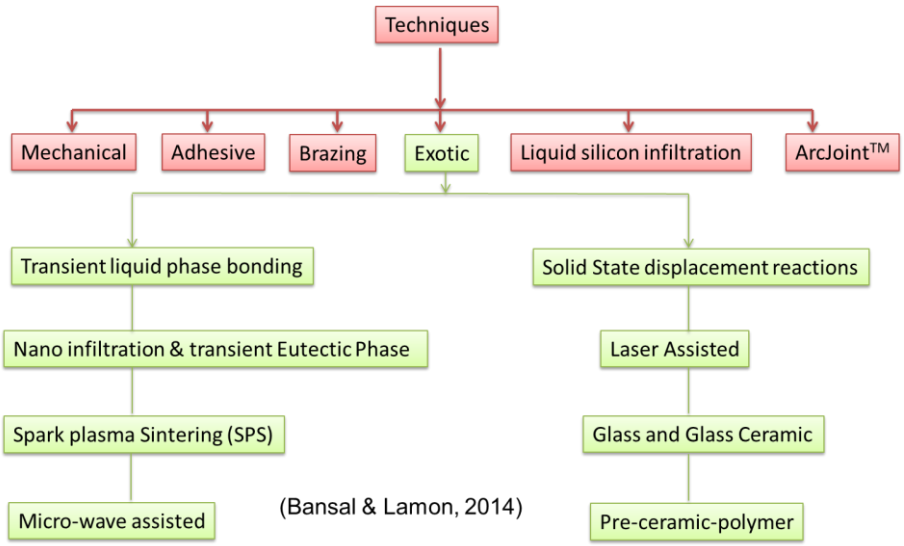


**Figure 9 Overview of joining techniques [1]**

The selection of joining technique is subjected to the "services required by the joints and its suitability in producing the final design" [19].

Joining techniques shown in Figure 9 are discussed briefly in the following section to give an overview (state of the art) of available joining techniques and materials used for SiC-based CMC.

## 2.1 Mechanical Joining

Mechanical joining is one of the oldest joining technique used to join two machined (threaded, drilled) components with the help of external part (screws/nuts and bolt rivet mechanism), only recently used for SiC-based CMC. The typical external part can be of metallic or ceramic (screws/nuts and bolts/rivets) depending on the joining system and area of application. Mechanical joining adds weight to the final component (screws/nut weighs an average of 100 g per piece). [15, 17]. Moreover, the machining cause stress concentration, microcracks, delamination, thermal stress which affect the strength of SiC based ceramics and composites component. Mechanical joining is low cost, with the possibility to dismantle the joined structures [20, 21]. Joints produced by this technique have moderate strength, applicable for low to moderate temperature applications. There are specific applications (automotive) where joints need to be produced without heat treatment and to replace the parts in case of damage [22].

## 2.2 Adhesive Joining

Adhesive joining of SiC based ceramics and composites are limited due to their lack of high-temperature stability. However, considering the ease of application and other benefits, recently there is a growing interest to join the ceramics and CMC for high-temperature applications by using modified adhesives (reinforced with ceramic particles, fibers and carbon nanotubes) [23].

The organic part in adhesives has the drawback of giving high porosity and low-temperature stability. Therefore, a recent research trend shows the effectiveness of reinforcement of adhesives with inorganic particles to minimize the porosity and strength issues for high-temperature applications. For example, a modified polymethyl silasesquioxane resin as a matrix is reinforced by inorganic fillers (Si, Al, B4C, SiC whiskers) to join carbon composites resulting in improved mechanical properties at room temperature [23-25]. Polymer based adhesive joining is one of the simplest, low cost and high speed technique, which can be used for ceramics, metals and dissimilar materials (metal-ceramic) but the use is limited to low temperature applications [26].

## 2.3 Glass and Glass-Ceramic Joining

Glass and glass-ceramics as joining materials have been studied due to their unique tailorable properties, such as coefficient of thermal expansion (CTE), viscosity, wettability, and most important high-temperature and oxidation stability. Moreover, with a suitable thermal treatment desired crystalline phases can be achieved. Glass and glass-ceramic joining is one of the very few tailorable pressure-less joining techniques used for SiC-based materials [27, 28].

Recent research trends show the use of reinforcement (particles, fibers) in the glass-ceramic materials to produce the composite joint structure. Glasses can create hermeticity, and this is one of the reasons why several glass compositions have been developed and successfully used in joining [29, 30].

In nuclear applications, SiC/SiC are highly demanded due to their radiation stability and low neutron induced activation. Therefore, joining materials needed for joining SiC/SiC to be used in energy production applications (nuclear fusion and fission) must be stable under nuclear environment. Materials used in fusion reactors must be resistant to high energy irradiations (14.1 MeV) neutrons.

A calcia-alumina (CA) glass-ceramic having composition (CaO = 49.77 and $Al_2O_3$ = 50.23 Wt%) was used as a joining material for SiC/SiC composites at 1500 $^oC$ for 1 hour in an inert environment. Average lap joint shear strength reported is 28 MPa and microstructure consists of $3CaO.Al_2O_3$ and $12CaO.7Al_2O_3$ [31, 32]. In another study CA glass-ceramic joined SiC at 1480 $^oC$ in an inert environment for 10 minutes. Joined SiC were irradiated with 5.1 MeV $Si^{2}$+ ions to 3.3 x $10^{20}$ ions/$m^2$ at temperatures of 400 and 800 $^oC$. No cracking, damage, detachment and peeling was observed after $Si^{2+}$ irradiation at elevated temperature [33]. Moreover, CA glass was also tested at 5.5 MeV $^4He^+$ ion irradiations and it shows CA glass-ceramic is a promising material for joining SiC intended for nuclear applications [34]. SiC-CA-SiC joints were also tested under neutron irradiation at 500 °C (3.0-3.4 x $10^{25}$ n/$m^2$) and 800 °C (5 x $10^{25}$ n/$m^2$). The slightly decrease shear strength was observed due to increase in transverse cracks density after irradiation. The unirradiated shear strength is 115 MPa while as the 93 MPa is of irradiated at 500 °C and 800 °C [35].

Magnesium alumino-silicate (SAMg) glass ($SiO_2$–$Al_2O_3$–MgO) has been proposed as a joining and coating material for SiC/SiC composites at 1180 $^oC$ with a high heating rate (3000 $^oC$/hour) for 1 hour in an inert environment. High temperature resistant crystalline phases cordierite and mullite were detected [36]. SAMg glass was tested under neutron irradiation for one year at 50 $^oC$, 6.92 x $10^{24}$ n/$m^2$ (E > 1 MeV) to investigate the microstructure changes caused by neutron irradiation. EDS analysis before and after irradiation shows no change in elemental composition and no cracking [37].

A low activation glass-ceramic having composition based on $SiO_2$–$Al_2O_3$–$Y_2O_3$ (SAY) was used in joining of SiC/SiC composites at 1375 $^oC$ for 20 minutes and then at 1235 $^oC$ for 1 hour under an inert environment. Joint microstructure contains three crystalline phases cristobalite, mullite and yttrium disilicate (keivyite) and 4-point bending test results gave 120 MPa as joint strength [38]. SAY glass-ceramic was tested at 5.5 MeV $^4He^+$ ion irradiations in order to investigate the microstructural changes at elevated dpa. No phase and microstructural variation was detected by XRD and SEM-EDS analysis [34]. SAY joined SiC/SiC were neutron irradiated for 1 year at different conditions (i) 550 $^oC$, 9-11 x$10^{24}$ n/$m^2$ (ii) 600 $^oC$, 16–22 x $10^{24}$ n/$m^2$ and (iii) 820 $^oC$ 31–32 x $10^{24}$ n/$m^2$. SAY morphology and elemental composition before and after irradiation showing very similarity. No significant effect on 4-point strength values before and after neutron irradiation were measured [37].

In another study, a C/C-SiC composite was joined by multilayer interlayer glass-ceramics. Two glasses based on magnesium aluminum silicate (MAS) and lithium aluminum silicate (LAS) were used: C/C-SiC-*MAS+(MAS+LAS)+LAS*-C/C-SiC slurry was applied on faying surfaces and joined in a hot press at 1200-1300 $^{o}$C for 30 minutes with a pressure of 20-25 MPa under vacuum. Joint shear strength was measured in the range of 12-20 MPa on CVD SiC coated and uncoated composites [39].

Literature reports many other glass and glass-ceramics compositions for joining ceramics (SiC, $Zr_2B$, $Si_3N_4$, $Al_2O_3$) based on calcium aluminosilicate, yttrium aluminosilicate and rare earth (RE) aluminosilicates (with Yb, La or Ce) [26]

## 2.4 Preceramic Polymer Joining

Preceramic polymers are kind of polymers that can be converted into ceramics by heat treatment. Joining by a preceramic polymer is an easy, inexpensive method, gives stable joining structures and compositions. Development of preceramic polymers have gained special attention in the past couple of years [40]. There are many commercially available preceramic polymers developed by Ceramatec USA, one example of preceramic polymer used in joining of SiC is a mixture of allyl-hydridopolycarbosilane (aHPCS; Starfire Systems, USA), silicon carbide powder, and an un-pyrolyzed polymer. A viscous preceramic was applied on the faying (e.g. silicon carbide) and heat treated up to 1200 $^{o}$C [41].

A hybrid preceramic polymer in combination with chemical vapor infiltration (CVI) technique has been used to join SiC/SiC tubes. This is a three step process starting with low-temperature curing, followed by pyrolysis and finally CVI at 1300 $^{o}$C to densify the interlayer [42].

In another study, cork and ceramic matrix composites (C/C-SiC) were successfully joined for thermal protection system with high-temperature commercial adhesives: based on alumina 670 Ceramabond$^{TM}$ (maximum use at 1650 °C), 669 Graphi-bond$^{TM}$ (maximum use at 760 °C), and 835 Ceramabond$^{TM}$ (maximum use at 1371 °C), from Aremco products Inc [43].

A liquid preceramic polymer named (V-PMS) was used in joining of sintered SiC at room temperature by applying the V-PMS liquid on faying surfaces with the help of brush and cured under a $N_2$ for 2 hours at 200 $^{o}$C. SiC cured specimens were

then heat treated at 800 $^{o}$C, 1000 $^{o}$C and 1200 $^{o}$C under a $N_2$ environment for 2 hours with a heating rate of 2 $^{o}$C per minute at each temperature in order to investigate the joint strength with respect to joining temperatures. Shear strength produced by V-PMS was measured 11.9 MPa (at 800 $^{o}$C), 34.5 MPa (at 1000 $^{o}$C) and 29.9 MPa (at 1200 $^{o}$C). V-PMS pre-ceramic polymer was obtained by two steps (i) Polymethysilane (PMS) was synthesized by a condensation reaction of methyl dichlorosilane and metallic sodium and (ii) PMS and D4Vi mixed and heated at 130 $^{o}$C for 2 hours, and the final product is yellowish liquid V-PMS [44].

## 2.5 Liquid Silicon Infiltration Joining (LSI)

LSI is an in situ joining technique originally adopted for manufacturing of carbon-based CMC. In LSI, silicon and silicon-based alloys are used as a joining material. LSI is a two-step process; the first step involves the preparation of porous composites (C/C) structure and in the second step molten silicon/alloy flows through the porous components of carbon (C/C) under a controlled condition (vacuum), and it reacts to form the silicon carbide. LSI is a low cost joining technique able to produce complex shapes without residual open porosity. This technique is well established and it is being commercially used in the integration of CMC brake systems by joining the C/SiC with a metallic part [45-48].

In one study 2D C/SiC prepared by low pressure chemical vapour infiltration was joined by liquid infiltration process with the Ni-based interlayer. The joining was performed at 1300 $^{o}$C under a vacuum with a pressure of 20 MPa for 15-60 minutes. During joining the interlayer melted and infiltrated partially within the pores of composites. Joint strength increased with increasing holding time; 58 MPa was reported with 3-point bending test [49].

## 2.6 ARCJOINT $^{TM}$

This joining technique was developed at NASA and named as Affordable Robust Ceramic Joining. It consists of two steps, (i) carbonaceous materials are applied on the surfaces to be joined and left for curing (for 10-20 minutes) at 110-120 $^{o}$C. (ii) silicon, and silicon-based alloys are applied over the carbonaceous surface as a paste, tape, slurry or whatever could be the solution for intended joint and thermally treated at around 1250-1450 $^{o}$C. The silicon starts melting and reacting with available carbon to form silicon carbide. This technique is very suitable for large and complex designed components [50, 51]. This joining technique is rapid and simple which can be applied to monolithic SiC and composites as well. SiC can be

replaced with other materials in second step such as $Si_3N_4$; it enables to join other materials as well [26].

## 2.7 Nano-Infiltration and Transient Eutectic Phase (NITE)

NITE technique was initially developed for the manufacturing of SiC/SiC composites for nuclear applications. This novel process was developed based on liquid phase sintering. NITE joining technique uses a mixture of SiC and some oxide powder such as $SiO_2$, $Al_2O_3$ and $Y_2O_3$ as a joining material. Oxide transient liquid phases are formed during the joining process. Joining is carried out under an inert environment (i.e. in the presence of Ar) at elevated temperature of around 1700-1900 $^oC$ and a pressure of 20-30 MPa. The joint composition is same as of SiC in SiC/SiC matrix and has good mechanical strength [1, 52-54]. NITE is considered a promising joining technique for joining SiC-based materials to be used in nuclear applications. SiC ceramic can be joined with mixed powders of $Al_2O_3$, $Y_2O_3$, $SiO_2$ and SiC as joining materials at 1800 $^oC$ with a pressure of 20-30 MPa for 1 hour. The torsional test on NITE joined SiC exceeded 200 MPa and crack initiating with the grip of specimen holder [55].

## 2.8 Spark Plasma Sintering (SPS)

SPS is a sintering technique used to fabricate a dense bulk material. SPS uses electrical energy which creates a local plasma in the porous regions of powder, results in heat and mass transfer necessary to achieve full densification. Localized heating of particles occurs due to electrical discharge. SPS has unique features such as short processing time, low sintering temperature, no prior compaction step, and high heating rate that help in keeping nanostructures with better particle and matrix interface characteristics [14, 56, 57].

SPS use has been extended in joining of SiC and CMCs [58]. Recently considerable attention has been paid to join the SiC and CMCs by SPS. The SPS processing allows broad flexibility in the processing parameters including the applied pressure (0-100 MPa), the current density (up to 10000 Ampere), heating rate (up to 500 K/min). Such flexibility in the processing parameters is always desired for joining CMC, ceramics and refractory metals. SPS is quite an expensive process requires the pulsed DC generator and can only produce small symmetrical shapes [59]. The heating efficiency and homogenous temperature distribution is dependent on the electrical conductivity of die and powders (Raw materials) being used. Maintaining low temperature gradient within specimens is desired to obtain

homogeneous sintering which is difficult in case of heterogeneous materials have different coefficients of conductivities [60].

CVD SiC-coated composite (C/SiC) was joined by SPS with a high heating rate of 150-200 $^{o}$C/ minutes and pressure of 60 MPa with three different joining materials:

(i) Ti (30 -130 µm thick) at 1700 $^{o}$C for 3 minutes, joint microstructure consists of $Ti_3SiC_2$, $TiSi_2$ due to inter-diffusion Si and C. Joint apparent lap shear strength was measured 12-14 MPa.

(ii) glass-ceramic (CA= $CaO–Al_2O_3$) at 1480 $^{o}$C for 10 minutes, apparent lap shear strength of CA joint was measured 13-22 MPa

(iii) SiC+ $BC_4$ (wt % 5) at 1900 $^{o}$C for 3 minutes having joint apparent lap shear strength of 12-18 MPa [61].

SPS was demonstrated to be a new and very effective joining technique for CMC irrespective of joining material. SPS has potential to use pure metals, glass-ceramics and ceramic powders as a joining material, *possibly* in a pressure-less and localized heating regime: research is going on in these directions.

## 2.9 Laser-Assisted Joining

Laser-assisted joining is a localized melting of joining materials by using a laser as heating source. Localized heating by laser radiations is advantageous to avoid the adverse effects deriving from heating the entire CMC, as in the previous techniques, however it is difficult to locally control the process conditions. Several joining materials are available such as metals, silicides and oxides: glass–ceramic solder (Y–Al–Si–O) successfully joined SiC-based and other CMC such as silicon carbon nitrite (SiCN) [62]. Joining CMC by this technique has limitations such as: gradient in thermal conductivity within substrates, which influence joint quality and processing, ambient environment which may lead to the formation of undesired compounds, limited specimen size to be joined [16, 29, 63].

Pure Zirconium (Zr) foil (40 µm thickness) was used in joining of SiC by a laser scanning with a maximum power of 3000 W. Zr has very low neutron capture thus highly demanded in neutron irradiations environment for nuclear reactors. Zr melting (1852 $^{o}$C) was controlled by controlling the power at 180 W. Ar was blown from the laser nozzle in order to minimize the oxidation. Microstructural analysis

shows the presence of $ZrSi_2$, $Zr_5Si3Cx$, and $Zr_4Si$ due to diffusion of Si in Zr, however Zr diffusion was also observed in SiC up to 120 μm [64].

## 2.10 Micro Wave Assisted Joining

Microwave processing is one of the emerging technology adopted in fabrication of ceramics, ceramic matrix composites, polymer and polymer matrix composites due to rapid source of heating [65]. The foremost benefit of using microwaves in joining is that it does not heat the complete assembly, but only the joint area or interfaces, as for laser joining previously discussed. The high temperature and detrimental pressure effect on the whole substrates can also be avoided. This is one of the fastest joining technique, in principle, large and complex pieces/parts can be joined at a low cost. Microwaves are capable to achieve a temperature 2000 $^oC$ with a frequency of 2.45 GHz and a power of 700 W [15, 17, 66]. Microwaves have been effectively employed for joining of ceramics (alumina, zirconia, SiC), ceramic matrix composites (SiC/SiC) [67-69] metals (Copper, stainless steel) [70, 71] and polymer matrix composites [72]. Different fillers such as glasses [73, 74], alumina gel [75], Al-Si-powders [76], TICUSIL paste [77, 78] and NiTi foils [79] were used in microwave assisted joining.

## 2.11 Solid State Displacement Reactions (SSDR)

Displacement reactions are obtained when more reactive metals displace the less reactive metals in a compound. Such reaction can occur in liquid and solid state, in case of solid it is known as solid-state displacement reactions. Ti-Si-C based SSDR reactions have been proposed for SiC-based and other CMCs for joining [80, 81].

## 2.12 Transient-Liquid-Phase Bonding (TLPB)

TLPB is quite a new joining technique which uses interlayers based on metals. During heating, the constituents melt and react forming phases which have a higher melting point than the joining temperature. TLPB has an immense potential for high-temperature applications. Understanding reactions and formation of final phases during TLPB is key to produce strong joints with desired compounds. The liquid phase formed while heating reduces the use of high pressure [82, 83]. Careful design of the microstructure is needed to get the required properties [82, 84].

## 2.13 Brazing

Brazing involves joining via interlayers (metallic) having melting temperature over 450 $^{o}$C. Brazing is one of the most well-established joining technology used for metals, ceramics and CMCs. Several commercial brazes are available for joining SiC-based ceramics and CMCs, based on active metals (Ti, Cr), Gold (Au), Silver (Ag) and Nickel (Ni) along with additional alloying (filler) elements (Ti, Si, Mo, V, B) [1, 15, 17, 21, 52, 85].

Capillary flow of braze against the parent substrate is a fundamental physical force that ensures the quality of joint. More specifically, it is a relative force of attraction among the molecules of the molten liquid and to the solid surfaces [15]. In other words, the wettability of molten material must be good enough to wet the joining surfaces. Wettability is always measured in terms of contact angle: higher the contact angle lower will be the wettability and vice-versa. [86].

Joint quality depends on the base metal and can further be enhanced by additional alloying elements. Alloying elements can enhance wettability, viscosity, melting point, reactivity and CTE. Faying surfaces play a critical role in successful joining. Clean surfaces can help to produce the desired crack free strong joints.

Brazing CMC is quite challenging because of several reasons such as the difference in CTE of CMC and metallic braze, uneven surfaces, low diffusivity coefficient and high porosity [26]. Higher porosity is more detrimental when the braze reaches its liquids point and infiltrates into the pores instead of staying in the joint area. Brazing or joining of CMCs can be done in two ways (i) indirect brazing requires the pre-metallization of surfaces with active metals (i.e. Cr, Ti, Zr) in order to improve the wettability and (ii) direct brazing also known as active metal brazing where active metals/elements are alloyed in braze, resulting in single step brazing [87].

Interlayers can have more than one function in brazing; they may enhance bonding and relieve stresses; such as a thin layer of gold (Au) can reduce the temperature required for bonding, or a thin layer of tungsten (W) can alleviate stresses in joining of dissimilar materials [26].

Molybdenum (Mo) has been used in many studies because of its low coefficient of thermal expansion (CTE Mo = 5 x$10^{-6}$/K ) close to SiC-base materials and mullite. Mo interlayer (100 µm) was used in joining of mullite at 1650 $^{o}$C under a vacuum hot pressed at 10 MPa resulting in good bonding strength of 140 MPa [88].

In another study, CVD SiC was joined with a Mo interlayer (25.4 µm) at 1500 $^{o}$C for 10 hours. SiC-Mo-SiC joint phases formed are $Mo_2C$ (at center) and $Mo_5Si_3C$ with a Si diffusion from SiC due to longer duration at both interfaces (with SiC). Flexural strength (4-point bend) was measured at 183 ± 83 MPa at room temperature and 258 ± 157 at 1090 $^{o}$C [89].

Moreover, Mo interlayer has been used to reduce the residual stress in SiC bonding [90], whereas Nickel (Ni) and Copper (Cu) interlayers were used in joining of $ZrO_2$ at 1000- 1200 $^{o}$C and 700-900 $^{o}$C respectively, with pressure of 10 MPa. [91, 92].

In another study, refractory metals Niobium (Nb), Titanium (Ti), Molybdenum (Mo) and tungsten (W) were adopted in joining of SiC at 1200-1500 $^{o}$C in a vacuum atmosphere for 10 hours with a pressure of 4-18 MPa. Niobium carbide (NbC) and niobium silicides ($NbSi_2$ and $Nb_5Si_3$) phases were formed in the SiC-Nb-SiC joint. Ti, $Ti_3SiC_2$ and titanium silicides ($TiSi_2$, $Ti_5Si_3$) were formed in SiC-Ti-SiC joint region. SiC-Mo-SiC bonding has better diffusion than Nb and Ti. SiC-Mo-SiC bond region consists of $Mo_2C$ in middle and molybdenum silicides ($Mo_5Si_3$) at the interface with SiC. W interlayer was fully converted into $W_2C$ and $W_5Si_3$ in case of SiC-W-SiC joints [93]. Using pure refractory metals interlayers requires high temperature for longer duration may add adverse effects on the substrates.

Cu–Au–Pd–V and Cu-Pd-V fillers were used in joining of 3D C/SiC composites at 1200 $^{o}$C and 1170 $^{o}$C respectively for 10 minutes. The joint microstructure consists of a solid solution of Cu (Au, Pd), $Pd_2Si$ (formed by reaction with C/SiC) as Pd has strong affinity with Si and $Cu_3Pd$, whereas active metal V diffuses into composite surface: 135 MPa and 128 MPa joint strength was obtained at room temperature, respectively [94, 95].

CVD SiC was joined by two commercial brazes based on Ag, Cu and Ti named CuSil ABA at 815 $^{o}$C and TiCusil at 900 $^{o}$C under a vacuum with the addition of 5, 10 and 15 wt % SiC particles (20-30 µm)by using glycerine as a fugitive binder [96].

Sintered SiC was joined to itself by using active metal brazing (Ag–Cu=35.25 wt%, Ti=1.75 wt%) under a vacuum at 860 $^{o}$C -900 $^{o}$C - 940 $^{o}$C for 10-30-and 60 minutes. Joint microstructure consists of TiC and $Ti_5Si_3$ layer, 4-point bending strength reaches 324 MPa at room temperature. Longer holding time results in poor mechanical properties due to thicker reaction layers which increase mismatch of

CTE between SiC and reaction layer. With increasing test temperature flexural strength decreases due to softening of filler [97]. In another study, sintered SiC was joined by using brazing (Ag-27.25Cu 12.5 In- 1.25Ti wt%) at 700-800 $^{o}$C under vacuum. Joint microstructure consists of TiC and Ti5Si3 as reaction layer, 234 MPa joint strength (4-point bending) was measured [98].

SiC ceramics were joined by a tape cast interlayer of $TiB_2$-C with reactive Si infiltration at 1450 $^{o}$C in a vacuum with a heating rate of 20 $^{o}$C/minute. A very dense composite interlayer of $TiB_2$-C-Si was formed. The average 3-point bending strength of SiC joints bonded with $TiB_2$-C-Si was measured 360-420 MPa with fracture failure in SiC [99].

BraSiC$^{TM}$ is one of the commercial braze used for joining 2D and 3D CMCs (SiC/SiC), consists of Si with reactive metals such as Ti, Cr, V and Rh. The presence of Si improves the wettability, and reactive metals enhance joint strength [100, 101]. All refractory metals have a melting point over 2400 $^{o}$C and are highly resistive to heat, wear, creep. However, they are not chemically stable metals and have poor oxidation resistance at elevated temperature. These metals find their applications due to the high melting point, and high-temperature strength, however, their use is limited to non-oxidative applications only. The silicides of refractory metals (Mo, Nb, Ta and W) are oxidation resistive and high temperature stable materials; their melting temperature is above 1900 $^{o}$C. Oxidation resistive and high temperature stable materials are demanded in aerospace and energy (nuclear) applications.

Table 1 summarizes the literature reported in previous sections for joining of SiC based materials. It presents the joining materials used, joining technique or process adopted, process parameters, joint strength and phases formed in the joint seam. However, there are some studies without mechanical tests and joint phases. Some glass and glass ceramics studies report the stability of joining material under irradiations (Si, He and neutron).

**Table 1 Summary of Joining materials and methods for SiC based substrates**

| Joining substrate | Joining material | Joining (technique/process) | Process parameters (T, t, p) | Strength/other tests | Phases formed | Ref: |
|---|---|---|---|---|---|---|
| SiC/SiC | CaO- $Al_2O_3$ (49.77-50.23 %) | Glass and glass ceramic (Ar flow) | 1500 °C, 1 hour | (Lap Shear Strength) 28-33 MPa | $3CaO.Al_2O_3$ and $12CaO.7Al_2O_3$ | [31] |
| SiC/SiC | CaO- $Al_2O_3$ (49.77-50.23 %) | Glass and glass ceramic (Ar flow) | 1500 °C, 1 hour | (Single lap offset Shear Strength) 28 MPa self-healing | $3CaO.Al_2O_3$ and $12CaO.7Al_2O_3$ | [32] |
| SiC | CaO- $Al_2O_3$ (49.77-50.23 %) | Glass and glass ceramic (Ar flow) | 1480 °C, 10 min | Irradiated with 5.1 MeV $Si^{2}$+ ions to 3.3 x $10^{20}$ ions/$m^2$ at temperatures of 400 and 800 °C. | $3CaO.Al_2O_3$ $12CaO.7Al_2O_3$ | [33] |
| SiC/SiC | $SiO_2$–$Al_2O_3$–$Y_2O_3$ | Glass and glass ceramic (Ar flow) | 1375 °C, 20 min, then at 1235 °C for 1 hour | (4-point bending) 24 MPa (Type 1) 122 MPa (Type 1) 149 MPa (Type 1) | Mullite Cristobalite Keivyite | [38] |
| SiC/SiC | $SiO_2$–$Al_2O_3$–MgO<br>$SiO_2$–$Al_2O_3$–$Y_2O_3$ | Glass and glass ceramic (Ar flow) | SAMg 1180 °C, 1 hour<br>SAY1375 °C, 20 min, then at 1235 °C for 1 h | (4-point bending) 122 MPa unirradiated<br>SiC/SiC were neutron irradiated for 1 year at<br>(i) 550 °C, 9-11 x$10^{24}$ n/$m^2$<br>(ii) 600 °C, 16–22 x $10^{24}$ n/$m^2$ and 118 MPa | SAMg cordierite and mullite<br>SAY Mullite Cristobalite Keivyite<br>No significant effect of irradiation | [37] |

| | | | | | | |
|---|---|---|---|---|---|---|
| | | | | (iii) 820 °C 31–32 x $10^{24}$ n/$m^2$<br>89 MPa | | |
| SiC/SiC | SiO2–Al2O3–MgO | Glass and glass ceramic (Ar flow) | 1180 °C, 1 hour | - | cordierite and mullite | [36] |
| CVD SiC | $CaO–Al_2O_3$<br>(49.77-50.23) wt % | Glass-Glass ceramic<br>(Ar Flow) | 1480 °C, 10 min | (Torsion Shear strength)<br>Unirradiated<br>115 MPa<br>Irradiated (neutrons)<br>93 MPa (500 °C)<br>93 MPa (800 °C) | $12CaO.7Al_2O_3$,<br>$3CaO.Al_2O_3$ | [35] |
| C/C-SiC | $Li_2O$-MgO-$Al_2O_3$-$SiO_2$ | Hot-Pressing | 1200-1300 °C<br>30 min, 20-25 MPa | (Shear Strength)<br>12-20 MPa | SiC-C/C and SiC-LMAS interfaces | [39] |
| SiC | allyl-hydridopolycarbosilane SiC Powder unpyrolysed polymer | Pre-Ceramic polymer (Ar flow) | 1200 °C | (Shear Strength)<br>25 MPa as joined<br>12 MPa exposed 50/50% to $H_2O/O_2$ at 1000 °C for 1000 hours<br>12 MPa exposed to $N_2$ at 1000 °C for 1000 hours | - | [41] |
| SiC | Pre-ceramic Polymer (V-PMS) | Pre-Ceramic polymer | 800 °C, 1000 °C and 1200 °C 2 hours, 0.1 MPa | (Shear Strength)<br>12 MPa (800 °C)<br>34 MPa (1000 °C)<br>30 MPa (1200 °C) | - | [44] |
| Cork and C/C-SiC | Commercial adhesives<br>670 Ceramabond™ Alumina based<br><br>669 Graphi-Bond™ Graphite based | Adhesive | 93 °C, 2 hours with a small load | (Shear Strength)<br>Room Temp: RT<br>liq: Nitrogen: LN<br><br>(i) Alumina based<br>RT: 0.54 MPa | - | [43] |

| | | | | | | |
|---|---|---|---|---|---|---|
| | 835 Ceramabond™ Zirconia based | | | LN: 0.85 MPa<br><br>(ii) Graphite based<br>RT: 0.52 MPa<br>LN: 0.60 MPa<br><br>(iii) zirconia based<br>RT: 0.78 MPa<br>LN: 1.07 MPa | | |
| C/SiC | Ni-base alloy | LSI (Vacuum) | 1300 °C, 15-30-45 and 60 min 20 MPa | (3-Point bending) 58 MPa (45 min) | - | [49] |
| SiC | $Al_2O_3$, $Y_2O_3$, $SiO_2$ and SiC powders | NITE | 1800 °C, 1 hour 20 MPa | (Torsion Shear strength) 200 MPa | - | [55] |
| CVD SiC | Ti (Foil) | SPS | 1700 °C 3 min, 60 MPa | (Shear Strength) 12-14 MPa | $Ti_3SiC_2$, $TiSi_2$, SiC | [61] |
| CVD C/SiC | $CaO$-$Al_2O_3$ (49.77-50.23 %) | SPS | 1480 °C 10 min, | (Shear Strength) 13-22 MPa | 3CaO.Al2O3 and 12CaO.7Al2O3 | [61] |
| CVD SiC | SiC+5%$B_4C$ | SPS | 1900 °C 3 min, 60 MPa | (Shear Strength) 12-18 MPa | - | [61] |
| SiCf-SiCN | $Y_2O_3$- $Al_2O_3$- SiO (16.5-26.05-57.4) | Laser | 1420 °C with 140 W $cm^{-2}$ 70 seconds | (4-point bending) 122 MPa | - | [62] |
| SiC | $Y_2O_3$-$Al_2O_3$-$SiO_2$ (6.55-26.05-57.4) | Laser | 1450 °C 70 seconds (3100 W and with 808 and 904 nm) | (4-point bending) 112 MPa | corundum, mullite and yttrium disilicate | [102] |
| SiC | Zr sheet | Laser | 1852 °C (180 W) Few seconds | - | $ZrSi_2$, $ZrSi_3C_x$ & $Zr_4Si$ | [64] |

| | | | | | | |
|---|---|---|---|---|---|---|
| CVD SiC | Powders<br>Ti-Si-C<br>(1:1:1)<br>molar ratio | Microwave | 2.45 GHz<br>(1.2 kW)<br>10 min<br>20-40 Mpa | (Lap Shear Strength)<br>Compact powders<br>7-45 MPa<br>Loose powders<br>3-10 MPa | $TiSi_2$,TiC, C | [103] |
| SiC | TiSi2 + SiC (Powder) (0-30 vol%) | Microwave | 12 kW power<br>Less than 1 min | - | $TiSi_2$ + SiC | [104] |
| SiC | Alloy<br>(Zn-8.5Al-1Mg) Wt% | Brazing (ultrasonic) | 420 $^oC$ with for 2, 4, 8 and 16 seconds | (Shear Strength)<br>148 MPa with 8 seconds | Zn Al phase and intermetallic compound $MgZn_2$ phases | [105] |
| C/SiC | Cu-Au-Pd-V<br>(40-18-32-10) Wt% | Brazing (Vacuum) | 1196 $^oC$, 10 min | (3-point bending)<br>135 MPa at RT<br>189 MPa at 600 °C | $Pd_2Si$<br>Cu (Au-Pd), V-C | [94] |
| C/SiC | Cu-Pd-V<br>(48-42-10) Wt% | Brazing (Vacuum) | 1170 $^oC$<br>10 min | (3-point bending)<br>128 MPa at RT | $Pd_2Si$, $Cu_3Pd$, V-C<br>(Cu, Pd) | [95] |
| SiC | Ti and Mo foils | Brazing (Vacuum) | 1400 $^oC$<br>1hour, 7 MPa | (Shear Strength)<br>67 MPa for Ti<br>76 MPa for Mo | $Ti_3SiC_2$,$TiSi_2$<br>$Mo_5Si_3C$, Ti and Mo | [106] |
| CVD SiC | Ticusil + SiC Powder<br>Ag–26.7Cu–4.5Ti<br><br>Cusil ABA + SiC Powder<br>Ag–35.3Cu–1.75Ti<br><br>SiC powder (5-10-15) wt% | Brazing (Vacuum) | Ticusil<br>900 °C<br><br>Cusil ABA<br>815 $^oC$<br><br>15 min<br>0.2–0.4 MPa | - | Si–Ti–C-rich reaction layers<br>Cu-rich secondary phase | [96] |
| SiC | (Ag-Cu-In-Ti)<br>(60-27-12-1) Wt% | Brazing (Vacuum) | 700, 740, 780 and 800 $^oC$, 10 min | (4-point bending)<br>220 MPa (700 °C)<br>234 MPa (740 °C) | TiC layer<br>$Ti_5Si_3$ layer | [98] |

| | | | | | | |
|---|---|---|---|---|---|---|
| | | | | 180 MPa (780 °C)<br>130 MPa (800 °C) | | |
| SiC | Ag-Cu-Ti<br>(63-35-2) Wt% | Brazing (Vacuum) | 860, 900 and 940 °C<br>10-30-60 min | (4-point bending)<br>Max: values<br>110 MPa (860 °C)<br>263 MPa (900 °C)<br>316 MPa (940 °C) | TiC, $Ti_5Si_3$, | [97] |
| SiC | Cusil-ABA<br>(63Ag-35.25Cu-1.75Ti | Brazing (Vacuum) | 820 °C, 5 min | (Shear Strength, SLO)<br>42 MPa at 650 °C and<br>25 MPa at 750 °C | TiC, TiSi | [107] |
| SiC | Tape cast TiB2–C<br>interlayer with Si | Brazing (Vacuum) | 1450 °C<br>Heating rate of<br>20 °C /min<br>without dwell | (3-point bending)<br>358-422 MPa | $TiB_2$, Si | [99] |
| SiC | Ni–56Si filler/paste<br>Mo as interlayers | Brazing (Vacuum) | 1350-1400 °C<br>10, 30 and 50<br>min | (Shear Strength)<br>27-41 MPa | Ni-Si/Mo | [108] |
| SiC | SiC/C tapes | Brazing (Vacuum) | 500 °C 1 hour<br>then<br>1450 °C 30 min | (4-point bending)<br>346 MPa at RT<br>439 MPa (1250 °C) | SiC and Si | [109] |
| SiC and C/SiC | $Ti_3SiC_2$ | Brazing (Vacuum) | 1200–1600 °C<br>30 min, 20-40<br>MPa | (3-point bending)<br>110 MPa Max: | $Ti_3SiC_2$ and TiC | [110] |
| CVD SiC | Ti (Foils) | Hot Pressing<br>(Ar Flow) | 1160 °C<br>3h, 20 MPa | (Shear strength)<br>unirradiated<br>124 Mpa<br>Neutron Irradiated<br>125 Mpa | $Ti_3SiC_2$, $Ti_5Si_3$ | [35] |
| CVD SiC | Ti-Si-C Max | Brazing (Vacuum) | 1425 °C<br>2h, 30-40 MPa | (Shear strength)<br>unirradiated<br>117 MPa<br>Neutron Irradiated | $Ti_3SiC_2$, SiC | [35] |

| | | | | | | |
|---|---|---|---|---|---|---|
| | | | | 98 MPa | | |
| Mullite/$MoO_2$ | Mo foil | Hot Pressed (Vacuum) | 1650 °C, 10 MPa | (3-point bending) 140 MPa (mullite) 136 MPa (mullite/$MoO_2$) | Mo, $MoO_2$ | [88] |
| CVD SiC | Mo foil | Diffusion bonding (Vacuum) | 1500 °C,10 hours, | (4-point bending) 183 MPa (RT) 257 MPa (1090 °C) | $Mo_2C$ (at center) and $Mo_5Si_3C$ | [89] |
| SiC | Nb, Ti, W and Mo foils | Diffusion bonding (Vacuum) | 1200-1500 °C 10 hours 4-18 MPa | - | ($NbC$, $NbSi_2$ and $Nb_5Si_3$) ($Ti_3SiC_2$, $TiSi_2$ and $Ti_5Si_3$) ($Mo_2C$ and $Mo_5Si_3$) ($W_2C$ and $W_5Si_3$) | [93] |
| SiC | Mo foil | Hot-Pressed (Vacuum) | 1200 - 1400 °C 1 hour, 10 MPa | - | - | [90] |

# Chapter 3

# Experimental

This chapter is divided into three sections

(i) Development of the RM-Wrap joining (*)
(ii) Brief introduction of materials (CMC, ceramics) used in this study and
(iii) Characterisations techniques of the joints performed in this study.

The key properties of substrates and their intended applications are highlighted, not all the characterizations presented in this chapter are performed on each joint.

*(*) Since the RM-wrap technique is a new joining technology, thus not available in the literature, its development and the rationale behind it are described in this experimental Chapter and not in Chapter 2.*

## 3 RM-Wrap joining (Development)

To meet the ever increasing need for high temperature oxidation resistant joining materials for space and energy production, new reliable joining materials and joining techniques are highly demanded. Silicides are well known for oxidations resistance at elevated temperature.

However, joining of SiC-based composites with pure refractory metals (Mo, Ti, V, Cr, W) to form the silicides at interfaces requires high pressure and temperature. [89, 106].

A novel joining technique “RM-Wrap” (RM=Mo, Nb, Ta, W, Refractory metals) has been developed during this study.

The developed technique is a novel brazing technique brazing named RM-Wrap after the metal used as a wrap to contain one or more silicon foils (e.g. Mo-Wrap when a Mo wrap is used to contain a Si foil).

To the best of author’s knowledge for the first time ever, superior properties of refractory metals are exploited in a pressure-less joining of SiC-based ceramics and ceramic matrix composites.

## 3.1 Mo-Wrap

Molten Si is very reactive and forms alloys and silicides with most metals. $MoSi_2$ is one of the most suitable material to be used at a high temperature (up to 2000 $^oC$) for a long time and in a harsh environment, i.e. oxidative [111].

Molybdenum (Mo) has a high melting temperature (2650 $^oC$): it has many attractive properties such as high strength and stability at high temperature although it has poor oxidation resistance. Mo and its alloys have many versatile, attractive properties for many applications such as electrical and electronic devices, materials processing equipment’s (heating element in high-temperature furnaces) aerospace and defense equipment [112].

The binary reaction of Si-Mo forms three silicides $MoSi_2$, $Mo_5Si_3$ and $Mo_3Si$ as shown in phase diagram Figure 10, [113]. All the silicides have high melting points, above 2000 $^oC$, moreover, $MoSi_2$ has an excellent oxidation and corrosion resistance at elevated temperature due to development of thin protective coating of $SiO_2$ which reduces the diffusion of oxygen [114]. This compound is much more performant than superalloys based on Nickel (Ni) and Cobalt (Co) which are limited in 800-1000 $^oC$ temperature range. $MoSi_2$ has many rich, attractive properties such as high melting temperature (2020 $^oC$), low density (6.24 $g/cm^3$), higher thermal & electrical conductivity, high modulus, low cost, non-toxic and environmentally sustainable.

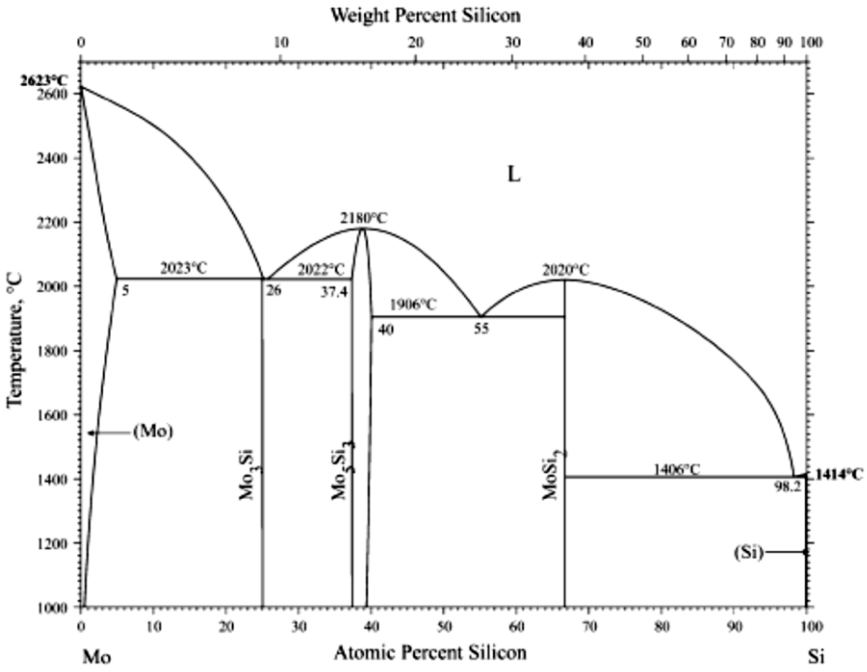


Figure 10 Mo-Si Phase diagram [113]

$MoSi_2$ is well known as inorganic filler used for oxidation resistant applications and as reinforcement materials for composites [112, 115-118]; it has been commercially used in an electric heating element of furnaces up to 1900 $^oC$ in air and has high thermal shock resistance. Other two silicides, $Mo_5Si_3$ and $Mo_3Si$, have a higher melting temperature, but $MoSi_2$ is superior in oxidation resistance [112].

### 3.1.1 Preparation of $MoSi_2$

Various processing techniques are available for synthesis of $MoSi_2$ such as arc melting, hot pressing, casting, powder pressing-sintering, reaction bonding, self-propagating high-temperature synthesis (SHS), infiltration and mechanical alloying (MA) and reactive synthesis (RS). SHS and MA are widely adopted processes/techniques for the synthesis of high temperature refractory materials. In SHS raw powders of Mo and Si are mixed in a molar ratio of 1:2 for 8 hours following by pressing under a hydrogen atmosphere. The combustion synthesis is performed under the argon atmosphere at 1355 $^oC$ with a very rapid heating few seconds to reach the target temperature; it is regarded as a fastest process. The reaction equation of Mo and Si is simple, and is given below [112, 119-124].

$$Mo + 2\ Si \rightarrow MoSi_2$$

**Equation 1 Mo and Si reaction**

Silicon has a lower melting temperature (1412 $^{o}$C) than Mo (2600 $^{o}$C). Thus liquids silicon is available to Mo for reaction.

The mechanical alloying is a well-known powder processing technology. It has gained much attention in past years and it has been widely adopted for the preparation of silicides of molybdenum and tungsten [125-127]. Stainless steel balls and containers are used to mill the desired powders in specific stoichiometric ratios. MA is a lengthy process, and it is quite complicated to synthesis intermetallic compounds, as it takes a long time and it is subjected to high level of contamination. [128, 129].

Reactive sintering synthesis (RS) is also one of the possible technique that reduces the processing time, but it is difficult to synthesize the pure compounds due to rapid oxidation of powder at elevated temperature [130]. High energy vibratory ball milling machines are used with stainless steel container and balls under an argon gas atmosphere to avoid the oxidation. Many advancements have been made in past couple of years in the optimization of process parameters such as balls to powder mixture, processing cycles, temperature, etc. [112]. $MoSi_2$ has a self-passivating behavior which leads its usage to various high-temperature applications, the most prominent and matured application is as the heating element in furnaces.

To summarize, the conventional manufacturing routes are lengthy and need very sophisticated equipment, hindered by the high melting point of $MoSi_2$. Moreover, undesirable phases can be formed while processing. Silicides obtained by these routes have high oxygen contents and other impurities thus cannot be used for high-temperature structural applications [18, 131].

Four Mo-Si based procedures were adopted in this study to synthesise molybdenum disilicide ($MoSi_2$) in situ while joining by using powders and foils.

Silicon wafer (thickness of 584 μm, MEMC Electronic Materials, Italy, and Si powders of (<150 um particles size) 99.95% purity from Alfa Aesar were used. Refractory Metal foils (Mo, Nb, Ta, thickness of 25.4 μm and Mo powder (<74 um) of 99.9% purity Alfa Aesar were used as a joining material.

**1. Mo-Si slurry:** Si and Mo powders were mixed in a different weight ratio (from 70:30 to 30:70) were mixed for 12 hours to ensure homogenization. The slurry of Si-Mo powders was prepared with ethyl alcohol as a fugitive binder and sandwiched between composites and heated at 1450 $^{o}$C for 1 to 10 minutes with heating rate of 1000 $^{o}$C/ hour and cooled naturally under an inert environment (Ar flow).

**2. Mo-Si foils:** Si and Mo foils were placed in between sandwiches of composites in different configurations and heated at the same temperature and time as for in Mo-Si slurry joining.

**3. Two steps joining:** in a two-step joining process (i) Si foil was heat treated on the composite at 1420 $^{o}$C for 1 minute and (ii) Mo (slurry) was deposited on partially Si infiltrated faying surfaces and heated treated at 1450 $^{o}$C for 5 minutes for reaction of Si-Mo or Mo slurry as sketched in Figure 11.

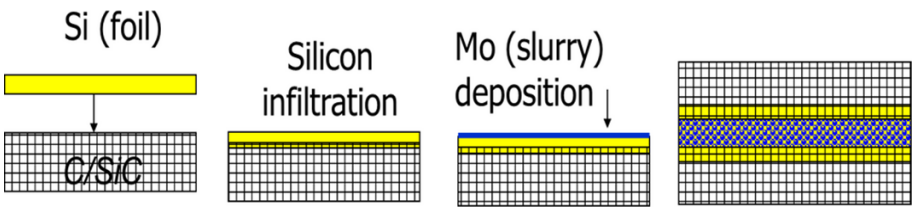


**Figure 11 Two-step joining by Si and Mo [18]**

Silicon viscosity is 0.7-0.9 mPa.s at 1415-1600 $^{o}$C, close to water viscosity (0.7 mPa.s) at room temperature [132]: controlling the silicon infiltration within the specific joining area above its melting temperature is quite challenging.

Joining according to three methods described above was not successful: Figure 12 shows the problem encountered in joining of C/SiC by using the powder of Si and Mo weight ratio (70:30 and 30:70) as a slurry and foils. The discontinuous, poor joint is well evident due to infiltration of Si within the pores of composites and out of the joint area.

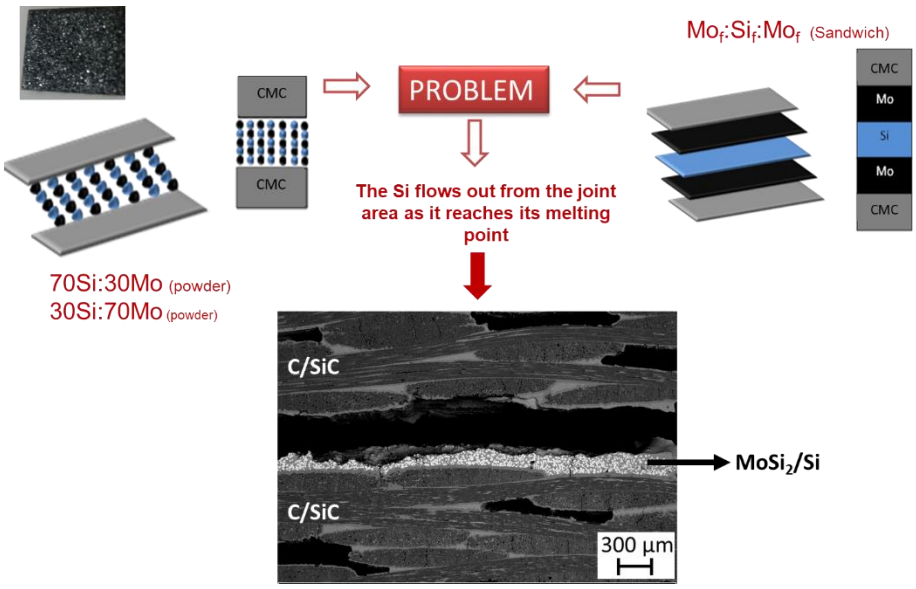


**Figure 12 Discontinuous joint obtained by using the powder of Si and Mo with a weight ratio of 70:30 and 30:70, as a slurry and foils**

A new solution has been developed after series of experiments resulting in a novel, pressure-less, one-step and cost-effective joining technique named "Mo-Wrap."

**4. Mo-wrap:** The new "Mo-wrap" technique consisting in wrapping one Si foil in a Mo foil folded as a wrap; the optimized heating conditions are: 1450 °C, dwell of 5 minutes, as shown in Figure 13 [18].

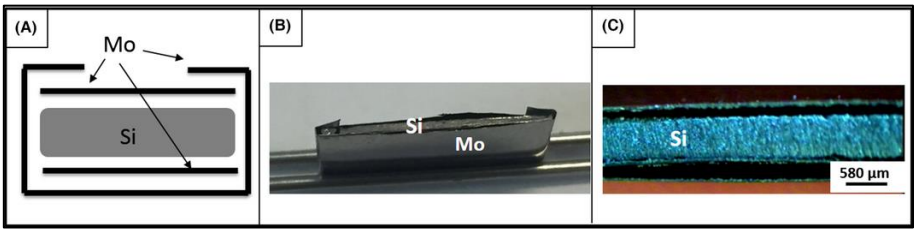


**Figure 13 Mo Wrap Joining [18]**

Joints produced by "Mo-Wrap" are continuous, well bonded without infiltration of Si within C/SiC pores shown in Figure 14.

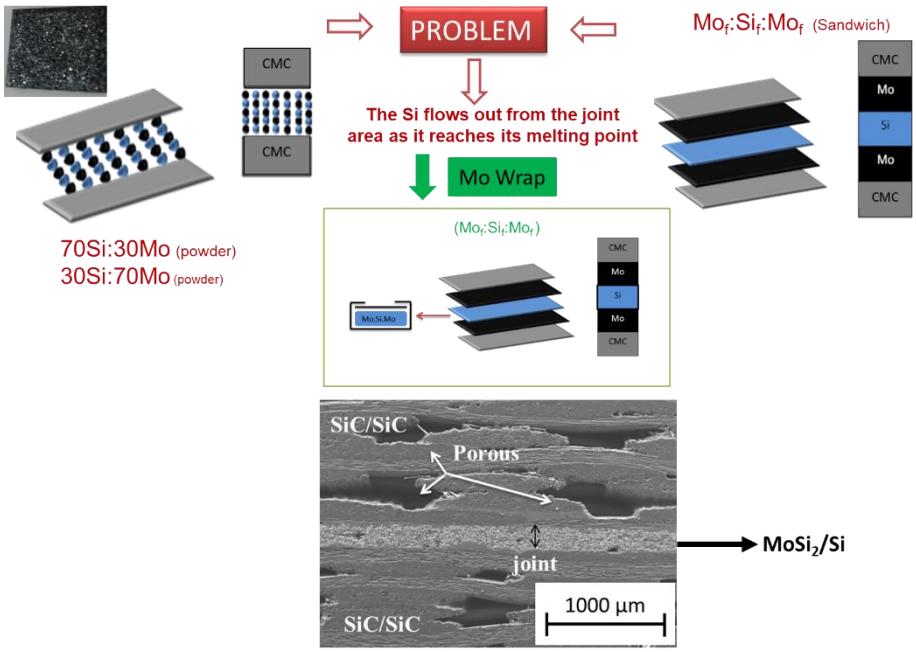


Figure 14 Mo-Wrap joined C/SiC [18]

The joining material is an in-situ formed composite made of $MoSi_2$ particles well embedded in a Si matrix. Si has a dual function:

(i) it provides the liquid phase which is very beneficial for wetting the faying surfaces

(ii) it forms the silicides by reacting with Mo.

Presence of free silicon is not desired in certain applications such as nuclear, but certain amount of silicon is required to achieve the good wettability and crack-free continuous joints (Figure 14). Likewise, the presence of free (un-reacted) Mo is not desired due to its poor oxidation resistance at 300-400 ºC.

The quantity of free silicon has been minimized in this work and the unreacted Mo completely avoided, as it will be discussed in the following sessions.

Mo-Wrap is a **tailorable pressure-less** joining technique in which quantity of each phase can be controlled according to end user requirement. The X-ray diffraction analysis (reported in chapter 4) confirmed the formation of $MoSi_2$ and Si only.

"Mo Wrap" has been fully optimized regarding phase composition, treatment time and temperature. The optimized parameters are 1450 $^{o}$C, dwell time of 5 minutes, heating rate of 1000 $^{o}$C/hr, under an inert Ar. Compositions ranging between 35-50 wt % Mo and 65-50% Si have been tested to optimize the joining process, as sketched in Figure 15, Figure 16 and Figure 17.

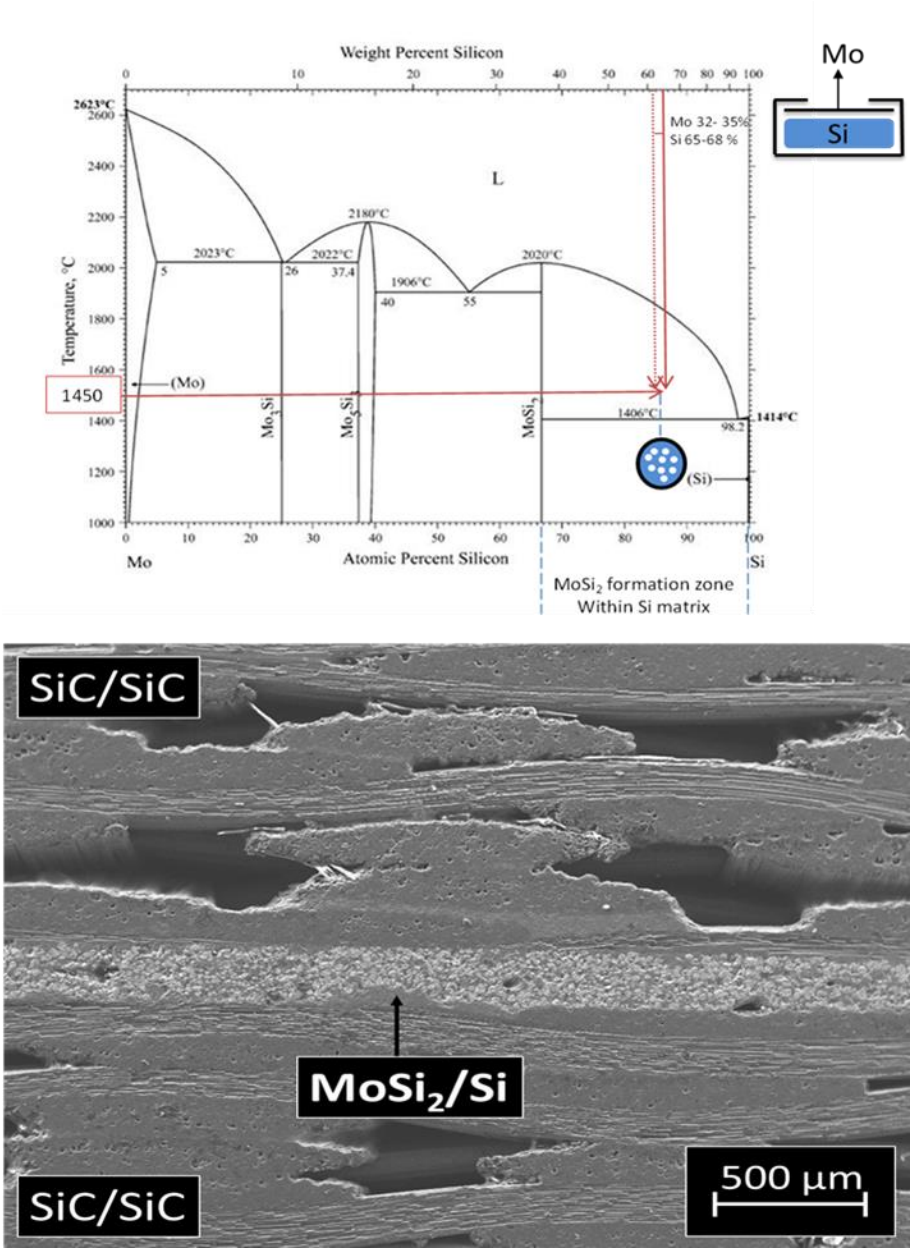


**Figure 15 Mo-Wrap (32-35 Mo %) and (65-68% Si) optimized conditions shown on Mo-Si binary phase diagram and SiC/SiC joint**

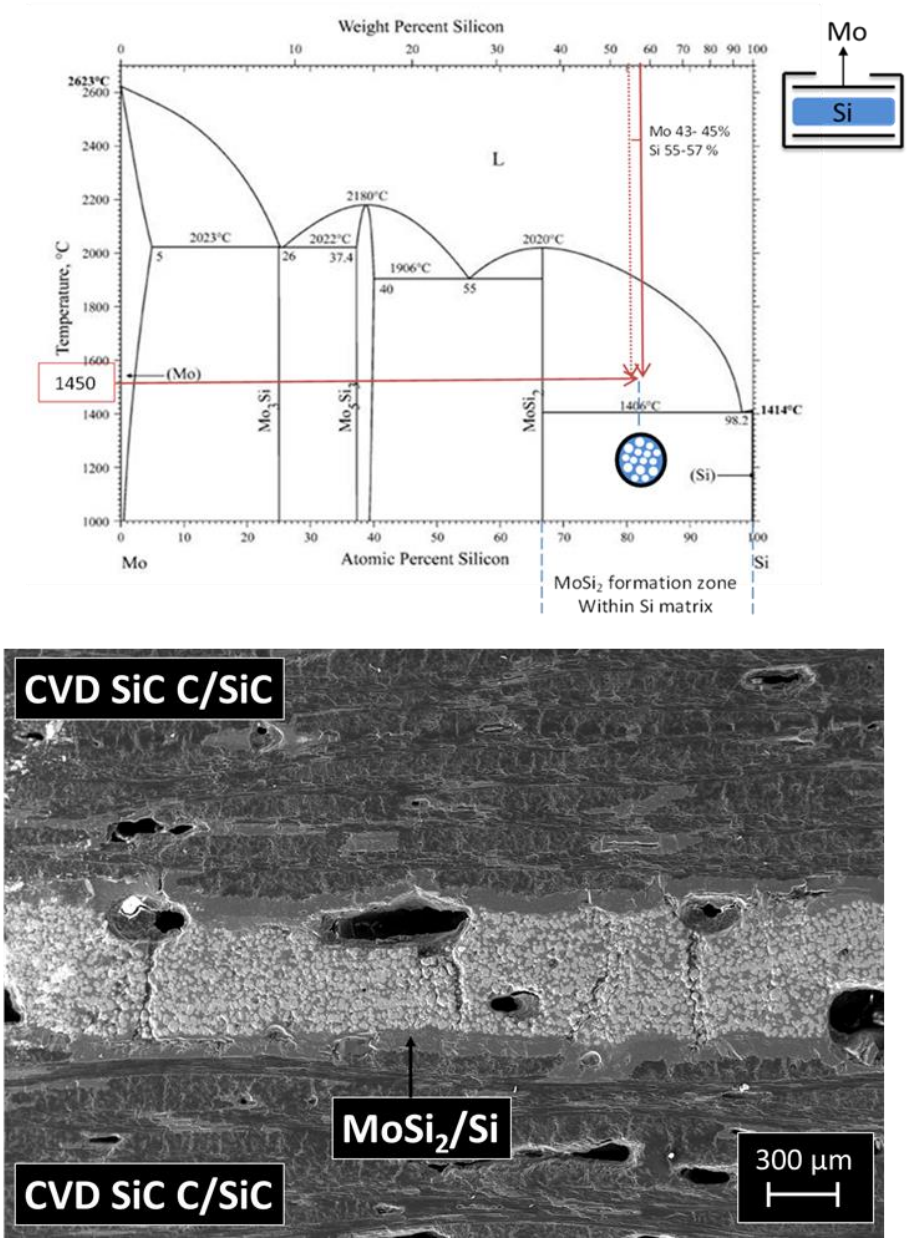


**Figure 16 Mo-Wrap (43-45 Mo %) and (55-57% Si) conditions shown on Mo-Si binary phase diagram and CVD SiC coated C/SiC joint.**

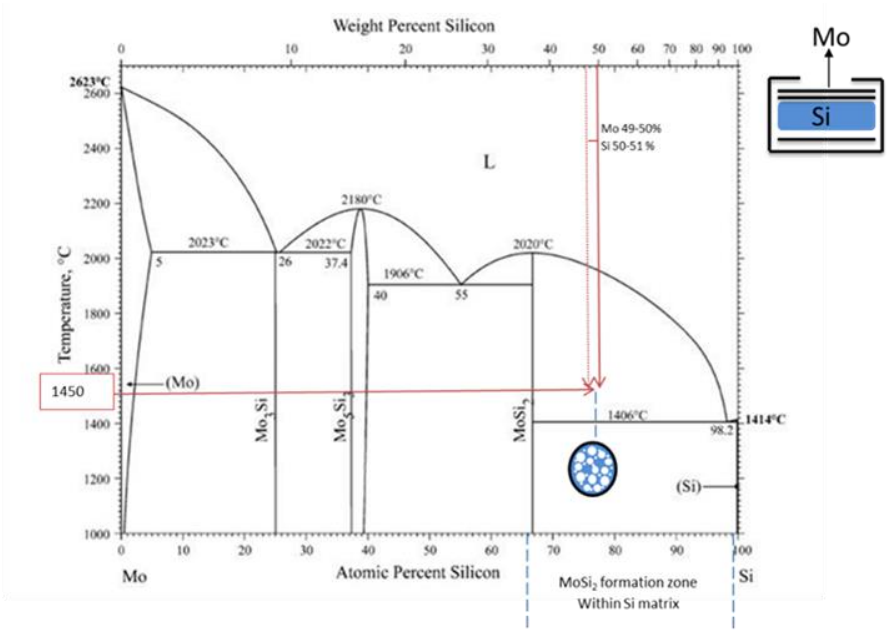


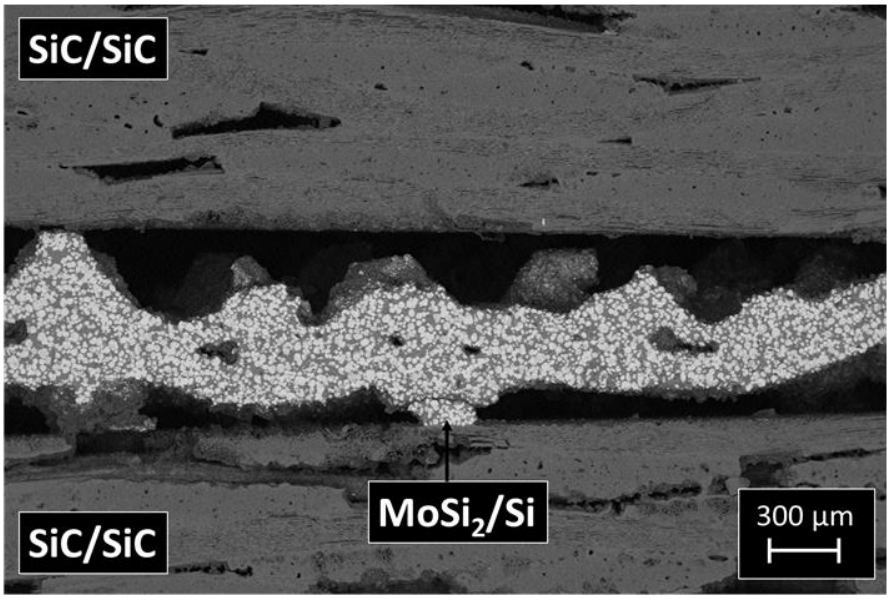


**Figure 17 Mo-Wrap (49-50 Mo %) and (50-51% Si) conditions shown on Mo-Si binary phase diagram and SiC/SiC joint**

Mo-wrap joining best results were obtained with (65-68 % Si) and (32-35 % Mo) composition.Increasing the amount of Mo (or RM) consume most of Si in formation of disilicides, results in low amount of Si (Liquids) and discontinous joints (Figure 17). Minimum (55 wt % of Si) is required in Mo-wrap within joint interface in order to wet the surface and obtained the continous crack free joints.

"Mo-Wrap" joining was then successfully used to join several ceramics (SiC, SiSiC (SiC obtained by LSI process), Mullite, Alumina, SiC foam), SiC based CMC (coated and uncoated C/SiC and SiC/SiC) [18, 133]. Moreover, and most importantly since are very porous substrates, SiC foams having porosity higher than 80 % were successfully joined by using the RM-Wrap technique. Each substrate's joining is discussed in detail in chapter 4.

Following the success of Mo-Wrap, its scope has been extended to the other refractory metals specifically Nb, Ta and W to form the suitable silicides. Nb and Ta are most versatile ones because of excellent room temperature ductility and relative ease of fabrication and corrosion resistance.

## 3.2 Nb-Wrap

Nb-Si based alloys are considered suitable candidates for high-temperature structural application in aircraft engines and rockets [134]. Niobium cannot be considered a light refractory metal having density 8.57 g/cm$^3$, but it is close to that of nickel superalloys and has good thermal conductivity. Nb-Si based silicides are frequently manufactured by two processing routes named ingot metallurgy (IM) and powder metallurgy (PM). Details of manufacturing routes are beyond the scope of this thesis, but can be found in [14, 135].

$NbSi_2$/Si composite joining material has been developed as a new joining material like the $MoSi_2$/Si one, by using the RM-wrap methodology.

The binary phase diagram of Si-Nb is similar to the Si-Mo one, where ($NbSi_2$, $Nb_5Si_3$ and $Nb_3Si$) compounds can be formed; X-Ray diffraction analysis (reported in chapter 4) confirms the presence of $NbSi_2$ and Si after Nb-wrap joints. Figure 18 shows the optimized Nb-Wrap conditions on Si-Nb binary phase diagram.

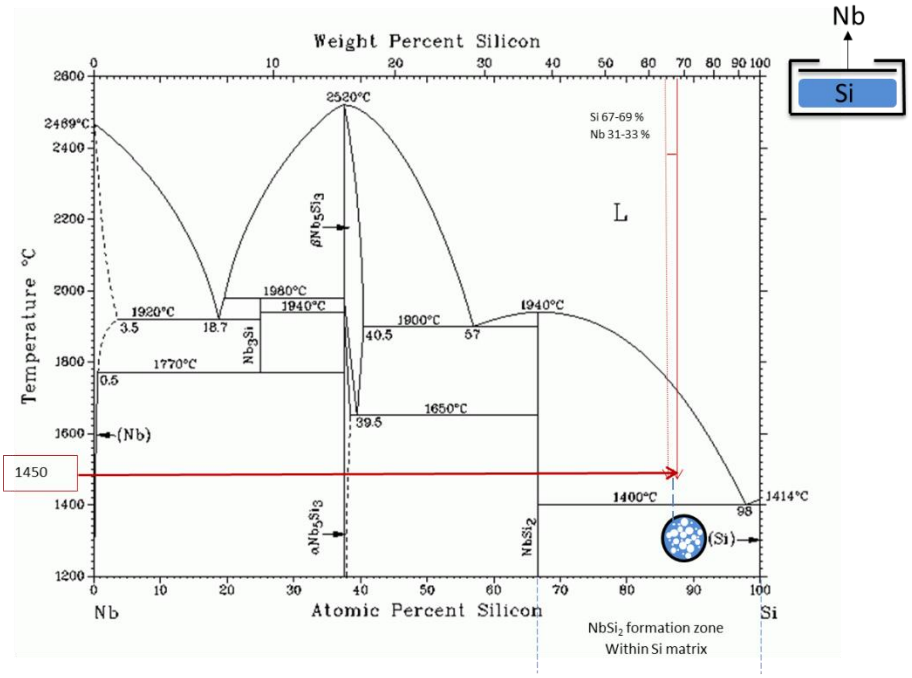


**Figure 18 Nb-wrap optimized conditions [136]**

Nb shows a good corrosion resistance except for hydrofluoric acid, concentrated hot sulfuric acid and hot alkaline solutions. Ta corrosion resistance is better than Nb, but still, Nb is better than nickel-based superalloys used in chemical industries. Presently 95% of total Nb annual production (1000 ton) is used in steel and nickel-based alloys for increasing strength [14]. Nb applications are limited due to its poor oxidation resistance over 250 $^{o}$C and rapid oxidation above 500 $^{o}$C. Nb can be alloyed to improve these shortcomings. Alloying Nb (with other metals) is potentially under research and development since the 1970s and is constantly under investigation for nuclear structural components of aircraft, space vehicles, rockets.

Several coating systems of $NbSi_2$ have been proposed to permit the use of Nb in oxidative environments [14, 137-139]. A recent study on Nb-Si system in [140, 141] by first principle studies finds out that shear modulus, Young's modulus and hardness of Nb-Si compounds increases with increasing Si concentration. Hardness and elastic properties are directly related with the presence of bonds among the formed compounds. Nb-Nb has a metallic bond while as the Si-Si have the strong covalent bonds, therefore, $NbSi_2$ exhibits the strongest shear resistance and highest hardness among the Nb-Si compounds ($Nb_5Si_3$ and $Nb_3Si$). $NbSi_2$ has a better oxidations resistance than $Nb_2Si_3$ [142].

## 3.3 Ta-Wrap

Tantalum has a unique combination of interesting properties having high melting point (3000 $^{o}$C), excellent ductility at room temperature, low ductile to brittle transition (DBT) temperature, reasonable modulus of elasticity and high density (16.69 g/cm$^3$). Due to high density, initial efforts were not successful to use the Ta in aerospace applications. It has been reported that only 2% of total production of Ta used in nuclear and defense industries, 22% in cutting tool applications and 66% in the electronics industry [14].

Binary Ta-Si phase diagram is shown in Figure 19: four phases can be formed, $TaSi_2$, $Ta_5Si_3$, $Ta_2Si$, and $Ta_3Si$. Also, $TaSi_2$, as other silicides previously mentioned, has low electrical resistivity, high oxidation stability due to $SiO_2$ layer formation on its surface [143]. Like Mo and Nb silicides synthesized by different powder processing techniques, Ta silicides can be synthesized by hot pressing, sintering, mechanical alloying, self-propagating high-temperature synthesis (SHS) [143, 144].

$TaSi_2$ has a great potential to be used in the high-temperature oxidative environment as a bulk and coating material. $TaSi_2$ thin films have been fabricated by various techniques such as sputtering (direct sputtering, co-sputtering, reactive sputtering), ion beam layer by layer deposition of Ta and Si, vacuum plasma spray etc. [145].

Figure 19 shows the optimized Ta-Wrap conditions on Si-Ta binary phase diagram. X-Ray diffraction analysis (reported in chapter 4) confirms the presence of $TaSi_2$ and Si in the Ta-wrap joints.

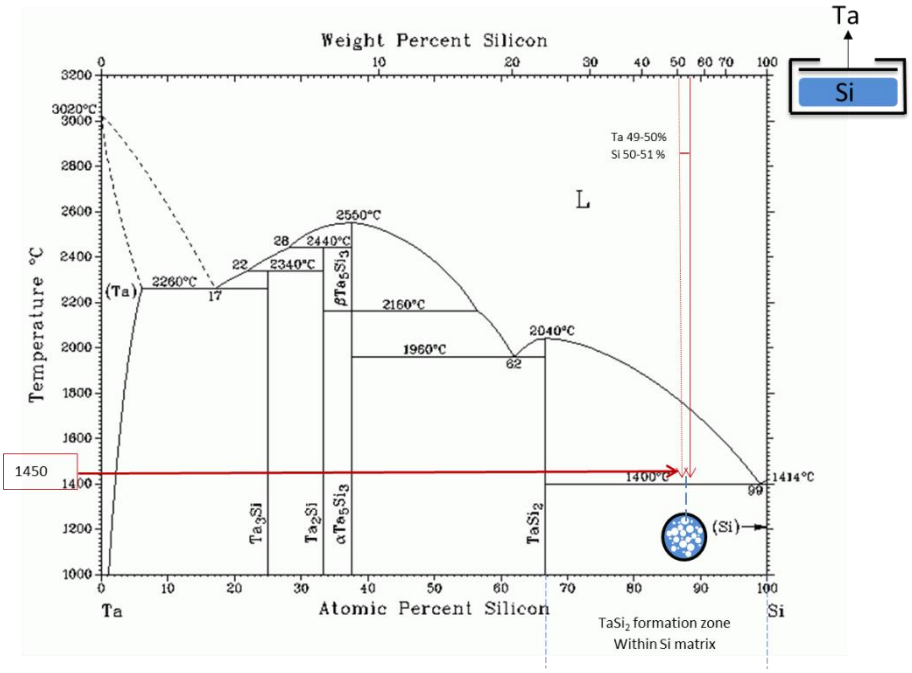


Figure 19 Ta-Wrap optimized conditions [146]

## 3.4 W-Wrap

As shown in the Si-W binary phase diagram, $WSi_2$ and $W_5Si_3$ are the two silicides formed [147]. The crystal structure, electronic structure and coefficient of thermal expansion of $WSi_2$ are similar to those of $MoSi_2$ [135]. $WSi_2$ has high melting temperature 2160 $^oC$ and good oxidation resistance (inferior to $MoSi_2$). Among the tungsten silicides, $WSi_2$ is more oxidation resistive than $W_5Si_3$, and oxidation kinetics is slow due to the formation of $SiO_2$ on its surface [148]. Like other refractory silicides, $WSi_2$ can be synthesized by mechanically alloying, field activation with pressure, reaction synthesis, combustion synthesis (CS) or self-propagating high-temperature synthesis (SHS) [149, 150]. $WSi_2$ has a high potential to be used in oxidative high-temperature applications.

W-Wrap method was adopted with tungsten (W) to form the $WSi_2$ phase along with silicon (Si) matrix. Figure 20 presents the optimized W-Wrap conditions on Si-W binary phase diagram. X-Ray diffraction analysis (reported in chapter 4) confirms the presence of $WSi_2$ and Si in the W-wrap joints.

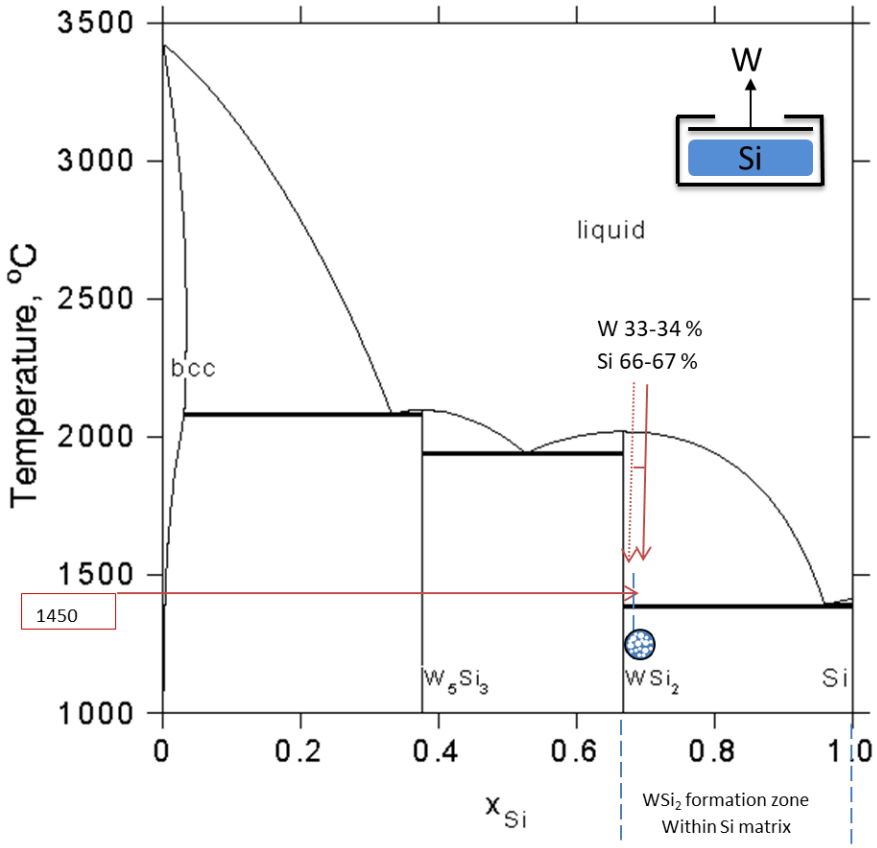


**Figure 20 W-Wrap optimized conditions (two-step) [147]**

The properties of silicides such as melting temperature, density and crystal structure of all four disilicides are given in Table 2

**Table 2 Properties of Silicides**

| Silicides | Melting Temperature °C | Density g/cm$^3$ | Crystal Structure |
|---|---|---|---|
| $MoSi_2$ | 2020 | 6.24 | Tetragonal |
| $NbSi_2$ | 1920 | 5.62 | Hexagonal |
| $TaSi_2$ | 2040 | 9.25 | Hexagonal |
| $WSi_2$ | 2160 | 9.86 | Tetragonal |

## 3.5 Combo-Wrap

Successful joining by RM-Wraps led to a combination of more than one Refractory Metal in the wrap joining technique, as shown in Figure 21 and named as "Combo-Wrap."

Tailorable joining materials are highly demanded: besides the tailoring capability of RM-Wraps, Combo-wrap has the more possibilities to develop/tailor the required phases from more than one element in a particular ratio.

Figure 21 shows the combination of Mo with W, Nb and Ta; however, more combinations are possible by changing the refractory metals. In this thesis, one possible combination of Mo with W wrap is reported and named MoW-Wrap.

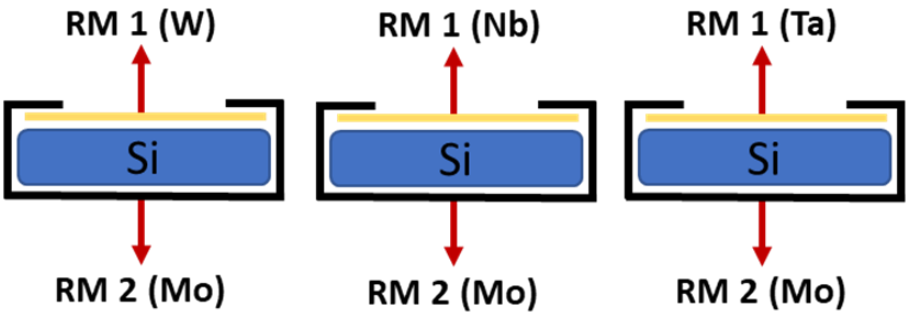


Figure 21 Typical Combo-Wrap Schemes (Mo with another RM)

### 3.5.1 MoW- Wrap

MoW-Wrap was developed as an example for the "Combo-wrap" technology. It is proven that alloying/compounding is a good method to overcome the shortcoming of a single compound [151]. As stated earlier, $MoSi_2$ is an attractive candidate for various high-temperature applications. However, it has intrinsic limitations such as low ductility at room temperature (below 1000 $^oC$), and poor creep at high temperature (above 1000 $^oC$) [152]. Therefore, MoW-Wrap is a challenging solution based on $MoSi_2$ and $WSi_2$ forming a joining material along with silicon as a matrix. The Si-Mo-W ternary system is shown in Figure 22 indicates the presence of $MoSi_2$, $WSi_2$ and Si; the joint interface and EDS analysis reported in chapter 4.

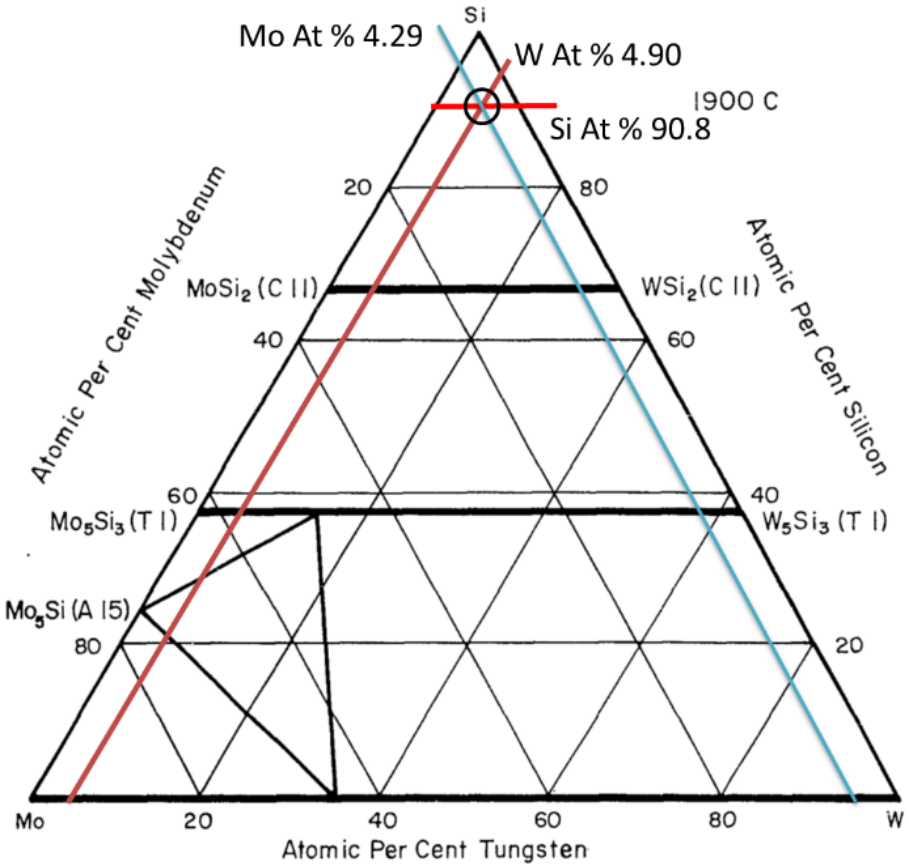


Figure 22 MoW-Wrap optimized conditions (two-step) [153]

## 3.6 Si-Coat as additional step for RM-Wraps

The best joining can only be achieved if the joining surfaces have good wettability to the joining material. The RM-Wrap technology is very flexible and can be used with various materials (ceramics, composites, foams) even with materials that have a poor wettability toward the final wrap material.

Silicon is a unique element which has the viscosity of water and can wet most of the materials used in high-temperature applications. The additional step of Si coating before RM-wrap joining is shown in Figure 23, and it was introduced for uncoated C/SiC; a Si foil of 80-100 µm was put on the C/SiC uncoated surface then heated at 1450 $^{o}$C for 2 minutes in Ar flow. Then, Mo, Nb, Ta, W and MoW-wraps were successfully used to join uncoated C/SiC.

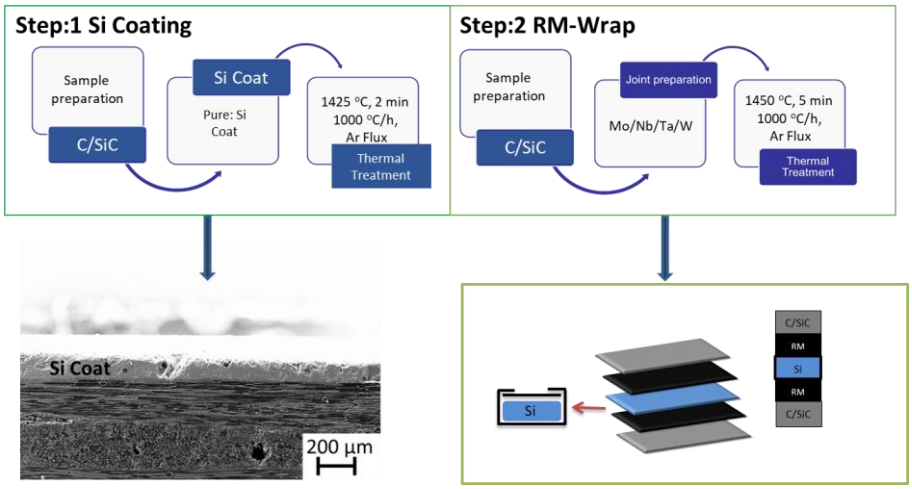


Figure 23 Two-step RM- Wrap for uncoated C/SiC

The optimized weight percentages of each element for the single and double (two) step process aresummarized in Table 3

Table 3 RM-Wrap weight % of each element used in joining (single and two step joining process)

| wrap | wt % | | | | Materials joined (Single Step) | Materials joined (Two steps) |
|---|---|---|---|---|---|---|
| | Single step | | Two steps | | | |
| | Si | RM | Si | RM | | |
| Mo | 65-68 | 32-35 | 79-80 | 20-21 | • CVD SiC coated C/SiC to themselves<br>• CVD SiC coated SiC/SiC to themselves<br>• SiC/SiC to themselves<br>• CVD SiC coated C/SiC- to SiSiC foam<br>• SiC to themselves<br>• SiC to Mullite<br>• Alumina to Alumina | • C/SiC to C/SiC<br>• SiSiC disc to SiSiC foam |
| Nb | 67-69 | 31-33 | 82-83 | 18-17 | SiC to SiC | C/SiC to C/SiC |
| Ta | 50-51 | 49-50 | 67-68 | 32-33 | SiC to SiC | C/SiC to C/SiC |
| W | - | - | 66-67 | 33-34 | - | C/SiC to C/SiC |
| MoW | - | - | Si 66 | Mo 11 / W 23 | - | C/SiC to C/SiC |
| In two step, Si coat is the first step, and the corresponding Wrap is the second one<br>Si coating of 100 microns; wt = 0.1772 g<br>RM = Refractory metal Wrap | | | | | | |

## 3.7 Chromium Silicides as Joining Materials

Chromium silicides are also potential candidates for the high-temperature oxidative environment. The Cr-Si compounds can form two oxide coatings, $Cr_2O_3$ and $SiO_2$ respectively at a low and high temperature, which protect from the oxygen diffusion [154-156]. Chromium is an active metal which can also improve the wettability of surfaces. A two-step joining process was adopted:

(i) coating of C/SiC surface with pure chromium

(ii) joining with silicon to form the chromium silicides.

A Cr slurry was prepared with ethanol as a fugitive binder and uniformly applied to the joining surfaces and thermally treated at 1330 $^oC$ in the presence of Ar for 10 min. The Cr reacts with Si, C and with some residual amount of oxygen from the furnace atmosphere. Two layers of Cr were developed (i) chromium oxide layer (greenish) top layer and (ii) Si/Cr/C reaction layer (silver) bottom layer, as shown in Figure 24.

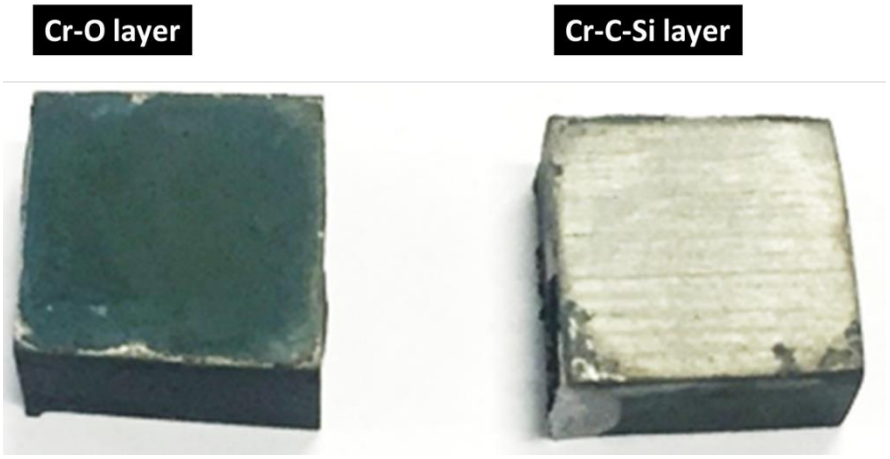


**Figure 24 Cr Coatings on C/SiC**

The brittle oxide layer can easily be removed and specimens can then be joined by a thin Si foil at 1450 $^oC$ in the presence of Ar flow, for 2 minutes.

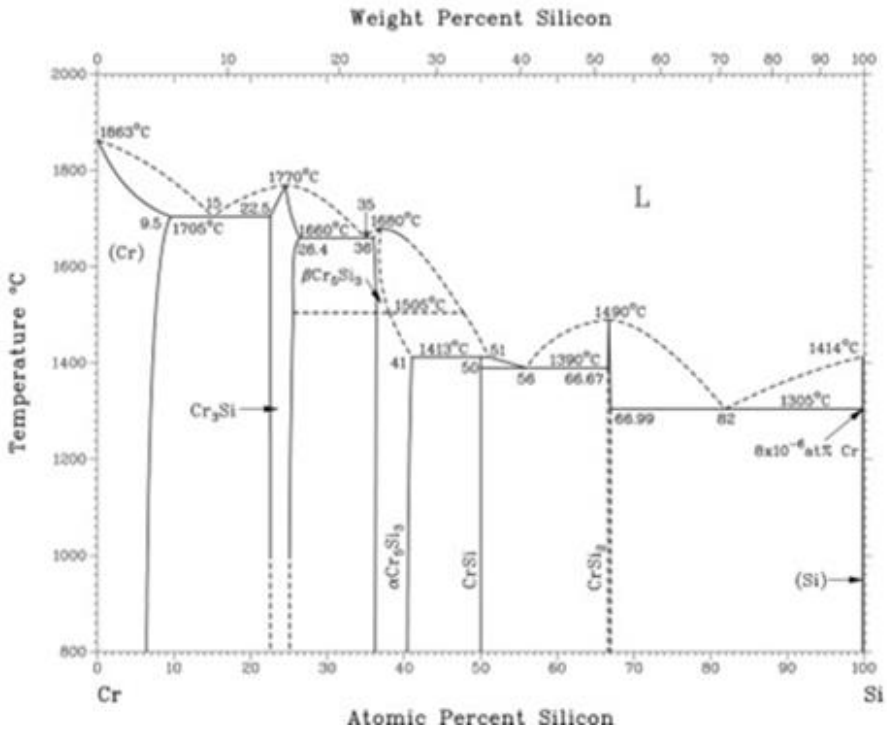


Figure 25 Cr–Si phase diagram [157]

Four chromium silicide compounds ($Cr_3Si$, $Cr_5Si_3$, CrSi, and $CrSi_2$) can possibly be formed, as shown in Cr-Si phase system (Figure 25). All these compounds have excellent oxidation resistance. Chromium silicide can also be synthesis by mechanical alloying and $CrSi_2$ is always the first phase formed if the Si is available in excess [158-160]. $CrSi_2$ is an attractive candidate for high-temperature applications [160]. A Si/Cr/C reaction layer of about 10 microns containing two phases ($Cr_3Si$ and $Cr_7C_3$) was developed. After joining with Si, a continuous uniform cracks free joint has been developed containing in-situ formed $CrSi_2$ phase within Si matrix. Detailed results analysis is given in chapter 4.

## 3.9 Materials joined in this thesis

### 3.9.1 Alumina ($Al_2O_3$)

Alumina is one of the most significant engineering material that has superior properties such as high thermal/electrical insulation, mechanical strength, wear resistance and chemical inertness [161]. Pure alumina has only one

thermodynamically stable phase named hexagonal α-phase, i.e. corundum. Since the last decade, a new family of toughened ceramics have been developed where alumina has been toughened with zirconium oxide and SiC whiskers to enhance the performance (strength and fracture toughness) of ceramics for new demanding applications [14]. Alumina is produced from bauxite rocks by using the Bayer's process. Alumina is largely used in refractory, abrasive and technical porcelain industries. Typical alumina applications are seal rings, medical prostheses, laser tubes, electronic substrates, ballistic armors, thermocouples, electrical insulators, grinding media, thread guides, wear components, high-temperature furnace tubes, and internal walls etc. [162]. Pure Alumina is stable in both oxidizing and reducing environment up to 1900 $^{o}$C against many gases and regents except wet fluorine and hydrofluoric acid [163]. Alumina density (3.95 g/cm3) is half of the steel-based materials, and hardness is three times higher i.e. 19 GPa than hard steel. Elastic modulus is around 390-400 GPa, twice than steel, and high-temperature stability brings the alumina in many hi-tech structural applications such as rocket nozzles, engine parts, heat resistance titles for space-shuttles, nuclear materials, storage, and renewal energy sources [57, 164]. Alumina is a low-cost material with great properties; its ceramic components are manufactured by slip casting, injection molding and pressing.

Properties of alumina used in thesis are reported in Table 4.

**Table 4 Properties of Alumina [163]**

| Mechanical | Unit | $Al_2O_3$ |
|---|---|---|
| Density | gm/cm$^3$ | 3.89 |
| Porosity | % (%) | 0 |
| Color | — | ivory |
| Flexural Strength | MPa | 379 |
| Elastic Modulus | GPa | 375 |
| Shear Modulus | GPa | 152 |
| Bulk Modulus | GPa | 228 |
| Poisson's Ratio | — | 0.22 |
| Compressive Strength | MPa | 2600 |
| Hardness | Kg/mm$^2$ | 1440 |
| Fracture Toughness $K_{IC}$ | MPa x m$^{1/2}$ | 4 |

| | | |
|---|---|---|
| Maximum Use Temperature (no load) | °C | 1750 |
| **Thermal** | | |
| Thermal Conductivity | W/m K | 35 |
| CTE | $10^{-6}$/°C | 8.4 |
| Specific Heat | J/Kg•°K (Btu/lb•°F) | 880 |
| **Electrical** | | |
| Dielectric Strength | ac-kv/mm (volts/mil) | 16.9 |
| Dielectric Constant | @ 1 MHz | 9.8 |
| Dissipation Factor | @ 1 kHz | 0.0002 |
| Loss Tangent | @ 1 kHz | — |
| Volume Resistivity | ohm•cm | $>10^{14}$ |

### 3.9.2 Mullite ($3Al_2O_3$ .$2SiO_2$)

Mullite is an alumina-silicate compound ($3Al_2O_3.2SiO_2$), extensively used in the traditional refractory applications. It is an only stable phase in alumina-silica system at atmospheric pressure. Mullite is usually synthesized rather than mined, very rarely found naturally except in the Scottish island named "mull" and mullite is named based on this island. It is one of the most promising ceramic material due to its environmental stability, chemical compatibility, low coefficient of thermal expansion (like silicon carbide SiC), good creep resistance and high compressive strength at elevated temperature. It has excellent thermal shock resistance and low thermal/electrical conductivity. In comparison with alumina, mullite has a density of 2.8 g/$cm^3$, and other mechanical properties lower than alumina such as hardness, Young's modulus, mechanical bending strength and toughness values as shown in Table 5. However, its CTE is low which improves the resistance to thermal shock and rapid change/drop in mechanical properties with change in temperature unlike alumina above 1200 $^oC$. Diffusion in mullite is very slow which maintains its mechanical properties, i.e. creep which is also problematic during its sintering [165]. Mullite synthesis route can be classified as (i) sinter-mullite (ii) fused-mullite and (iii) chemical-mullite.

**Table 5 Properties of Mullite [163]**

| Mechanical | Unit | $3Al_2O_3$ .$2SiO_2$ |
|---|---|---|
| Density | gm/cc (lb/$ft^3$) | 2.8 |
| Porosity | % | 0 |
| Colour | — | Off-white |

| | | |
|---|---|---|
| Flexural Strength | MPa | 180 |
| Elastic Modulus | GPa | 151 |
| Shear Modulus | GPa | - |
| Bulk Modulus | GPa | - |
| Poisson's Ratio | — | - |
| Compressive Strength | MPa ($lb/in^2x10^3$) | 1310 |
| Hardness | $Kg/mm^2$ | 1070 |
| Fracture Toughness $K_{IC}$ | $MPa•m^{1/2}$ | 2 |
| Maximum Use Temperature (no load) | °C | 1650 |
| **Thermal** | | |
| Thermal Conductivity | W/m°K | 6 |
| CTE | $10^{-6}$/°C | 5.4 |
| Specific Heat | J/Kg•°K (Btu/lb•°F) | - |
| **Electrical** | | |
| Dielectric Strength | ac-kv/mm (volts/mil) | 9.8 |
| Dielectric Constant | @ 1 MHz | 5.8 |
| Dissipation Factor | @ 1 kHz | 0.003 |
| Loss Tangent | @ 1 kHz | - |
| Volume Resistivity | ohm•cm | > $10^{13}$ |

### 3.9.3 Silicon Carbide (SiC)

Silicon carbide (SiC) behaves almost like a diamond as one of the lightest and hardest material [166]. SiC has excellent physical, chemical, and mechanical properties. It has high melting point, hardness, Young's modulus, low density, excellent corrosion, abrasion and oxidation resistance [167]. Due to these tremendous properties of SiC, it has been used in many advanced engineering applications in aerospace, nuclear and ballistic materials. SiC has the excellent thermal conductivity, low coefficient of thermal expansion and excellent resistance to acids. SiC properties do not change up to 1400 $^oC$, compared to metals, SiC provides economical solutions for long terms aggressive environment applications. Various techniques have been developed so far for producing this highly demanding material such as (i) Hot-pressing (ii) sintering (iii) reaction sintering (iv) chemical vapor depositing and the recent one is (v) spark plasma sintering [14, 167].

Some common properties of SiC are given in Table 6.

Table 6 Properties of SiC [163]

| Mechanical | Unit | SiC |
|---|---|---|
| Density | $gm/cm^3$ | 3.1 |
| Porosity | % | 0 |
| Color | — | Black |
| Flexural Strength | MPa | 550 |
| Elastic Modulus | GPa | 410 |
| Shear Modulus | GPa | - |
| Bulk Modulus | GPa | - |
| Poisson's Ratio | — | 0.14 |
| Compressive Strength | MPa | 3900 |
| Hardness | $Kg/mm^2$ | 2800 |
| Fracture Toughness $K_{IC}$ | $MPa•m^{1/2}$ | 4.6 |
| Maximum Use Temperature (no load) | °C | 1650 |
| **Thermal** | | |
| Thermal Conductivity | W/m°K | 120 |
| CTE | $10^{-6}$/°C | 4.0 |
| Specific Heat | J/Kg•°K (Btu/lb•°F) | 750 |
| **Electrical** | | |
| Dielectric Strength | ac-kv/mm (volts/mil) | - |
| Dielectric Constant | @ 1 MHz | - |
| Dissipation Factor | @ 1 kHz | - |
| Loss Tangent | @ 1 kHz | - |
| Volume Resistivity | ohm-cm | $10^2$-$10^6$ |

#### *3.9.3.1 SiSiC Discs*

The SiSiC disc obtained by LSI contains Si and SiC and were provided by EngiCer SA, Balerna, Switzerland; their properties are given in Table 7.

SiSiC has low density, high modulus of elasticity and high thermal conductivity with respect to alumina, zirconia and nickel superalloys. This kind of materials has a wide range of applications in energy production, such as in concentrated solar power plants as an absorber. Their industrial exploitation has been so far hindered

by limitations in the materials used both for the central receiver - the core component - and for thermal storage.

Table 7 Properties of SiSiC disc

| Materials | Unit | SiSiC Disc |
|---|---|---|
| **Composition** | % | SiC (70-90%)<br>Si (10-30%) |
| **Physical properties** | | |
| • Density | ($g/cm^3$) | 2.8-3.1 |
| • Porosity | (Vol.%) | 0 |
| • Gas permeability | (Vol.%) | 0 |
| • Water absorption | (Vol.%) | 0 |
| **Mechanical properties** | | |
| • Modulus of elasticity | (GPa) | 350-400 |
| • Compressive strength | (MPa) | 1250-3000 |
| • Poisson ratio | - | 0.17- 0.20 |
| • Fracture toughness | ($MPa.m^{1/2}$) | 3.0 - 5.0 |
| • Shear modulus | (GPa) | 150 |
| **Thermal Properties** | | |
| • Maximum temperature | | |
| ○ Air | (ºC) | 1400 |
| ○ Inert gas | (ºC) | 1400-1500 |
| • Melting point | (ºC) | 2797 |
| • Thermal conductivity (25 ºC) | (W/mK) | 110-140 |
| • CTE | (µm/mK) | 4.2-4.8 |

### *3.3.3.2 SiC foams*

Light-weight high-temperature stable structures are highly demanded in aerospace and energy applications [168]. In the past years, porous ceramics were widely used in various versatile applications such as filters (liquid/gas), support for catalysis, insulators, gas distributors, implantable for bones, preforms for ceramic metal composites and many more. Ceramic foams currently available are oxide based, alumina-based, carbon-based, zirconia-based and silicon carbide based. Their intrinsic properties restrict the use of each kind of foam. Alumina is durable, low

cost, chemically inert, high temperature stable but have low thermal conductivity and poor thermal shock resistance. Zirconia is an expensive, high temperature stable but limited in thermal conductivity and thermal shock resistance. Carbon-based forms have good thermomechanical properties but poor oxidation resistance at elevated temperature (i.e. 400-600 $^{o}$C) thus their use is limited to the oxygen-free environment. Service conditions are prime factors in their selection.

Perhaps silicon carbide foams are one of the most promising candidates suitable for many applications because of lightweight, higher melting temperature, good mechanical strength, high thermal conductivity, low coefficient of thermal expansion, excellent oxidation resistance, inertness and good thermal shock resistance [169-173]. Various processing routes have been developed so far to obtain SiC foams; detail is given in [172]. Nature has optimized the cellular structure (wood, bone, coral, etc.). Development of synthetic cellular structures is just a history of the last couple of decades and very recently scientists have successfully developed cellular structures from ceramic materials.

In this research activity, foam used is **3D SiSiC foams** provided by EngiCer SA, Balerna, Switzerland: it is an open cell porous ceramic structure produced by replica method [174-176]. Polyurethane foams were impregnated with a slurry made of silicon carbide powder (α-SiC), binder and solvent. Dried green bodies were pyrolyzed in argon above 1000 °C. Molten silicon (Si) was then infiltrated at 1550 $^{o}$C, 10-20 mbar pressure, to form the β-SiC through the reaction bonding between molten silicon and carbon derived from the polymer. Table 8 presents physical properties of foam; the details on these foams are given in [175]. In this thesis, 30Si is used referred to as *SiSiC foam* in the text, and joined with C/SiC or SiSiC disk.

**Table 8 Properties of Si-SiC 3D foam**

| **I.D** | Free Si (Wt %) | Density (g cm$^{-3}$) theoretical | Density (g cm$^{-3}$) Actual | micro porosity (%) | Total porosity (%) |
|---|---|---|---|---|---|
| **30Si** | **30** | **2.95** | **2.68 ± 0.05** | **9.2** | **88.20** |
| 22Si | 22 | 3.07 | 2.66 ± 0.07 | 13.3 | 88.73 |
| 12Si | 12 | 3.10 | 2.55 ± 0.06 | 17.7 | 89.30 |

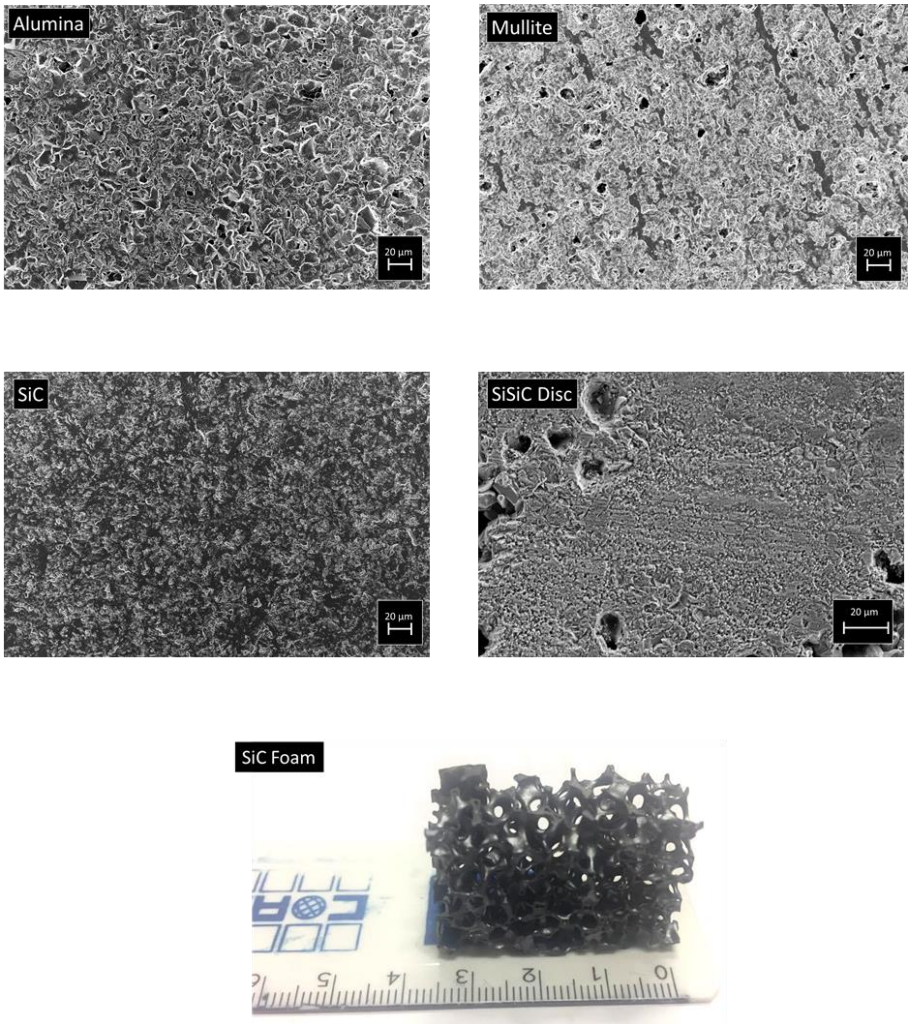


**Figure 26 Ceramics (Alumina, Mullite, SiC and SiSiC and SiC foam) used in this research activity**

## 3.9.4 Composites

Composite is a combination of more than one phase or materials (i) continuous phase is known as matrix and (ii) distributed phase is known as reinforcement. These materials have better characteristics than individual phase/ element/ components [177]. The reinforcement in composites can be of particles, whiskers, short fibers, continuous fibers and continuous sheets shown in Figure 27 [178]. The composites can further be classified into three different types based on matrix materials (i) Metal Matrix Composites (MMC) (ii) Polymer Matrix Composites

(PMC) and (iii) Ceramics Matrix Composites (CMC), as shown in Figure 28. CMC composites have been used in this study.


**Figure 27 Types of composite based on the form of reinforcement [178]**

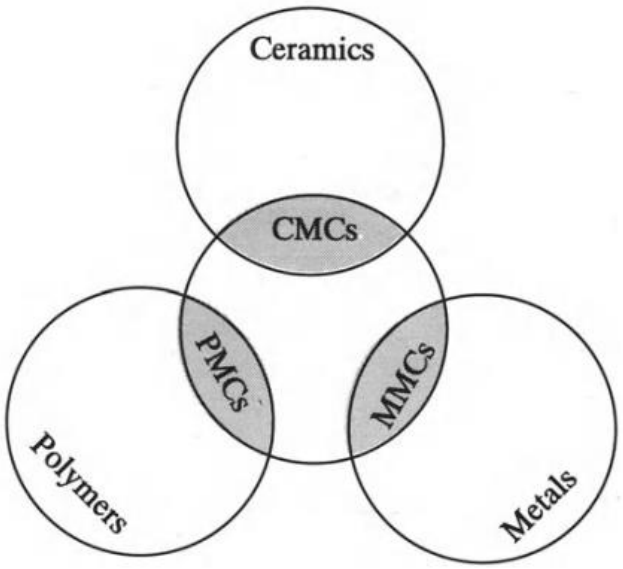


**Figure 28 Types of composite based on the matrix material [178]**

Ceramic matrix composites (CMC) are most often reinforced with textiles (fibers, yarns and fabrics sheets). Fiber reinforcement is aimed to achieve the crack resistance in composites. There are number of fibers available and used in different forms for matrix reinforcement. Among all the non-oxide continuous fibers (SiC and C) are most widely used. Oxide fibers have excellent oxidation resistance, but poor creep resistance, high density and high-temperature grain growth [178-180].

Textile structures are made of fibers which forms the yarns and woven structures. Yarn structure consists of thousands of fibers wrapped and twisted together. The woven structure is developed by two types of yarn direction (i.e. warp and weft) entangled at an angle with the specific arrangement. High-temperature

properties of CMCs are enhanced by the reinforcement of matrix with carbon and silicon carbide (fibers, yarn, and fabric sheets) [181, 182]. Textile reinforcement influences the mechanical behavior due to relative motion between fibers and yarn thus the resulting mechanical behavior is very specific. There are three scales in current use for textile substrates such as fibers (Microscopic, i.e. one to several micrometers), yarn (mesoscopic some millimeters) and fabric (macroscopic some centimeters to meters). Lot of research work is underway for simulating textile industry to work on fiber reinforced ceramic matrix composites.

CMCs have been developed to combine the properties of monolithic ceramics with better damage tolerance limit by fiber reinforcement. In CMC, the fracture behavior and other properties are dependent on reinforcing fiber, fiber/matrix reaction, interface and interphase formation during the in-situ reactions [1].

#### *3.4.4.1 Ceramic Matrix Composites (C/SiC & SiC/SiC)*

Superalloys have potential to be used up to 800 $^{o}$C and up to 1100 $^{o}$C with some protective coatings; beyond this temperature limit, use of ceramics is only the option. Ceramics low toughness, poor thermal shocks and catastrophic failure were the driving forces behind the development of ceramic matrix composites (CMC). The main disadvantage of ceramics is their brittleness which can be minimized in CMC with the help of ceramic textile reinforcement. [178, 179].

C/SiC is a modified carbon-carbon composite which has excellent properties but limited use at high-temperature oxidative environment (i.e. above 450 $^{o}$ C).

To improve the high-temperature oxidation stability and application lifetime, research has been extended to replace the carbon fiber with other ceramics fibers, particularly silicon carbide (SiC). SiC is well-known oxidation resistive, high temperature and thermal shock resistive material [14, 183].

Carbon fiber reinforced silicon carbide matrix composites need to be protected for high-temperature applications through thermal protective coatings (i.e. CVD SiC Coating). The scope and range of applications can significantly be increased by the use of oxidation resistive coating, modifying the matrix by adding some passivating elements to avoid the degradation in the oxidative environment or replacing the carbon fibers into silicon carbide ones [14].

Silicon carbide has no melting point and excellent thermo-erosive and oxidation resistance properties up to 2000 $^{o}$C which makes it an ideal candidate for high-performance applications such as rocket nozzles, brake discs, shuttle re-entry

components, high-temperature heat exchangers. Silicon carbide can be reinforced with continuous fibers (i.e. carbon and silicon carbide) to develop robust SiC-based composites. Fiber/matrix interfaces strongly influence their mechanical properties; therefore, high strength requires efficient load transfer ability fiber to the matrix and vice-versa. The primary function of the interface is to capture or deflect the microcracks, hence protecting it from premature failure and helps in transferring load when needed. Matrix microcracks at high temperature under oxidizing atmosphere facilities the diffusion of oxygen resulting in weak composites, therefore the interface has to be designed in a way to protect the oxygen diffusion at medium or high-temperature oxidative environment. Addition of boron like elements in the matrix (SiC) forms oxide phase (molten phases stable in the range of 500-1000 $^{o}$C and silicon rich phases stable in the range of 1000-1500 $^{o}$C) in a wide range of temperature which fills the cracks, hinders the oxygen diffusion and acts as self-healing materials. Proper design of interface reduces the cracks opening thus improves the composite stability at elevated temperature.

There are three commonly used process for the manufacturing of C/SiC and SiC/SiC composites listed below. Their detailed discussion is beyond the scope of this thesis work and can be found in [183].

**(i) Chemical vapor impregnation (CVD/CVI)**
**(ii) Polymer infiltration and pyrolysis (PIP)**
**(iii) Liquid silicon infiltration (LSI)**

In this thesis two different CMCs were used (i) manufactured via gradient chemical vapour infiltration (2D-fabric layers CVD SiC C/SiC and SiC/SiC) supplied by MT Aerospace (Germany) [184] and (ii) manufactured via polymer-infiltration-pyrolysis process (PIP), trade name SiCARBON$^{TM}$ supplied by Airbus Defense, and Space GmbH Germany [181]. The properties of composites used in this study are given in Table 9.

**Table 9 Properties of C/SiC and SiC/SiC**

| **Properties** | CVD SiC coated C/SiC | CVD SiC coated SiC/SiC and uncoated SiC/SiC | Uncoated C/SiC |
|---|---|---|---|
| Density (g/cm$^3$) | 1.7-2.2 | 2.3-2.4 | 1.8 |
| Tensile Strength (MPa) | 250-400 | - | 265 |
| Strain to failure (%) | 0.7 | 0.6 | |

| | | | |
|---|---|---|---|
| Compression Strength (MPa) | 300-500 | 300-500 | |
| Bending Strength (MPa) | 250-500 | 300-500 | |
| ILS (MPa) | 15-30 | 20-30 | 11-20 |
| Modulus (GPa) | 40-60 | 50-80 | 80 - 90 |
| Thermal expansion (1/K), parallel<br>Perpendicular | $2x10^{-6}$<br>$5x10^{-6}$ | $4x10^{-6}$<br>$4x10^{-6}$ | $2 \times 10^{-6}$<br>$5 \times 10^{-6}$ |
| Heat capacity (J/kgK) | 600-1600 (RT-1900K) | 670-1100 (RT-1300K) | 600 |
| Emittance (total hemispheric) | 0.8 | 0.8 | - |
| shear strength (kN)<br>tensile strength (kN) | 7.3<br>14.7 | - | - |

Figure 29 shows the cross-section and top surface view of CMCs used (i) CVD SiC Coated C/SiC, (ii) uncoated C/SiC, (iii) uncoated SiC/SiC and (iv) CVD SiC coated SiC/SiC.

C/SiC provided by Airbus Defence and Space GmbH Germany is less porous than the other three, as can be seen in Figure 29.

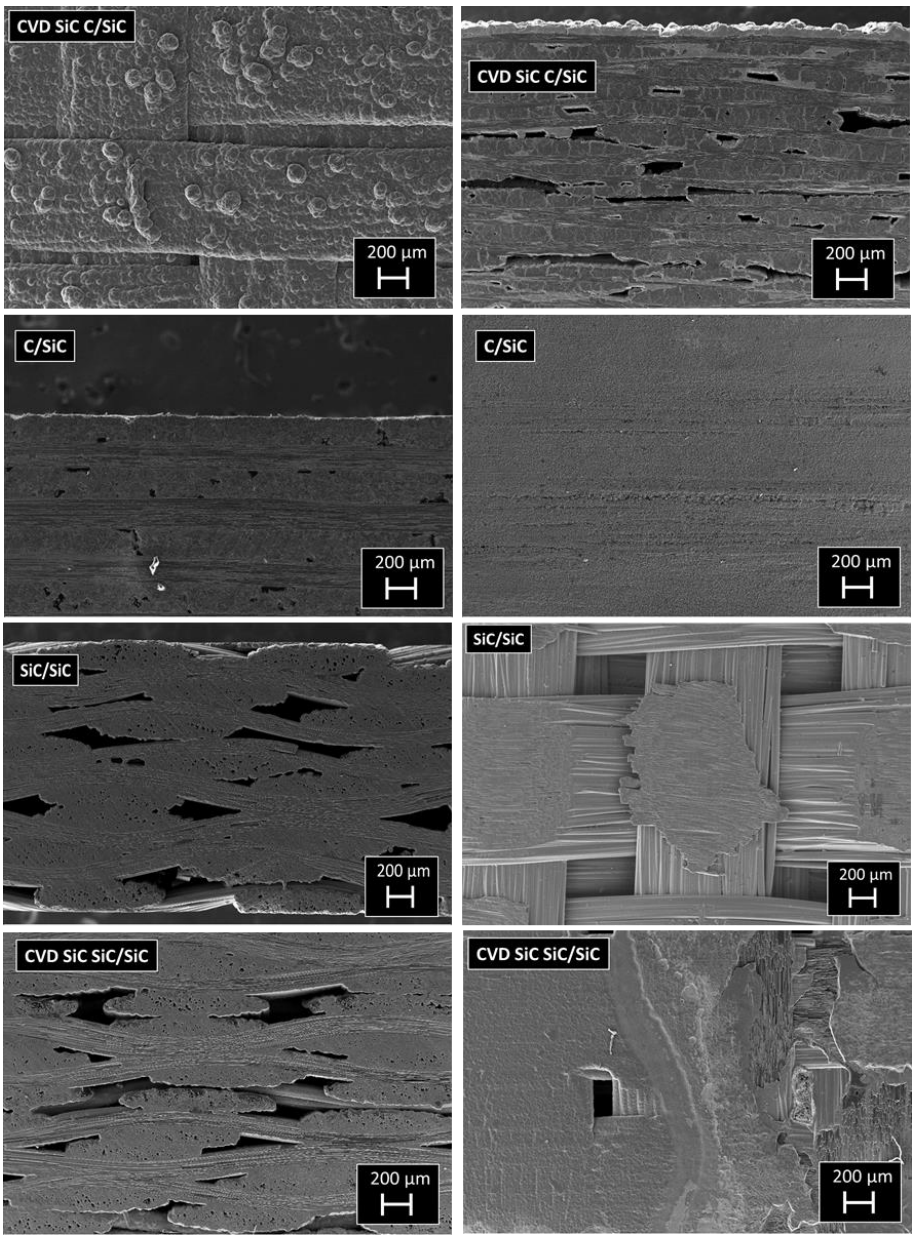


**Figure 29 SiC based CMC (C/SiC and SiC/SiC) used in this research activity**

## 3.9.5 Sandwich structures

Light-weight high-temperature stable structures are highly demanded in aerospace and energy applications. [168]. Ceramic sandwich structures offer weight reduction and high insulation potential: in particular ceramic foam/CMC sandwich structures are produced by joining two stiff/strong CMC skins with a porous ceramic foam

core [185, 186]. The core material has lower strength and low elastic modulus than skins but with a tailored porosity have exceptional properties which can be designed for a specific application not possible with conventional materials [174, 187]. The ideal structure can withstand high working temperatures, thermal shocks and mechanical loads.

Ceramic foams (i.e. SiC foams) have a great potential in high-temperature aerospace and energy applications as core materials for sandwich structures.

There is a strong need to develop the stable sandwich structures made of ceramics due to their high temperature stability, which is limiting factor (i.e., softening above 800-1000 $^{o}$C) in case of metallic structural components.

Fully ceramic made structures are very stable in many harsh applications, i.e., heat exchanger reactors offer excellent corrosion resistance and thermal conductivity [170, 188, 189].

The ideal joining materials/technique able to give a sound joint without the leakage of liquid phase outside the joining region and subsequent infiltration into the porous structure.

In literature, very few materials/techniques are reported to join cellular structures to CMC skins: Ortona et al. exploited the composite manufacturing technique i.e. Si infiltration to developed the sandwich structures for high-temperature heat exchangers where a higher amount of free Si causes many problems while in service. [190].

Two commercial adhesives (669 GrapibondTM and CeramabondTM) used in the development of a hybrid thermal protective system for aerospace by joining ablative (55-80 % Carbon fiber + 20-45% phenolic resin) to Ceramic (C/SiC) with increasing temperature decrease in shear strength has been observed [191].

A viscous, thick bonding layer of 30% + 30% thin and thick SiC powder in combination with 40% of Ceraset was used to develop the SiC foam sandwich structure joined to SiC fabric laminates [185]. A slurry of two different particle size (1-3 and 8-10 um) of SiC powder along with xylene solution was used to join the SiC foam with C/SiC composites, $SiO_2$ powder is used as a filler to fill in the SiC foam pores and used for insulation purpose [192].

NASA [193] manufactured a sandwich of C-SiC/SiC skins joined to SiC core, obtained by integral densification of the ceramic composite and the SiC foam; in this case, no joining process was required. The process of joining skin to foam by

*in situ* joining with additional densification via impregnation and pyrolysis allows the assembly of sandwich structures in any shape, but on the other hand, requires autoclave treatment and repetition of densification processes [185].

High-temperature brazing, high-temperature adhesives, joining processes based on preceramic polymers filled (or not) with ceramic particles [187, 194] need high temperature and in some cases the use of high pressure is required which can damage the SiC foam; to avoid and prevent the collapse of SiC foam lattice a pressure less joining is strongly needed.

Compared to oxides foams, SiC has a lower coefficient of thermal expansion, higher thermal conductivity, and good thermal shock resistance [185, 186].

The main problem encountered in the joining of the foams is infiltration of joining materials inside the highly porous core, thus causing blockage, discontinuous weak joints, inefficient insulation and low heat/energy recovery etc. SiC foams are used as core materials and are potentially suitable for applications between 1300 -1400 °C, with an excellent lifetime in combustion environment (e.g. burners).

These features make advanced sandwich structures suitable for several applications (industrial, space and energy) involves thermal loads, high temperature, harsh environment, heat exchangers, radiations (solar) burners, catalyst supports [195]. Specifically, it is the solution for leading-edge structures, controlled surfaces for thermal protection systems, in space vehicles high-temperature lightweight structures for space shuttles and many more. Space vehicles face a very aggressive aerodynamic heating due to the frictional effect of atmospheric gases, resulting in thermo-chemical reaction on the surface. Thus, sandwich structures are most widely used as thermal protection systems where the core acts as an insulator to keep internal temperatures under controlled conditions, and in energy applications where the core is used as a heat exchanger.

## 3.10 Characterizations Techniques

### 3.10.1 Morphology and Elemental Composition (FESEM, EDS)

The joint interphases and interfaces were investigated in cross-section using field emission scanning electron microscope (FESEM) by QUANTA INSPECT 200, Zeiss SUPRATM 40™. To analyze the specimen, FESEM uses a focused beam of an electron to scan across a specimen to produce an image. The analysis was made with two different detectors name secondary (SE) and backscattering (AB). The semi-quantitative elemental analysis was performed using Energy Dispersive Spectroscopy, (EDS, EDAX PV 9900™). Line scanning across the joint and elemental mapping for specific specimens were also done by using FESEM/EDS.

### 3.10.2 Computer tomography scan (CT-Scan)

CT-Scan X-ray Computer Tomography (CT) [196] is a non-destructive 3D inspection of internal/external geometry. Sandwich structure (C/SiC-SiCfoam-C/SiC) joined with Mo-Wrap was investigated at Nikon metrology X-Ray center of excellence UK. CT scan was performed with a beam energy of 210kV, current 130 up (27W), exposure of 500 ms, projection 3141 (1 frame per). The purpose of CT-Scan was to investigate void/discontinuity if present at joint interface, i.e. C/SiC-MoSi2/Si-SiC foam.

### 3.10.3 X-Ray Diffraction (Phase detection)

X-Ray diffraction (XRD) is an analytical method to identify the crystal structure of single and polymorphs materials. Typically, a diffractogram records the diffraction pattern by measure the intensity against the diffraction angle (Bragg's angle); generates intensity vs. diffraction plot. Obtained XRD patterns, can be analyzed to classify the crystalline structure and phase(s) of single or hetero-material, in relation with the database given by Joint Committee on Powder Diffraction Standards (JCPDS); using analyzing the patterns in programmed software with JCPDS database.

The joints fractured surfaces were analyzed for the identification of phases by using an X'Pert Phillips diffractometer, with Cu Kα radiation, under the following conditions: $2\theta = 10°-100°$, the XRD spectra were analyzed by using X'Pert High Score Plus software.

## 3.10.4 Mechanical Test

### *3.10.4.1 Single Lap Shear (SL)*

Single lap shear in compression loading according to (ASTM D1002-05) were performed on average of five joined samples. Commercial Scotch-Weld DP490 epoxy adhesive was used to attach the specimens to aluminum fixtures and cured for 45 min at 90 °C. Specimen size is 10 x 10 x (3 to 5) $mm^3$; geometry is shown Figure 30.

Single lap (SL) shear test in compression load was performed on SiC-Mo-wrap-SiC joints. It is worth mentioning here that SiC-Mo-Wrap-SiC joint did not break but the specimen detached from the aluminium fixtures; it was not possible to measure the joint strength by SL as the joints are stronger than that between the fixtures and Scotch-Weld DP490 epoxy adhesive.

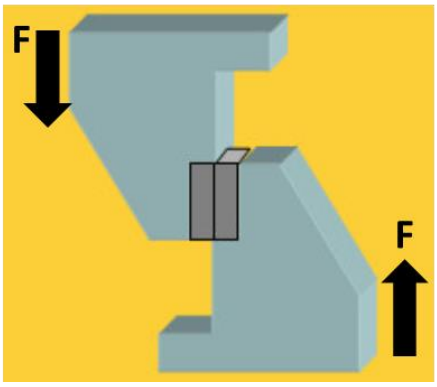


**Figure 30 single lap shear specimen geometry**

### *3.10.4.2 Single lap off-set (SLO)*

Single lap off-set ASTM-D905-03 was adapted to measure the joint strength of SiC joined by Mo-Wrap, the SLO specimen and test fixtures are shown in Figure 31. Specimen size is of 5 x 10 x (3 x 5) $mm^3$.

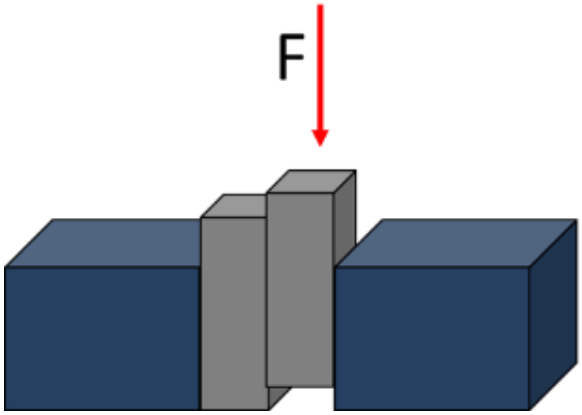


Figure 31 single lap off-set specimen geometry

### *3.10.4.3 High-Temperature Mechanical Testing*

Single lap shear test was inappropriate for measuring the joint strength of CMCs (uncoated SiC/SiC, CVD SiC coated SiC/SiC and CVD SiC coated C/SiC) joined by Mo-Wrap, as reported in [18], due to joint strength higher than the interlaminar shear strength of composites. Uncoated C/SiC joined in two steps (with an additional step of Si coat as discussed in section 3.6) were joined with Mo, Nb and Ta-wraps. C/SiC-RM-Wrap-C/SiC joints were prepared to measure the mechanical- and thermo-mechanical properties of joint by a single lap offset, at room temperature and 1000 $^{o}$C. Test system with vacuum and/or inert gas atmosphere chamber (Zwick/Roell-Messphysic-Maytec, at Inst. of Physics of Materials - Brno, Czech Republic) was used. During the test, a pre-load of 20 N and a test speed of 50 µm/min was applied. The specimen size and geometry is shown in Figure 32.

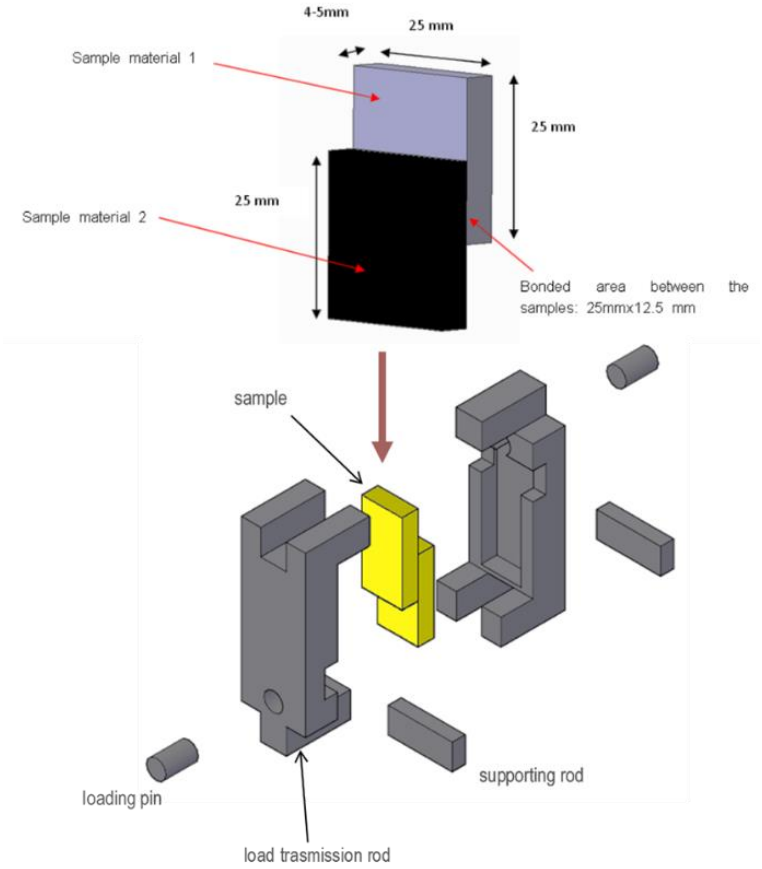


**Figure 32 Single lap-off set RT and HT testing at Inst. of Physics of Materials –Brno, Czech Republic**

### *3.10.4.4 Torsion*

To evaluate the pure shear strength of Mo-Wrap joined SiC, a torsion test was adopted. Small SiC hourglass shaped samples shown in Figure 33 with a circular joined area of 4 and 5 mm in diameter, were joined to find the actual/pure joint shear strength. Torsion test has a great potential to measure shear properties of the joint interface. Pure shear strength values are only considered when the failure is seen inside the joining material. If this is not the case then either the testing method is improper, or the substrate's and joint strength are similar. Both cohesive/adhesive failures can be observed.

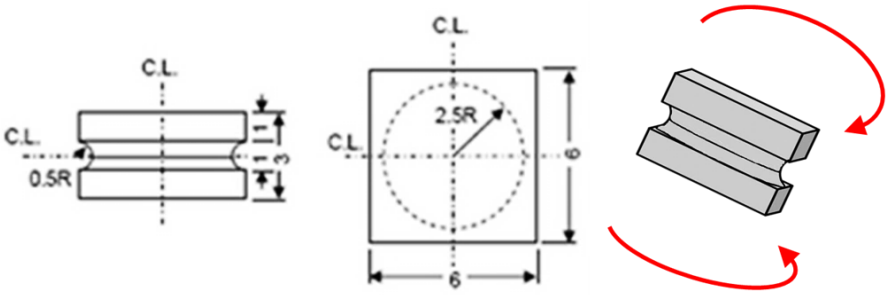


Figure 33 Torsion hourglass (THG)

The custom-made torsional testing machine developed at Politecnico di Torino is shown in Figure 34, and has potential to test different shapes of joints in torsion. Further details are described in [197-199], in this work only torsion hourglass of two different sizes (4 and 5 mm in diameter) were joined, named THG-4 and THG-5.

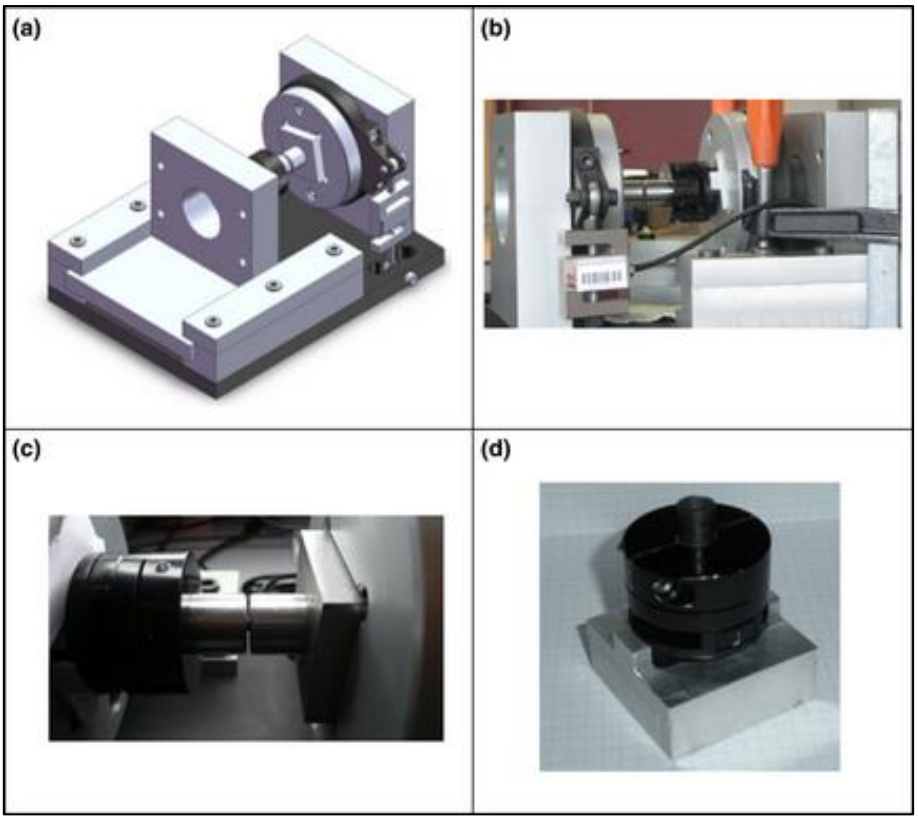


**Figure 34 Torsion machine set up: general view (a, b) and the sample holder (c, d): Oldham device (d) used to clamp the samples [197]**

### *3.10.4.5 Sandwich structures (Compression, Tensile)*

The sandwiches and as received SiC foams were tested in compression at room temperature with a crosshead displacement rate of 1 mm/min using a universal mechanical testing machine (SINTEC D/10) equipped with a 5kN load cell. Compression resistance test on specimen size of 25 x 12 x 17 $mm^3$ was performed in triplicate.

Tensile tests were done at room temperature on (i) sandwiches of size 10 x 10 x 25 $mm^3$, (ii) bare SiC foam as received (iii) SiC foam thermally treated at joining conditions (i.e. 1450 $^oC$ for 5 min with heating rate of 1000 $^oC$/hour and (iv) SiC form thermally shocked at 1100 $^oC$ for 2 min directly from room temperature and vice-versa. The tensile tests were performed on an electromechanical Universal Testing Machine (MTS Criterion model 43) having load cell capacity of 50 kN with a crosshead displacement of 1 mm/min, in triplicate. Commercial Scotch-Weld

DP490 epoxy adhesive was used to attach the sandwiches to the aluminum fixtures and cured for 45 min at 90 °C.

#### *3.10.4.6 Hardness Measurements*

Hardness, fracture toughness and elastic modulus can be determined by indentation [200]. It is based on an indenter of hard materials (e.g. diamond) to measure the resistance of surfaces to the penetration; depth and dimensions of the dent (imprint) are measured to obtain the hardness resistance.

Several methods are available since many years, such as Rockwell-, Vickers-, Knoop-Hardness, the last two mainly used for micro-hardness measurement; a more recent one, defined as nanoindentation, will be used in this thesis.

##### 3.10.4.6.1 Nanoindentation

Nanoindentation was carried out using Berkovich tip on Agilent G200 nanoindenter at room temperature. Continuous stiffness measurement (CSM) mode with a maximum penetration up to 1600 nanometers. The test was conducted at the Institute of Materials Research, Slovak Academy of Sciences.

##### 3.10.4.6.2 Micro-Indentation

Vickers Hardness test (ASTM E92-72) was adopted to measure the micro-hardness of silicides ($MoSi_2$, $NbSi_2$, and $TaSi_2$) with a load of 25 g for a dwell of 30 seconds. The indenter is a diamond pyramid with a square base and angle of 136°. The hardness was calculated by measuring the imprint area and by using the following equation:

$$HV = \frac{1.864 * P}{L^2}$$

**Equation 2 Vickers hardness measurement equation**

Where HV is Vickers hardness, P is applied load and L is the length of indentation across long axis.

### 3.10.5 Oxidation Resistance

The oxidation resistance of joined samples such as (i) SiC-based CMC joined by Mo-Wrap (ii) monolithic SiC joined by Mo-, Nb- and Ta-wraps were tested at up to 1100 $^{o}$C in the air.

The thermal treatment is close to possible working conditions for SiC-based CMC and was carried out in order to check the oxidation resistance and thermal stability of their joints at 1077 $^{o}$C for 30 minutes in the air.

Monolithic SiC joints were tested at 1100 $^{o}$C for 6 hours in the air, using FESEM prior and post thermal treatment for the examination of joint morphology.

### 3.10.6 Thermal Shock

Intense research is underway by the space agencies on the development of reusable launch systems/vehicles (RLS/V). The sudden change in temperature (thermal shock) while RLS/V is entering and existing the earth atmosphere develops high thermal stresses fails in the system.

Thermal shock tests were performed on the sandwich structures to evaluate the thermomechanical properties of in-situ formed joining material (i.e. $MoSi_2$/Si). The test is performed according to [201] on one sandwich with three cycles consisting in quickly transferring the sample from room temperature to a furnace at 1100 $^{o}$C in the air, keeping it for two minutes inside, then extracting it and letting it cool in air. Dual laser infra-red thermometer was used to measure the specimen temperature rise within two minutes of dwell inside the furnace. The measured parameters are furnace temperature, specimen temperature at the instant of removal from the furnace.

# Chapter 4

# Results and Discussion

This chapter presents the results on all joints prepared within this Thesis. The results are grouped separately for each joining technique accompanied by a discussion.

The joints obtained by RM-Wrap joining technology are summarized in Figure 35.

The results presented in this chapter have been published in two peer reviewed International Journals [18, 133], one oral presentation and seven poster presentations in international conferences.

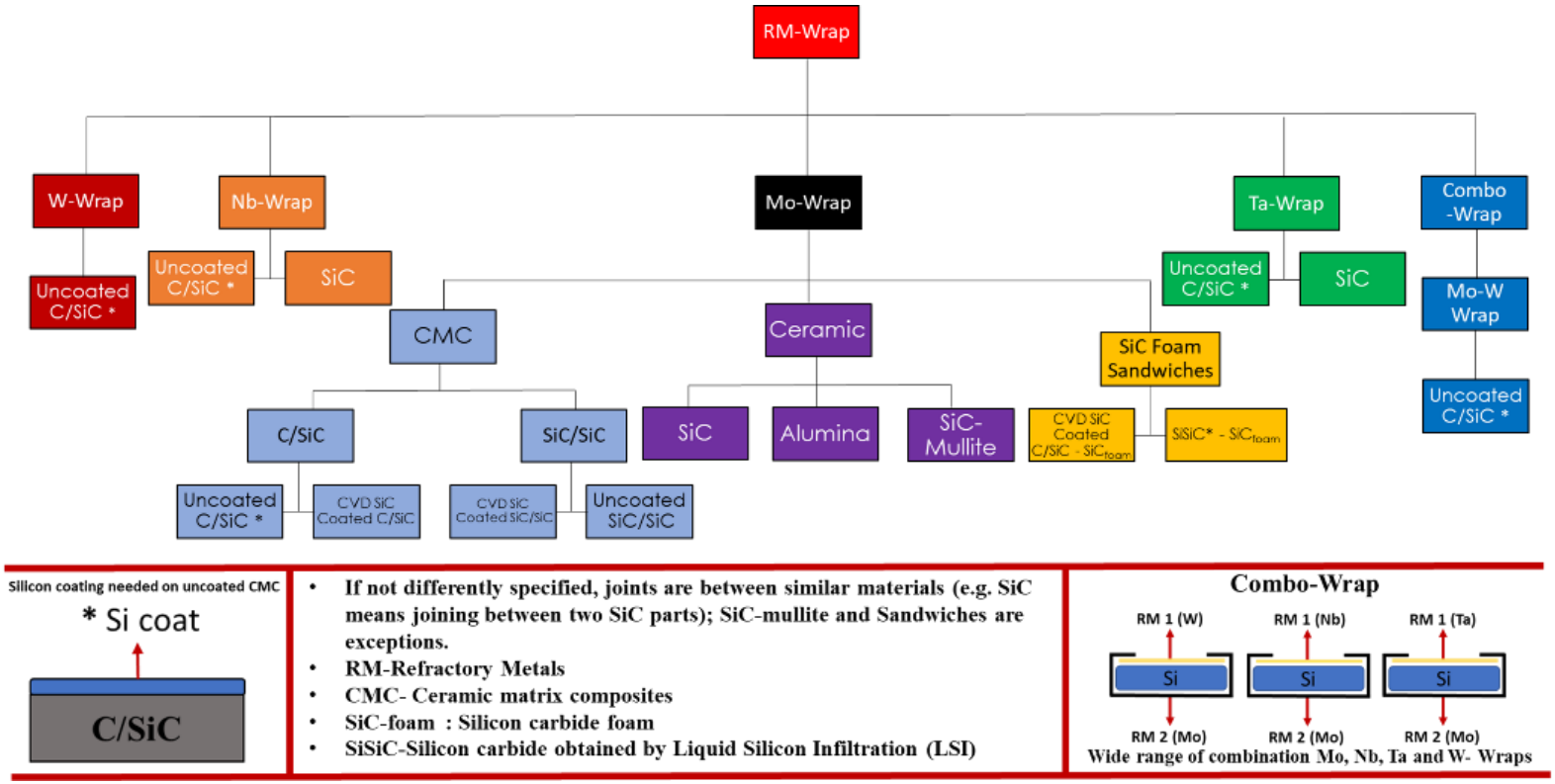


Figure 35 Joints obtained by RM-Wrap joining technique

# 4 Mo-Wrap

## 4.1 Joined CMCs

Mo-Wrap was successfully used to join the following CMCs pairs:

(i) **uncoated SiC/SiC joined to uncoated SiC/SiC**
(ii) **CVD SiC coated SiC/SiC joined to CVD SiC coated SiC/SiC**
(iii) **CVD SiC Coated C/SiC joined to CVD SiC coated C/SiC**

### 4.1.1 Uncoated SiC/SiC, CVD SiC coated SiC/SiC and CVD SiC coated C/SiC: Joints Morphology, Elemental and Phase Analysis (SEM, EDS and XRD)

**Uncoated SiC/SiC joined to uncoated SiC/SiC by Mo-Wrap:** the joint microstructure is shown in Figure 36. Continuous joint interface with the uncoated SiC/SiC composite is achieved without any joining material infiltration, with a final joint thickness of 220-250 µm. Joints are well bonded, without discontinuity, crack-free interface irrespective of the fibre orientation. $MoSi_2$ particles are uniformly dispersed across the whole cross-section. Round bright particles are $MoSi_2$ well embedded in the silicon matrix as shown in Figure 37.

Three phases ($Mo_3Si$, $Mo_5Si_3$ and $MoSi_2$) can possibly be formed according to Si-Mo binary phase diagram [113]. EDS confirms the elemental presence of Mo and Si while as XRD on fractured surfaces confirms the presence of two phases only: $MoSi_2$ and Si (Figure 37). No residual Molybdenum was detected, only $MoSi_2$ which is the most desirable phase due to its superior properties such as oxidation resistance and high melting temperature, i.e. 2020 $^oC$.

Silicon melting temperature is lower than Mo and its diffusion is faster in Mo than in C, thus only silicides are formed in the case of Mo-Wrap joining [202].

Mo-Wrap joined **CVD SiC coated SiC/SiC** morphology is shown in Figure 36: also, this joint is continuous and well bonded to the CVD SiC coated surfaces. Joint thickness in case of CVD SiC coated SiC/SiC is in range of 250-300 µm, a little

higher than for uncoated SiC/SiC joints. Mo-Wrap works very well with **CVD SiC coated C/SiC** composites too: continuous well-bonded cracks free joints were obtained, as shown in Figure 36 at low and higher magnification having thickness of 250-300 µm.

Figure 36 shows the microstructure of joints obtained by Mo-Wrap (i) uncoated SiC/SiC (ii) CVD SiC coated SiC/SiC and (iii) CVD SiC coated C/SiC Composites. All the three joints are well bonded, continuous, crack-free and exhibited a good continuity between joining material and composites surfaces (coated or uncoated) irrespective of the fibre orientation.

"Mo-Wrap" joining has a great potential to be used with various substrates including other CMC and monolithic ceramic materials. The formation of $MoSi_2$/Si (a composite joining material) has an excellent reproducibility.

The presence of $MoSi_2$/Si is likely to increase the toughness and creep behaviour of silicon at 1000 $^oC$.

The wrap is a tailorable joining technique where the percentage of each component ($MoSi_2$ or Si) can be tailored according to end-user requirements.

As an example, the volume % of silicides can be enhanced to improve the oxidation resistance, creep resistance and further extend the working temperature limit, as $MoSi_2$/Si is less prone to cracks than pure Si. $MoSi_2$ as reinforcing phase has the potential to deflect the cracks.

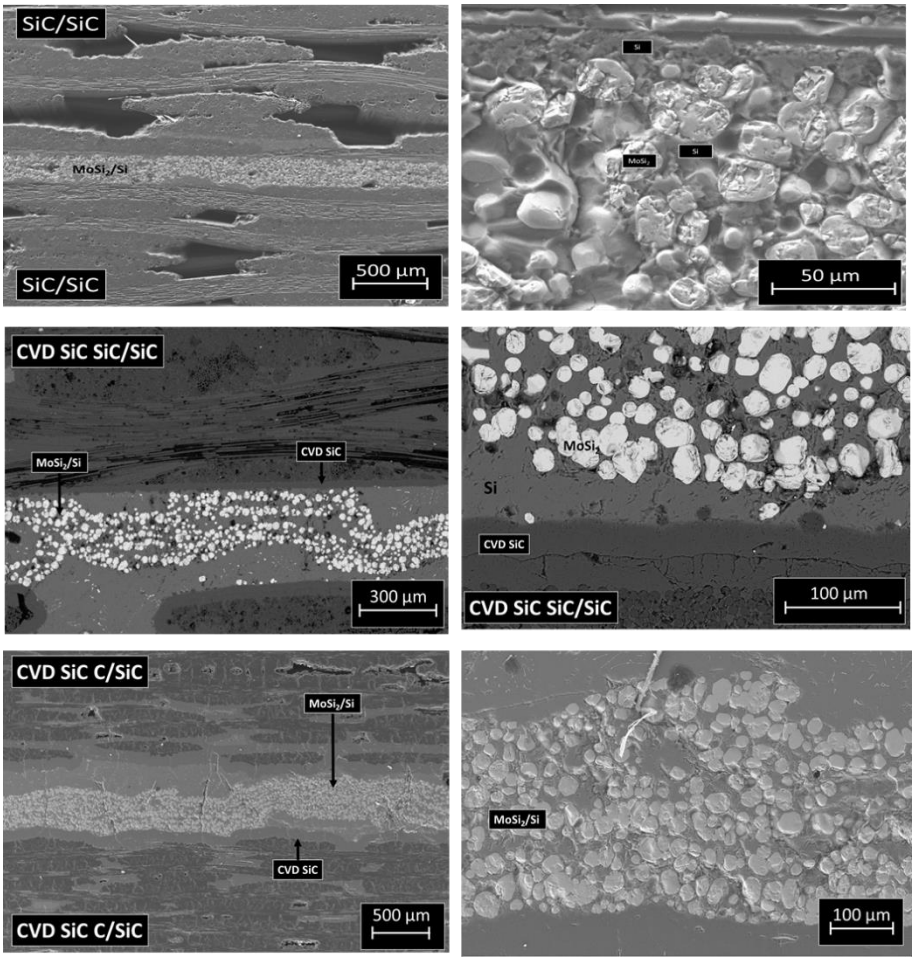


**Figure 36 Morphology of uncoated SiC/SiC, CVD SiC coated SiC/SiC and uncoated C/SiC joined by Mo-Wrap technology [18]**

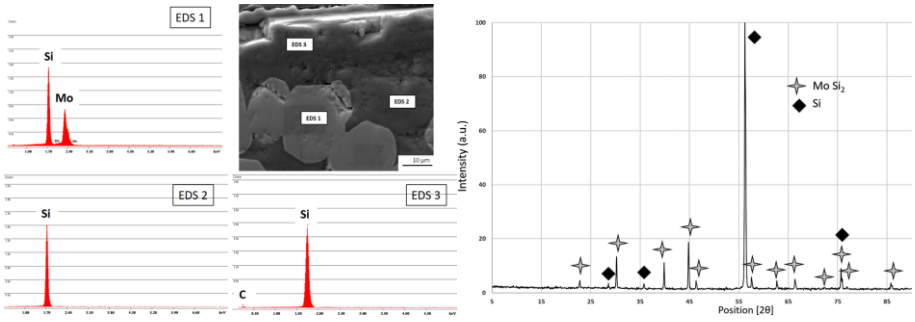


**Figure 37 EDS and typical XRD of the MoSi2/Si joined and fractured area [18]**

## 4.1.2 Mechanical Testing of Joints (Single Lap Shear)

**Uncoated SiC/SiC, CVD SiC coated SiC/SiC and CVD SiC coated C/SiC** joined specimens were mechanically tested to find their joint strength. Single lap shear in compression loading adapted from ASTM D1002-05 was performed on five samples as described in 3.10.4.1 section of chapter 3. The joint proved to be stronger than the interlaminar shear strength of all the composites joined and the crack propagates inside the composites, results in delamination of composites as shown in Figure 38. The joint remains firmly attached to one side of the composites. Fracture surface analysis shows composite layer on both sides, as shown in Figure 39.

Single lap shear testing in compression is not a good solution to find the joint strength, especially in case of composites. Therefore some other mechanical testing methods were followed such as single lap off-set and torsion testing, as it will be discussed in the section on joining of monolithic ceramics **Mo-Wrap joined SiC)**.

The $MoSi_2$ embedded in Si matrix acts as a crack deflector and can stop the crack as shown in Figure 40.

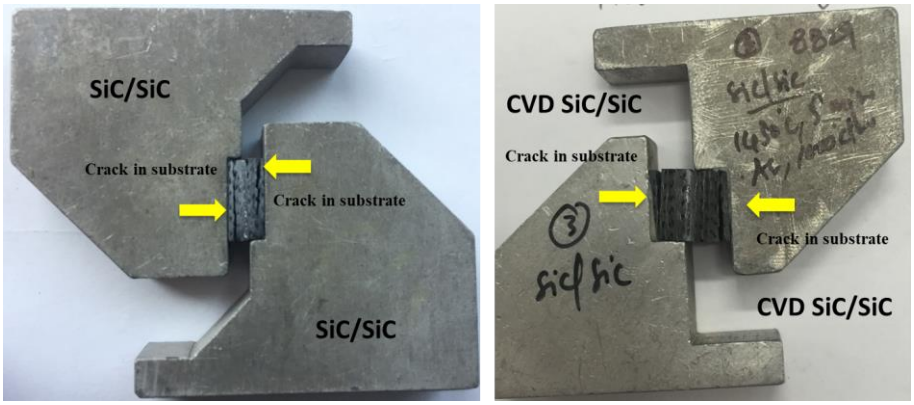


**Figure 38 Crack propagates in CVD SiC coated SiC/SiC and uncoated SiC/SiC composites**

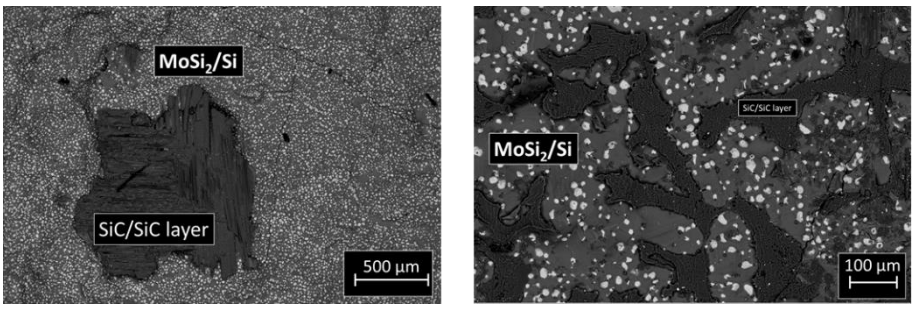


**Figure 39 uncoated SiC/SiC joined by Mo-Wrap, fractured surface (SEM, backscattering)**

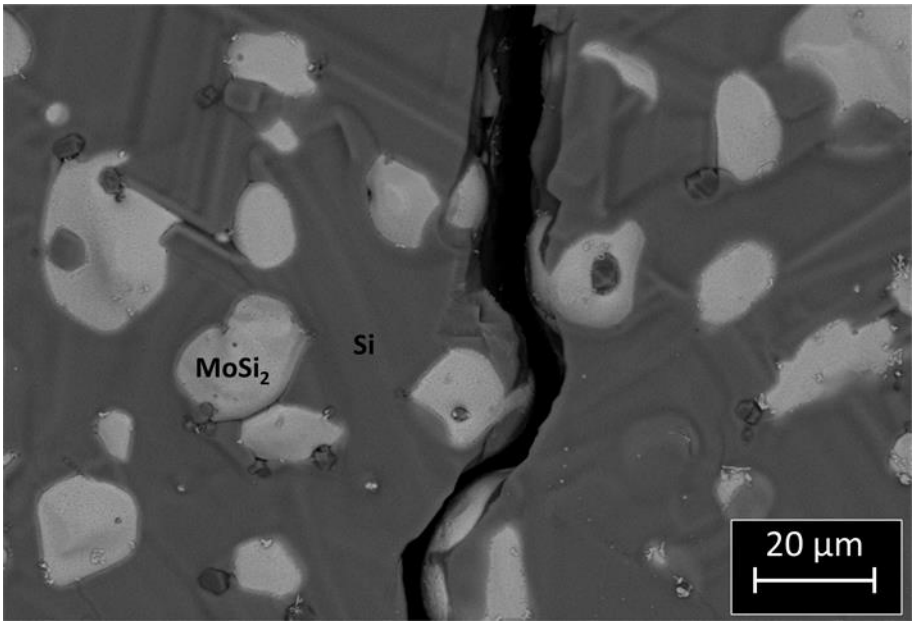


**Figure 40 Toughening mechanism by $MoSi_2$ particles in Si matrix, crack deflection in the fracture surface**

### 4.1.3 Oxidation Resistance

Thermal treatment close to possible working conditions of **CVD SiC coated C/SiC** joined with Mo-Wrap was carried out to check the oxidation resistance and thermal stability of **Mo-Wrap** joints at 1077 $^{o}$C for 30 minutes in the air. No change in morphology after aging at 1077 $^{o}$C was observed. Micro-structure before and after thermal treatment/aging is shown in Figure 41. The interface at lower magnification and interphase $MoSi_2$/Si of composite joining material are unaffected and resistant to oxidation at 1077 $^{o}$C, due to the self-passivating behavior of $MoSi_2$ and Si (potential formation of the $SiO_2$ protective layer).

Mo-Wrap joining produces oxidation resistant joining material suitable for high-temperature applications where commonly available brazes cannot be used. To the best of author's knowledge, for the first time, this material has been produced in-situ during joining. No literature is available on using silicides as a joining material. Considering excellent thermal stability of $MoSi_2$/Si and to further extend the limits of this newly developed joining material it was thermally treated at 1100 $^oC$ in the air for 6 hours, and results are discussed in the section on joining of monolithic ceramic (**SiC with Mo, Nb and Ta wrap)**.

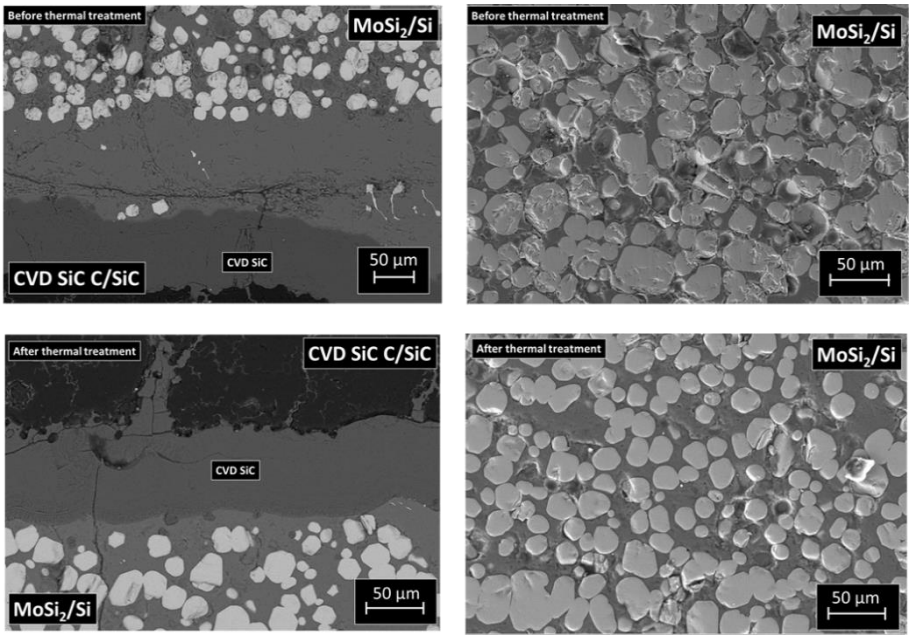


**Figure 41 Cross-section and microstructure of the $MoSi_2$/Si joined CVD SiC coated C/SiC before and after 1077 °C, 30 min in air**

## 4.1.4 Uncoated C/SiC: Joints Morphology and Elemental Analysis (SEM and EDS)

The uncoated C/SiC (SiCARBON$^{TM}$) was manufactured via Polymer-Infiltration-Pyrolysis Process (PIP), and supplied by Airbus Defence and Space GmbH Germany; C/SiC properties details have been summarized in chapter 3 and further details can be found in [181].

Joining the uncoated C/SiC by Mo-Wrap with a single-step process was not successful and produced weak and discontinuous joints due to poor wettability of

the composite with the Mo-wrap components. The surface wettability of C/SiC may vary a lot, possibly due to surface microstructure and oxygen-rich compound contamination [203, 204]. The surface morphology by SEM and elemental analysis by EDS of C/SiC composite is shown in Figure 42 and Figure 43 and cannot detect oxygen compounds. The poor wettability has been improved by the additional step of Si coating on C/SiC as shown in Figure 44 and discussed in 3.6 section of chapter 3. The additional step of Si coating improved the wettability [205] resulting in continuous, crack free, well-bonded joints shown in Figure 44.

Figure 44 shows the C/SiC after coating with Si at 1425 $^{o}$C, for 2 minutes under an inert environment (Ar flow), then joined with Mo-Wrap (second step) having joint thickness of 400-450 µm. The two-step Mo-Wrap is well optimized on uncoated C/SiC with a weight percentage of (79-80% Si and 20-21% Mo), as reported in section 3.6 of chapter 3.

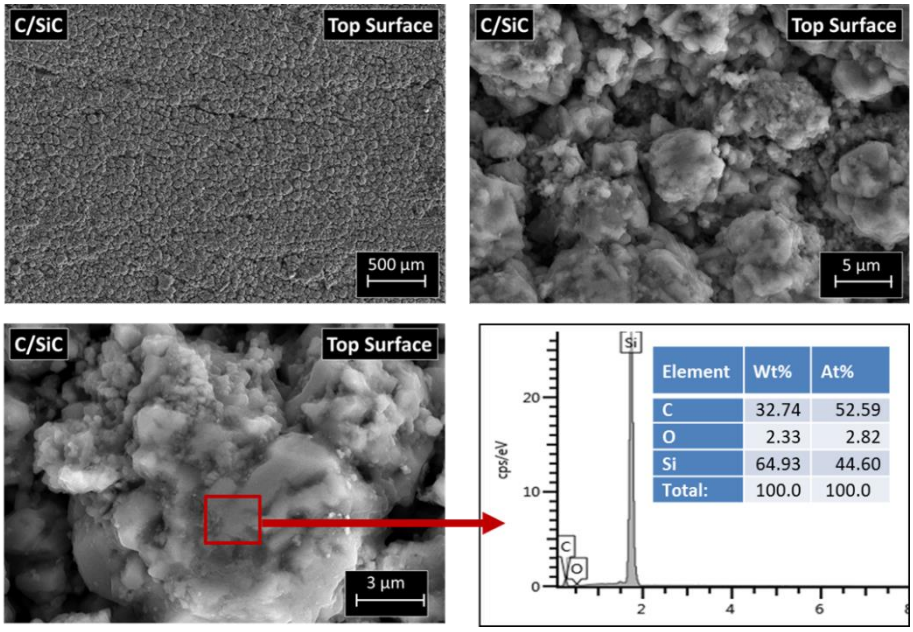


**Figure 42 As received uncoated C/SiC composites morphology top view**

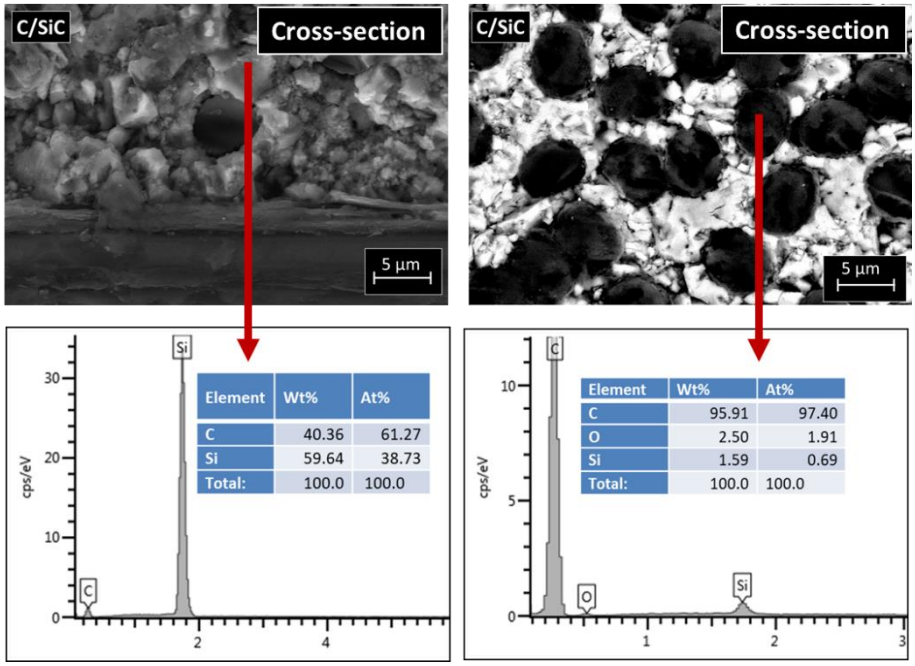


**Figure 43 As received uncoated C/SiC composites morphology cross-section (backscattered electrons image on the right)**

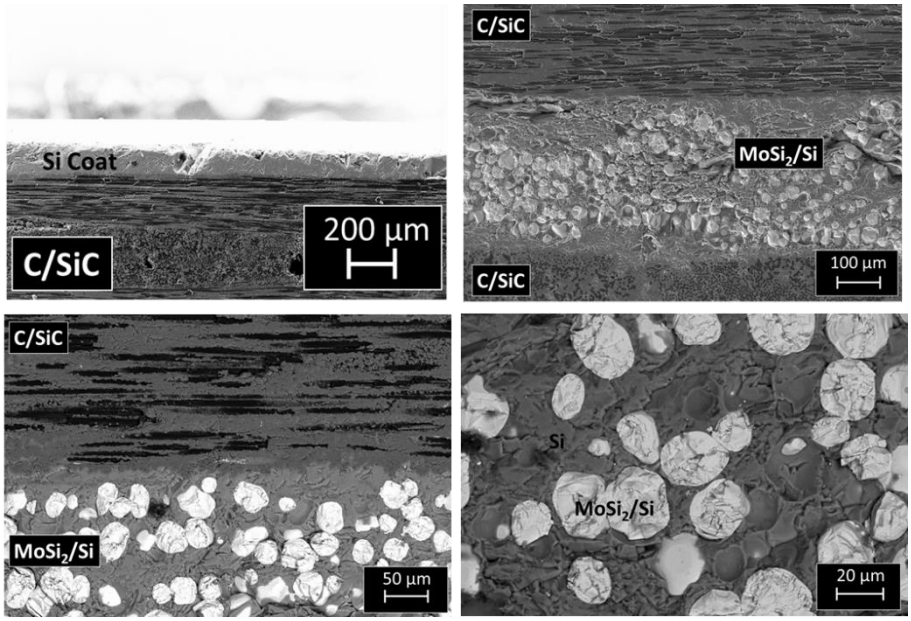


**Figure 44 Morphology of uncoated C/SiC joined in two steps (i) Si coat and (ii) Mo-Wrap**

### 4.1.5 Mechanical Testing of C/SiC (Single Lap Offset) Joints

Single lap shear testing was inappropriate for measuring the joint strength of SiC-based CMCs (SiC/SiC, CVD-SiC coated SiC/SiC and CVD-SiC coated C/SiC) joined by Mo-Wrap discussed in section 4.1.2, due to joint strength higher than the interlaminar shear strength of composites.

Therefore, **a single lap offset** was used: the specimen size and geometry are reported in 3.10.4.3 section of chapter 3.

Due to the good thermal stability of joining materials, single lap off-set shear tests were performed both at Room Temperature (RT) and high temperature (1000 $^{o}$C). ( section 4.1.3),

It is worth to mention here that not only **Mo, but Nb and Ta wraps** were successfully optimized to join the uncoated C/SiC in two steps. Joint micro-structure is discussed in their respective Sections (4.5.2 and 4.6.2).

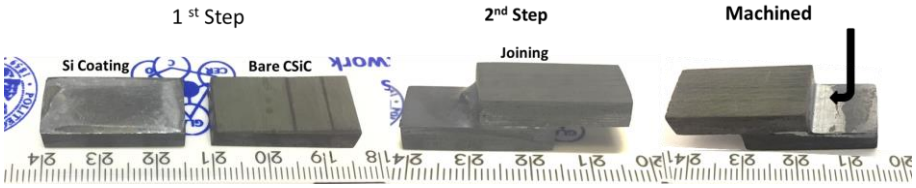


**Figure 45 C/SiC specimen preparation for SLO tests**

Figure 45 shows the C/SiC joined in two steps (first step: silicon coating of the uncoated C/SiC and second step: joining by RM-wrap); the additional machining step was required to remove the excess joining material. Since the machining step was done with workshop tools, it is worth to mention here that joined samples survived the stresses occurred while machining.

The SLO results are calculated as maximum force divided by nominal joined area, giving 15 MPa at room temperature and 37 MPa at 1000 $^{o}$C. The fracture surfaces obtained are of mixed failure mode (partially cohesive and partially adhesive); the cracks and delamination in composites are shown in Figure 46.

The primary limitation for silicides structural applications lies in their brittleness and poor fracture toughness at room temperature, which can be improved by alloying silicides with suitable elements, improving processing routes and tailoring microstructure [206]. Temperature has a substantial effect on the

deformation behavior of intermetallics, because of the insufficient number of independent slip systems being operative at temperatures less than the brittle to ductile transition (BDT) temperature. At or above the BDT temperature, the fracture toughness increases significantly, and the mode of fracture changes from cleavage to ductile, involving microvoid coalescence [135, 206].

Silicon single crystal is brittle at room temperature, but exhibits brittle to ductile behavior above 500 $^{o}$C [207-210]. BDT Temperature of $MoSi_2$ single crystal is believed to be around or above 1000 $^{o}$C: it shows ductile behavior between 1100-1300 $^{o}$C [211-213]. Literature also reports the thermomechanical behavior of monolithic single crystal $MoSi_2$ partially alloyed with SiC and $ZrO_2$ [135].

The silicides developed in this research work are polycrystalline $MoSi_2$, $NbSi_2$, and $TaSi_2$ embedded in a silicon matrix; the aim was to have reinforcing particles inside silicon, to improve silicon the creep behavior and increase its fracture energy. The higher shear strength values of at 1000 $^{o}$C observed for all three composites joints are due to the brittle to the ductile transition (BDT) of silicides at a higher temperature are in agreement with available literature.

The BDTT behavior of composite $MoSi_2$/Si, $NbSi_2$/Si and $TaSi_2$/Si as a joining material has never been reported in literature.

From the micromechanical point of view, with the ductility/toughness increase due to temperature increase and/or brittle to ductile transition with temperature increase (in case of RM disilicides) the critical defect dimension causing unstable fracture increases. It is generally known the relationship between defect size and strength, in which the intrinsic fracture resistance ($K_{IC}$ fracture toughness value) plays an important role ($\sigma_f = K_{IC} * (\pi a)^{-1/2}$). According to this equation, the strength decreases with increasing flaw size and decreasing fracture toughness. Thus, the increasing fracture toughness (in general ductility) results in strength increase at the same flaw population.

For the investigated Si-RM disilicide joints it means that at room temperature the critical defect size is small and the probability of the fracture is high, and thus strength is low. With the increase of the temperature, in particular when the material possesses brittle to ductile transition, and, in addition, with critical flaw size increase, the fracture probability decreases. At room temperature, something like premature fractures are observed whereas at high temperature plasticity can be fully developed.

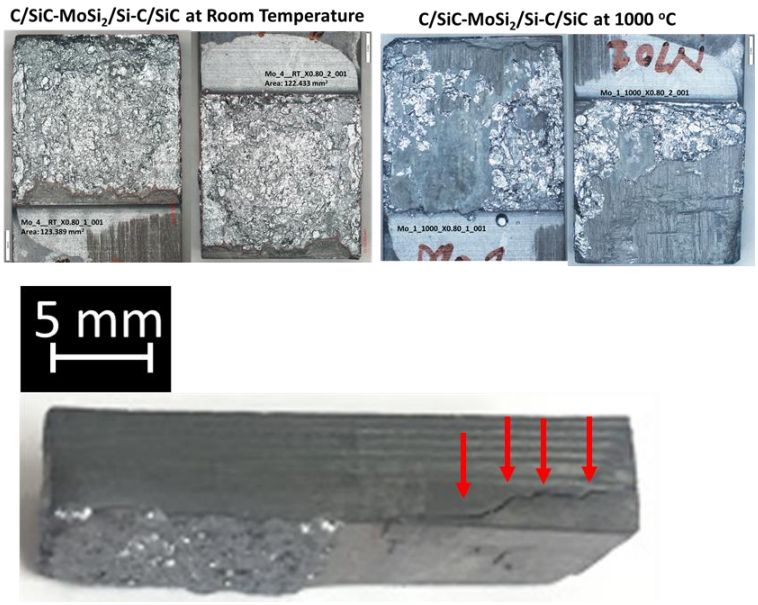


**Figure 46 Mixed cohesive and adhesive failure in SLO testing of C/SiC-Mo-Wrap-C/SiC joints at RT and HT**

## 4.2 Mo-Wrap: Monolithic Ceramics Joining

Since it was impossible to measure the Mo-wrap joint strength in CMCs due to their interlaminar shear strength lower than the joint one, the aim of this section is to measure it by single lap off-set (SLO) and torsion tests on Mo-Wrap joined monolithic ceramics.

### 4.2.1 SiC, Alumina and Mullite Joints Morphology (SEM)

Three monolithic ceramics joints were produced by Mo-Wrap joining (single step) (i) SiC-Mo-Wrap-SiC, (ii) Alumina-Mo-Wrap-Alumina and (iii) SiC-Mo-Wrap-Mullite having joint thickness in range of 200-250 µm in all three joints.

The ***SiC-Mo-Wrap-SiC*** joint microstructure is shown in Figure 47; the joint is continuous and well bonded. $MoSi_2$ particles are uniformly embedded in Si matrix, thus proving the excellent reproducibility of Mo-Wrap joining technology not only with the CMC (coated and uncoated) surfaces, but with monolithic surfaces too. Higher magnification of joint shows an excellent wettability on SiC surfaces and continuous and robust interface.

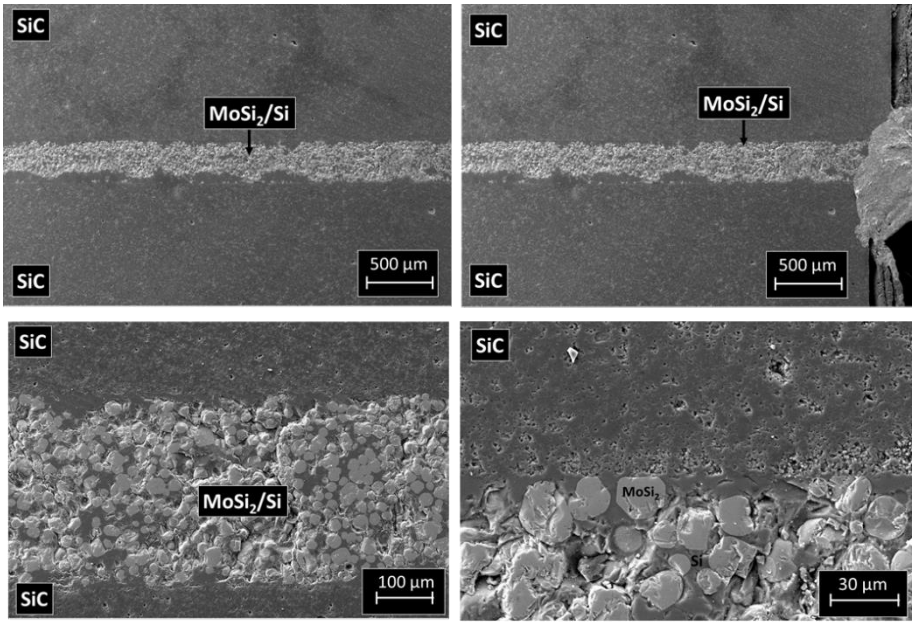


Figure 47 SiC-Mo-Wrap-SiC joint morphology

***Alumina-Mo-Wrap- Alumina*** joint microstructure is shown in Figure 48: also, in this case, the joint is continuous and uniform.

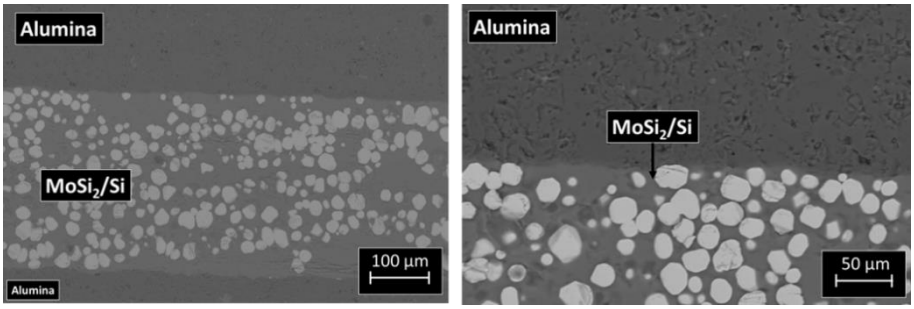


Figure 48 Monolithic alumina-Mo-Wrap-alumina joint morphology

***SiC-Mo-Wrap- Mullite*** joint morphology is shown in **Error! Reference source not found.**: in this case, two different materials (SiC and Mullite) were successfully joined. SiC has very good electrical and thermal conductivity, while the mullite ones are poor, as can be seen from the charge effect on the mullite during the SEM analysis.

Joining materials ($MoSi_2$/Si) and SiC have higher electrical and thermal conductivity than mullite.

***SiC-Mo-Wrap-Mullite*** is continuous, uniform and crack-free joint and can be used as a thermal barrier in various energy applications.

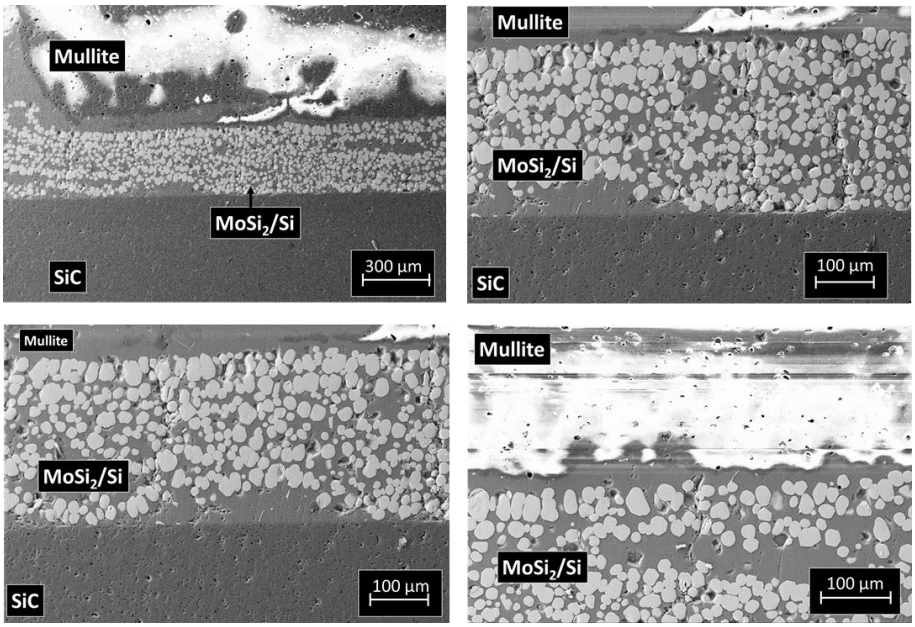


**Figure 49 Monolithic SiC-Mo-Wrap-mullite joint morphology**

## 4.2.2 Mechanical Testing of SiC-Mo-Wrap-SiC Joints (single lap shear, single lap offset and torsion)

To measure the **SiC-Mo-Wrap-SiC** joint strength, three different techniques have been used at room temperature: (i) single lap shear, (ii) single lap off-set and (iii) torsion.

Single lap (SL) shear test in compression load was done on SiC joints as discussed in 3.6 of chapter 3.: the joint did not break because the specimens were detached from the aluminium fixtures. Therefore it was not possible to measure the joint strength by SL as the joints are stronger than the bond between the fixtures and specimen itself.

Single lap off-set testing was adapted to measure the joint strength according to ASTM-D905-03; the SLO specimen, test geometry and fractured samples are shown in Figure 50.

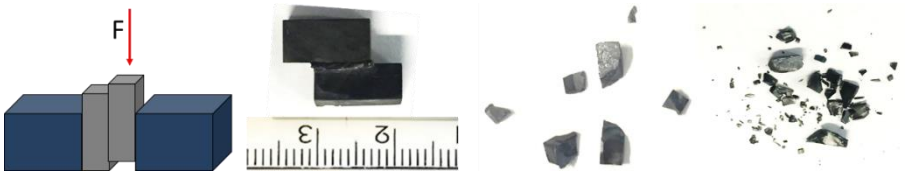


Figure 50 single lap off-set specimen geometry and fractured samples

The SLO results obtained on three samples gave values ranging between 133 and 175 MPa (unexpectedly low in one case, probably due to sample misalignment), with fracture surfaces showing a mixed cohesive and adhesive failure; samples failed catastrophically due to the brittle nature of monolithic SiC and it can be supposed that the joint strength is comparable to the SiC substrate one.

Table 10 SiC-Mo-Wrap-SiC SLO results

| Specimen | SLO (MPa) |
|---|---|
| 1 | 133.42 |
| 2 | 175.51 |
| *3* | *26.66* |
| Average: (1 and 2) | 154.47 |
| St. Deviation | 29.75 |

To evaluate the shear strength of Mo-Wrap joined SiC and not just the lap-shear one, torsion test was used as reported in 3.10.4.4 section of chapter 3. A small SiC hourglass shaped sample was joined, as shown in Figure 51, with a circular joined area of 4 or 5 mm in diameter.

Contrary to lap-tests, this torsion test can properly measure the shear strength of brittle joined materials, but shear strength values can only be calculated when the failure starts and propagates inside the joining material. If this is not the case, then either the test method is not correctly done, or the substrate and joint strength are similar.

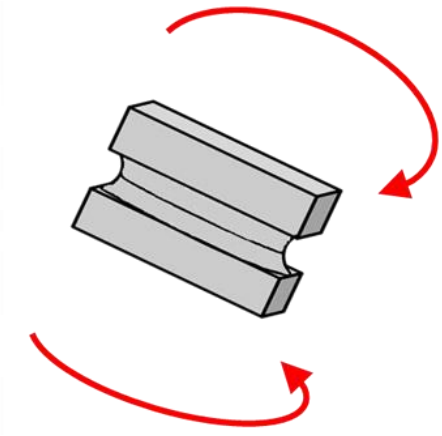

Figure 51 Torsion hourglass (THG)

The custom-made torsional testing machine developed at Politecnico di Torino can test different joints in torsion: details and comparison with other tests can be found in [197-199].

In this work, torsion hourglass of two different sizes (4 and 5 mm in diameter) were joined by Mo-Wrap, THG-4 and THG-5 respectively.

The fractured surfaces after torsion test are shown in Figure 52 and Figure 53: since the crack initiated and propagated in SiC substrates, also, in this case, we cannot measure the shear strength of these samples.

Moreover, the torsional results (MPa) calculated as maximum force divided nominal joined area (Table 11) are one order of magnitude lower than those measured on CVD-SiC joined by a glass ceramic in [214].

This can be due to a certain misalignment of joined hourglasses, thus giving to mixed mode loads together with torsion one. To obtain the reliable shear values in torsion, joints must be perfectly aligned. A few micrometres lateral shift in sample position may result in mixed shear along with bending load thus lower shear values observed. To avoid misalignment issues, large joined SiC tiles ( Figure 54) were prepared, then cut into small THG, which are going to be shipped here from the Japanese company (Morise), then tested in torsion.

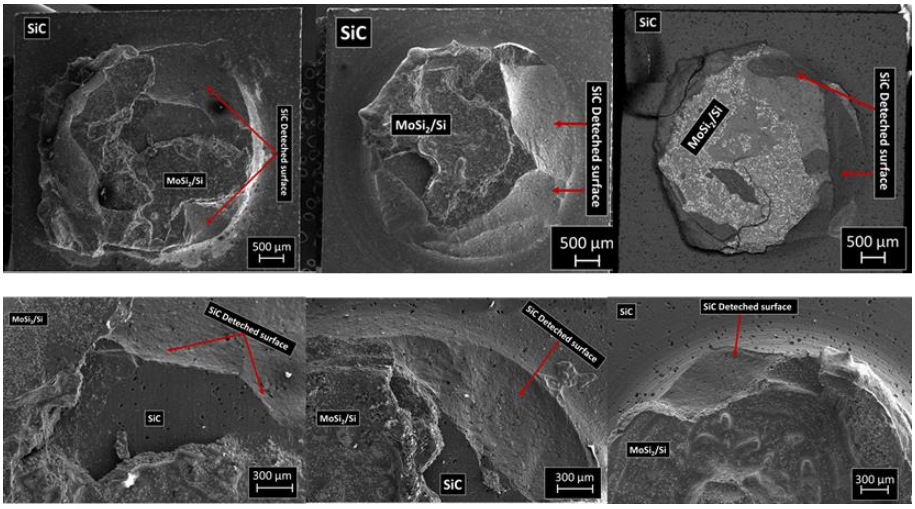


Figure 52 THG-4 fractured surfaces after torsion test

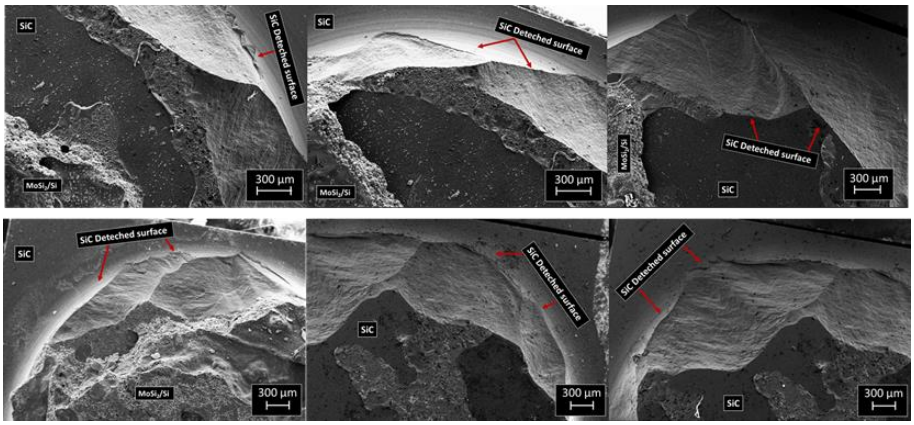


Figure 53 THG-5 fractured surfaces after torsion test

Table 11 Torsional results

| RM-Wrap joined SiC THG results (MPa) | THG-4 | THG-5 |
|---|---|---|
| 1 | 29.7 | 33.4 |
| 2 | 24.2 | 25.2 |
| 3 | 10.1 | 35.2 |
| 4 | 6.8 | 34.0 |


Figure 54 Larger SiC joined tiles

### 4.2.3 Mo-Wrap Joined Monolithic SiC Oxidation Resistance

Mo-Wrap joined CMC have good thermal stability and oxidation resistance as discussed in 4.1.3. To further extend the limits beyond the 30 minutes was not possible in case of composites, because of their interface limited oxidation resistance.

***SiC-Mo-Wrap-SiC*** (monolithic SiC joints) were tested at 1100 $^{o}$C for 6 hours in the air : the joint interface is shown in Figure 55; joined samples remained firmly joined and their morphology unchanged respect to prior treatment. **$MoSi_2$/Si** has a great potential to be used at high temperature for longer durations: silicon melting temperature, i.e. 1412 $^{o}$C can be the limiting factor. Good oxidation stability is also expected, due to a protective $SiO_2$ on silicon. Ta and Nb wrap joints for monolithic SiC were also tested under same conditions and discussed in their respective sections.

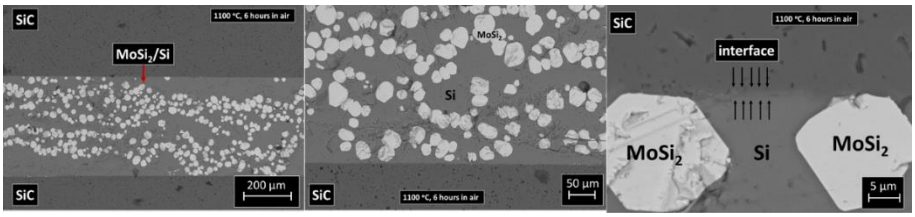


Figure 55 SiC-Mo-Wrap-SiC joint interface after 6 hours at 1100 $^{o}$C in air

### 4.2.4 $MoSi_2$/Si-Nano-Indentation

Indentation techniques measure the mechanical properties of individual phase/microstructure in a composite, thus allowing to predict in a first approximation the composite ones by the rule of a mixture [215].

Since the joint strength of Mo-wrap joints is still to be measured, micro and nanoindentation techniques were adopted in order to have some indications.

Nanoindentation was carried out on **SiC-Mo-wrap-SiC** joints interface and SiC substrate as described in 3.10.4.6.1 section of chapter 3.

Imprints of Berkovich tip are shown in Figure 56 on three different phases (i) Si matrix, (ii) $MoSi_2$ and (iii) joined monolithic SiC. The data obtained by an Agilent G200 Nanoindenter served to calculate the indentation hardness (H) and indentation modulus based on Oliver-Pharr method [216, 217]. Further details on evaluation and analysis process can be found in [218]. The hardness (H) and quantitative modulus obtained values are reported in Table 12.

The smaller imprints in SiC phase indicates that material has higher hardness and modulus values than the $MoSi_2$ and Si, as expected, and in agreement with values shown in Table 12. Only those indents which were precisely positioned on a particular phase were considered. The hardness and modulus values were averaged for each phase to the depth range of 900–1000 nm.

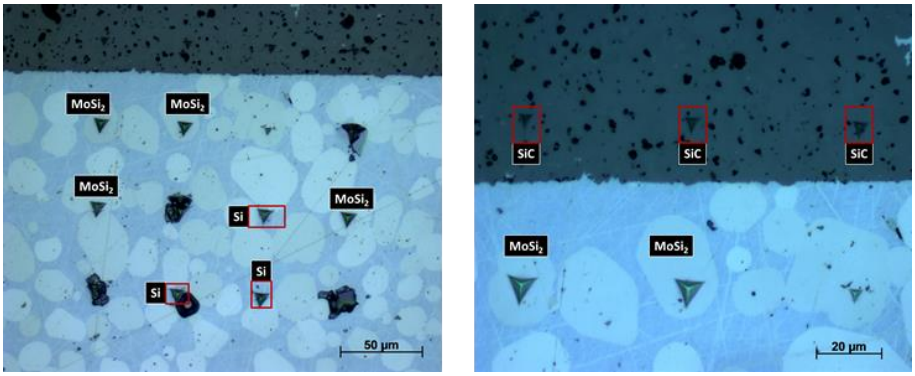


Figure 56 Nanoindentation imprints on Si, MoSi2 and SiC

Typical indentation modulus-displacement and hardness-displacement curves are shown in Figure 57. The curve profiles show more stable profile as the depth

increases which is the reason to choose the middle values to have more realistic analysis.

To the best of author's knowledge, this is the first time that in-situ formed silicides are tested. Literature reports the micro-hardness of monolithic $MoSi_2$ developed from commercially available powder and sintered at high pressure (15 MPa- 600 MPa) for about 24 hours and achieves the hardness values in the range of 11-15 GPa, which is in agreement with the values obtained by nanoindentation [216, 218-222].

**Table 12 Nanoindentation hardness and modulus values**

| | **Si** | **$MoSi_2$** | **SiC** |
|---|---|---|---|
| **Modulus (E) (GPa)** | 206.2 | 339.7 | 408.9 |

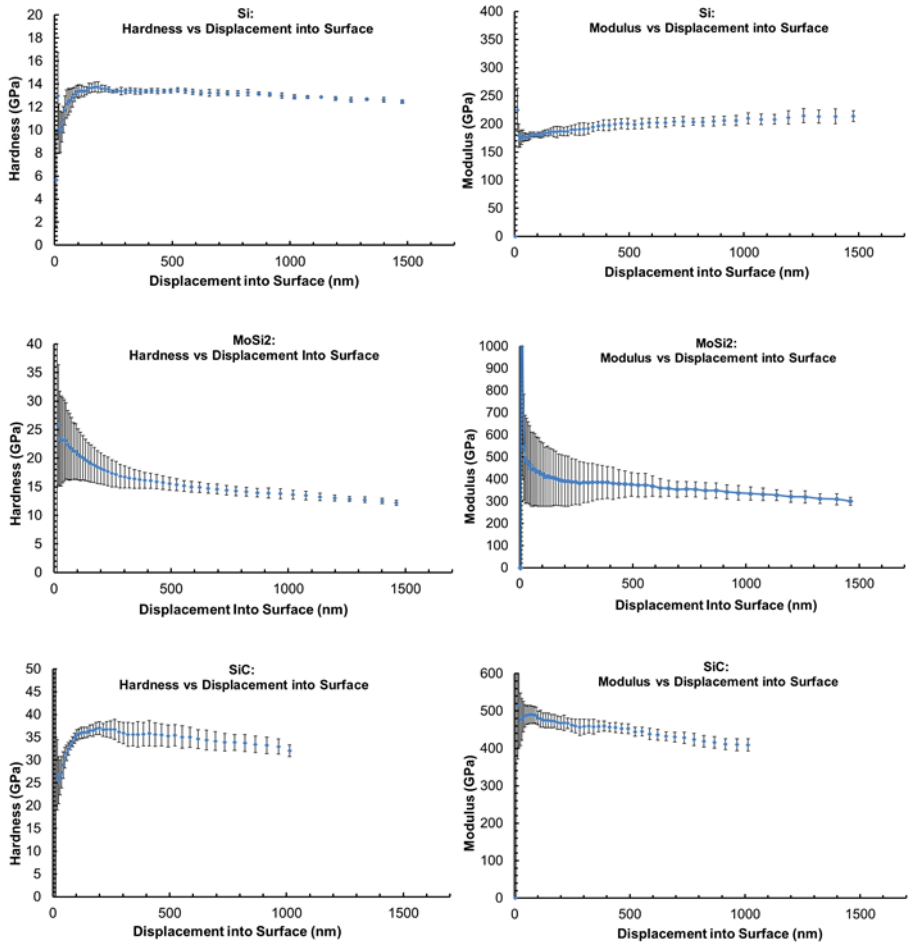


**Figure 57 Typical indentation modulus-displacement and hardness-displacement curves Si, MoSi2 and SiC**

## 4.2.5 Si Micro-Hardness (Vickers Hardness)

The conventional micro-hardness test was carried out to measure the Vickers-hardness of Si-matrix inside the joint as described in 3.10.4.6.2 section of chapter 3. Imprints on Si matrix are shown in Figure 58 and the obtained Vickers-hardness values are presented in Table 13. The indents in Si matrix show small cracks initiated from the edges of dents indicates the brittle behavior of silicon at room temperature [207-210]. Si hardness values obtained are in agreement with the reported values in [223].

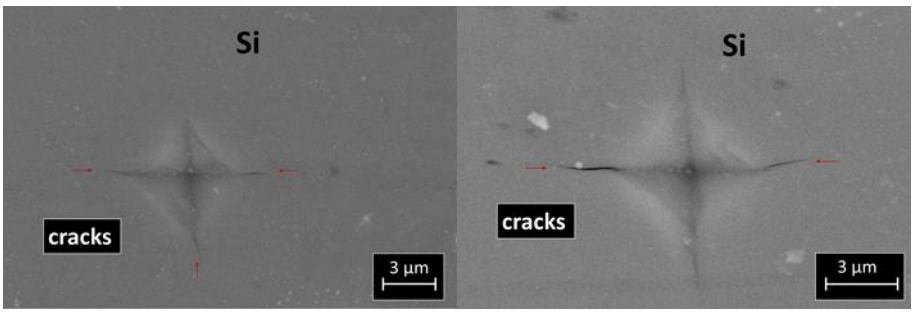


Figure 58 Vickers imprints on Si matrix inside the joint

Table 13 Vickers-hardness values of Si

| Vickers hardness | Si |
|---|---|
| 1 | 1091 |
| 2 | 1015 |
| 3 | 963 |
| 4 | 871 |
| 5 | 1071 |
| Avg | 1002 |
| MPa | $9.82 \times 10^3$ |

## 4.2.6 $MoSi_2$ Micro-Hardness (Vickers Hardness)

The conventional micro-hardness test was carried out to measure the Vickers-hardness of $MoSi_2$ as described in 3.10.4.6.2 section of chapter 3. Imprints on $MoSi_2$ are shown in Figure 59, and the obtained Vickers-hardness values are presented in Table 14.

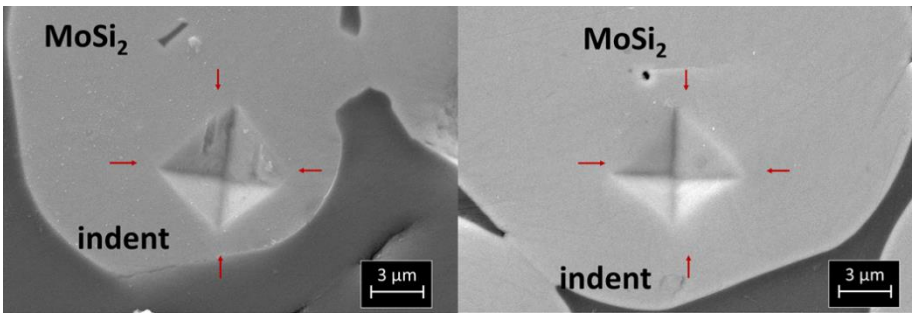


Figure 59 Vickers imprints on in-situ grown $MoSi_2$ inside the joint

The obtained values are in agreement with the values reported in the literature for monolithic $MoSi_2$ sintered with high pressure for longer time [216, 218, 220-222].

Table 14 Vickers-hardness values of $MoSi_2$

| Vickers hardness | $MoSi_2$ |
|---|---|
| 1 | 1199 |
| 2 | 1246 |
| 3 | 1111 |
| 4 | 1296 |
| 5 | 1091 |
| Avg | 1188 |
| MPa | $1.165 \times 10^4$ |

## 4.3 Mo-Wrap joined Sandwiches Structures

It is quite challenging to produce strong sandwich structures because of few connecting points between the skin and core especially when have high porosity (> 80%).

The following section will discuss the Mo-Wrap joining of SiC foams with CVD SiC coated C/SiC and C/SiC, their mechanical behavior (in compression and tensile mode) and their ability to withstand thermal shock.

### 4.3.1 Mo-Wrap: SiC Foam Sandwiches (SEM and MCT Scan)

The sandwich structures were produced by joining 2D CVD-SiC coated C/SiC and 3D SiSiC open cell foam (materials discussed in chapter 3) by Mo-Wrap.

The SiSiC foam is the core and CVD-SiC coated C/SiC the two skins on both sides of the sandwich; joined structure and joining scheme is shown in Figure 60.

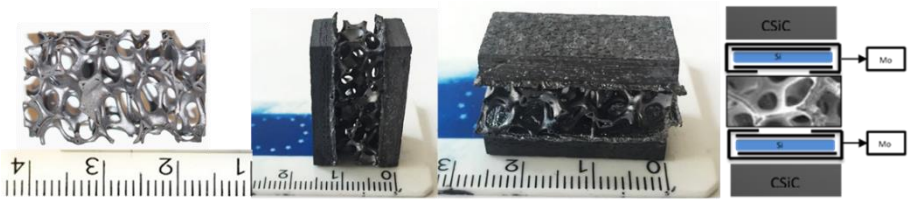


**Figure 60 Sandwich structures prepared by using the Mo-Wrap joining technique: the SiC foam is the core and CVD-SiC coated C/SiC the two skins**

Joint is uniform and continuous (200 -250 µm thick) as shown in Figure 61. The foam has few connecting points but firmly joined with the skins by $MoSi_2$/Si. The joining conditions were optimized to avoid any adverse effect on substrates (core and skin). One crack appeared in the foam while cutting by using a diamond blade and polishing. The continuous joint interface is evident at higher magnification in Figure 62: both interfaces (i) SiSiC foam-$MoSi_2$/Si and (ii) CVD-SiC coated C/SiC-$MoSi_2$/Si are continuous and crack free. In some spots (circled in Figure 62) there is a little capillary rise of joining material within SiSiC foam porosity.

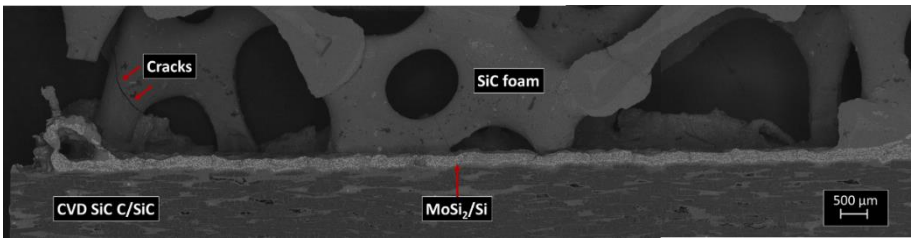


**Figure 61 Sandwich cross-section with C/SiC (bottom) joined to SiC foam by Mo-Wrap technique (SEM-back scattered electrons)**

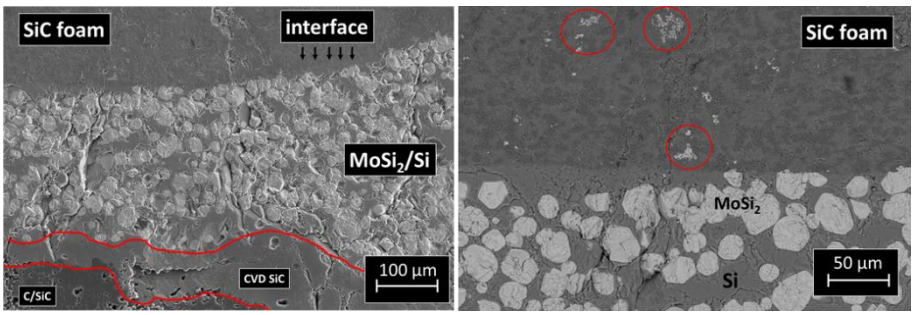


**Figure 62 Sandwich structure interface at higher magnification**

Uncoated C/SiC was also joined to SiC foam (by a two-step Mo-Wrap technique, involving silicon coating before joining, as described in 3.6 section of chapter 3.

Computer Tomography Scan (CT-Scan) was carried out to analyze inner characteristics of porous media and connecting points at the interface. CT-scan was carried out at Nikon metrological x-ray Center of Excellence, UK. The joining material is well spread and shows that Mo-Wrap has a good wettability on C/SiC and SiSiC foam which has few connecting points, but all are well connected to the joint, as shown in Figure 63.

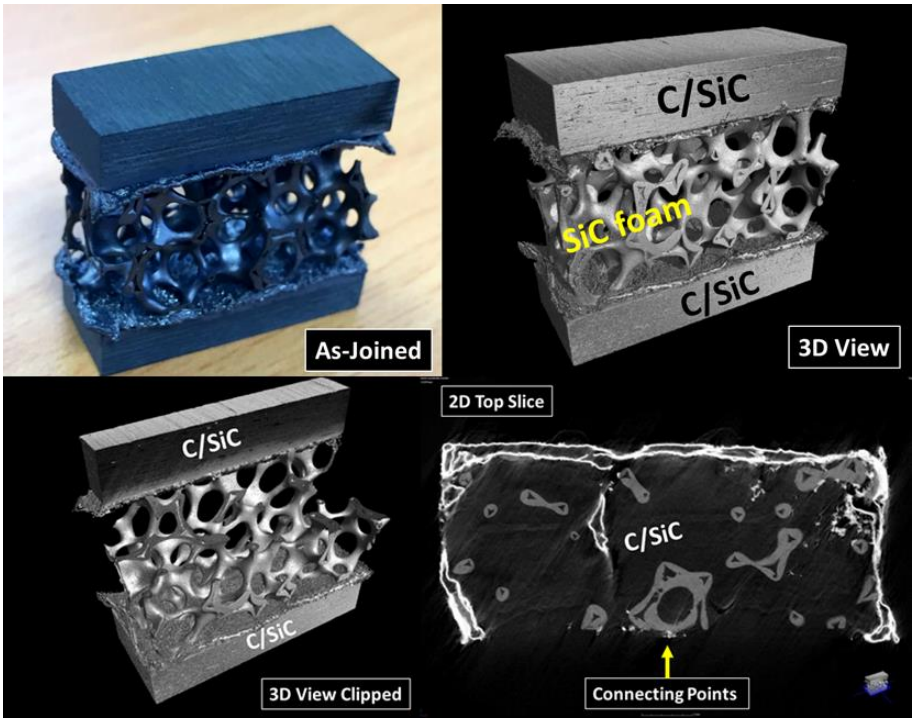


Figure 63 Sandwich structure, CT scan (2D & 3D)

### 4.3.2 Mo-Wrap Joined SiSiC Foam Sandwiches: Thermal Shock Resistance

The sandwich structures joined by Mo-Wrap were tested for thermal shock resistance as described in 3.10.6 section of chapter 3.

There are very few ceramic materials good at thermal shock resistance the prominent one is silicon carbide-based; this is the first time this newly developed joining material ($MoSi_2$/Si) is tested in as a sandwich structure. The sandwich was put in the platinum-rhodium crucible to be easily placed and removed from the furnace. The test is performed on one sandwich three times (cycles) as shown in Figure 64. Dual laser infra-red thermometer was used to measure the temperature of the sandwich was 830-950 °C during two minutes of dwell inside furnace, Figure 65. The sandwich structure remained bonded after three cycles of thermal shock at 1100 $^{o}$C.

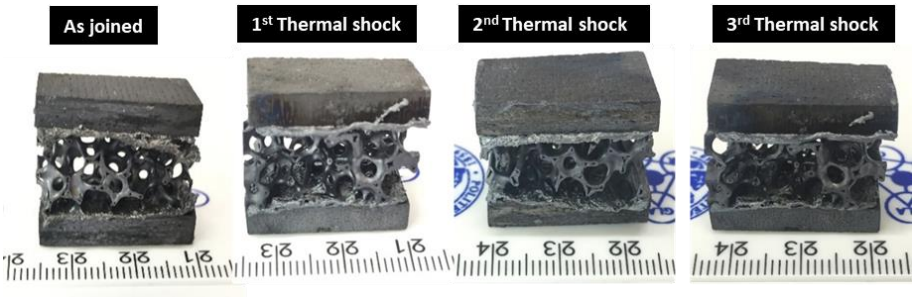


**Figure 64 Sandwich structure as joined, after first, second and third thermal shock at 1100 °C in air**

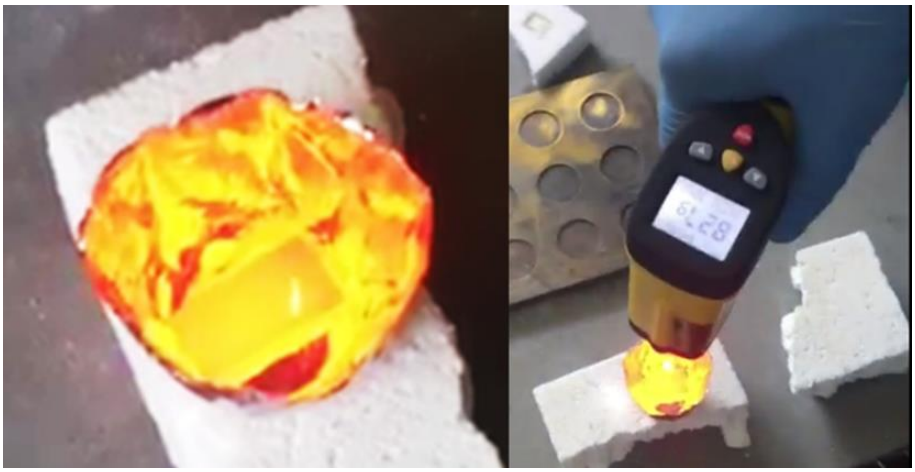

**Figure 65 Temperature measurement on the sandwich structure by using the dual laser infra-red thermometer at the instant of removing it from furnace**

Elemental mapping on the joint ($MoSi_2$/Si) was carried out before and after thermal shock. Figure 66 and Figure 67 shows the unchanged morphology of a sandwich after first and third thermal shock respectively. $MoSi_2$ particles play a dual role as toughing Si matrix and crack deflector, therefore, it is less prone to cracks in situ formed $MoSi_2$/Si due to thermal stresses [224]. After the thermal shock, the sandwich structure was analyzed in order to see the actual interface with foam, as shown in Figure 68. It is worth noting that neither the interface Mo-Wrap/SiC foam nor the Mo-wrap/CVD-SiC coated C/SiC itself changed morphology and composition (e.g. oxidation) after three thermal shock tests.

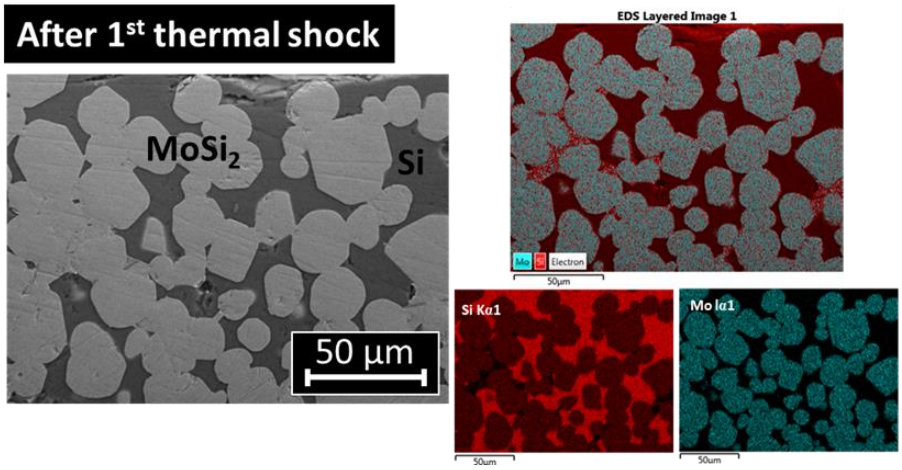


Figure 66 Elemental mapping of the sandwich joined region after first thermal shock at 1100 °C in air

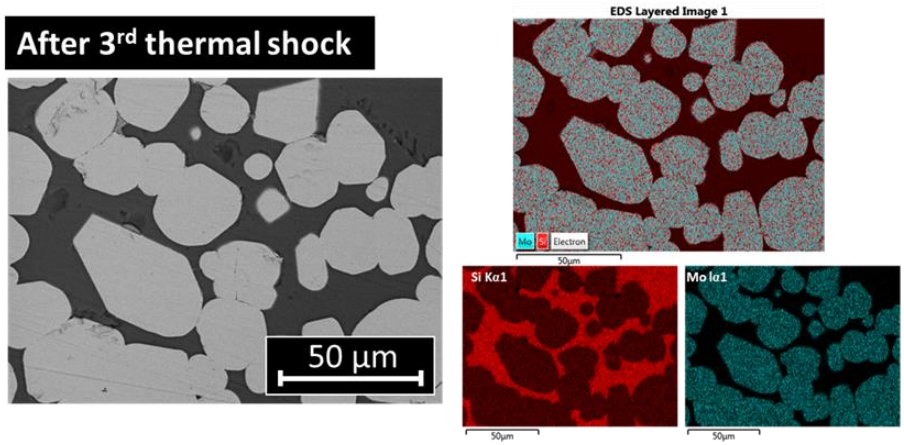


Figure 67 Elemental mapping of the sandwich joined region after third thermal shock at 1100 °C in air

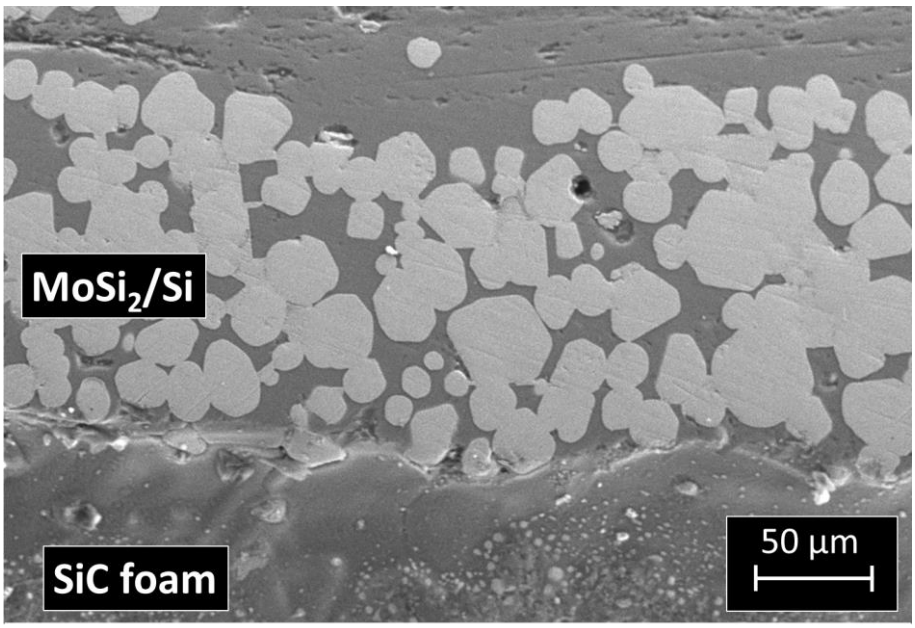


**Figure 68 cross-section (SEM) of the sandwich joined region after first thermal shock tests at 1100 °C in air**

### 4.3.3 Mechanical Testing of Sandwiches (Compression, Tensile)

The compression tests were carried out on (i) as joined sandwiches (ii) bare SiC foams and (iii) thermally shocked sandwiches (three cycles); samples are shown in Figure 60.

Tensile tests (samples shown in Figure 69) were carried out on (i) sandwiches of size 10 x 10 x 25 $mm^3$, (i) as received SiC foam (ii) SiC foam thermally treated at joining conditions (i.e. 1450 °C for 5 min with heating rate of 1000 °C/hour and (iv) SiC foams thermally shocked.

The corresponding load values are given in Table 15 It is worth noting that SiC foam breaks in middle/lattices in both test modes (compression and tensile). However, the connecting points remain firmly attached on both sides with joining material, and no detachment was observed from the skins (CVD-SiC coated C/SiC) even on the thermally shocked specimen. It proves the strong bonding not only with the smooth skins but with fewer connecting points in foam as well, as shown in Figure 70, Figure 71 and in Figure 72.

As a general comment on compression/tensile tests on these relatively small sandwiches, quite a large dispersion of results can be observed. It may be likely due to intrinsically non-regular pattern of these SiC foams, thus leading to a variable number, place and size of connecting points. Therefore, each specimen's load/displacement curves can be very different from another.

**Figure 69 Sandwiches and bare SiC foam for tensile tests inside test fixtures**

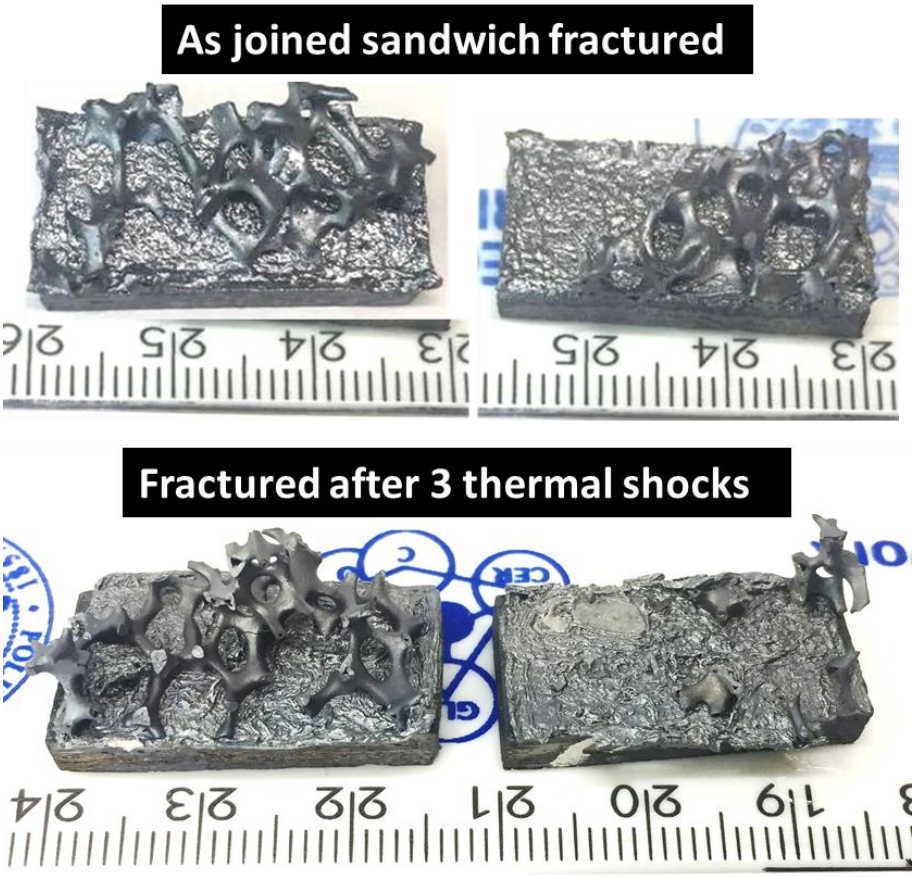


Figure 70 fractured surfaces after compression test

Table 15 Compression/tensile load vs. displacement on sandwiches and foams

| Mode | conditions | Maximum load (N) | Displacement at maximum load (mm) |
|---|---|---|---|
| Compression | | | |
| Sandwich as joined #1 | RT | 716 | 0.22 |
| Sandwich as joined #2 | RT | 369 | 0.15 |
| Sandwich as joined #3 | RT | 755 | 0.21 |
| Bare SiC | RT | 700 | 0.06 |
| Sandwich After thermal shocks | RT-1100 °C-RT 2 min | 259 | 0.27 |
| Tensile | | | |
| Bare SiC As received #1 | RT | 383 | 0.66 |
| Bare SiC As received #2 | RT | 29 | 0.34 |
| Bare SiC As received #3 | RT | 501 | 0.55 |
| Sandwich as joined #1 | RT | 34 | 0.13 |
| Sandwich as joined #2 | RT | 8 | 0.07 |
| Sandwich as joined #3 | RT | 18 | 0.62 |
| Bare SiC thermally treated #1 | 1450 °C, 5 min 1000 °C/hour | 151 | 0.36 |
| Bare SiC thermally treated #2 | 1450 °C, 5 min 1000 °C/hour | 388 | 0.28 |
| Bare SiC thermally treated #3 | 1450 °C, 5 min 1000 °C/hour | 91 | 0.25 |
| Bare SiC thermal shocked #1 | RT-1100 °C-RT 2 min | 456 | 0.50 |
| Bare SiC thermal shocked #2 | RT-1100 °C-RT 2 min | 108 | 0.11 |
| Bare SiC thermal shocked #3 | RT-1100 °C-RT 2 min | 132 | 0.08 |

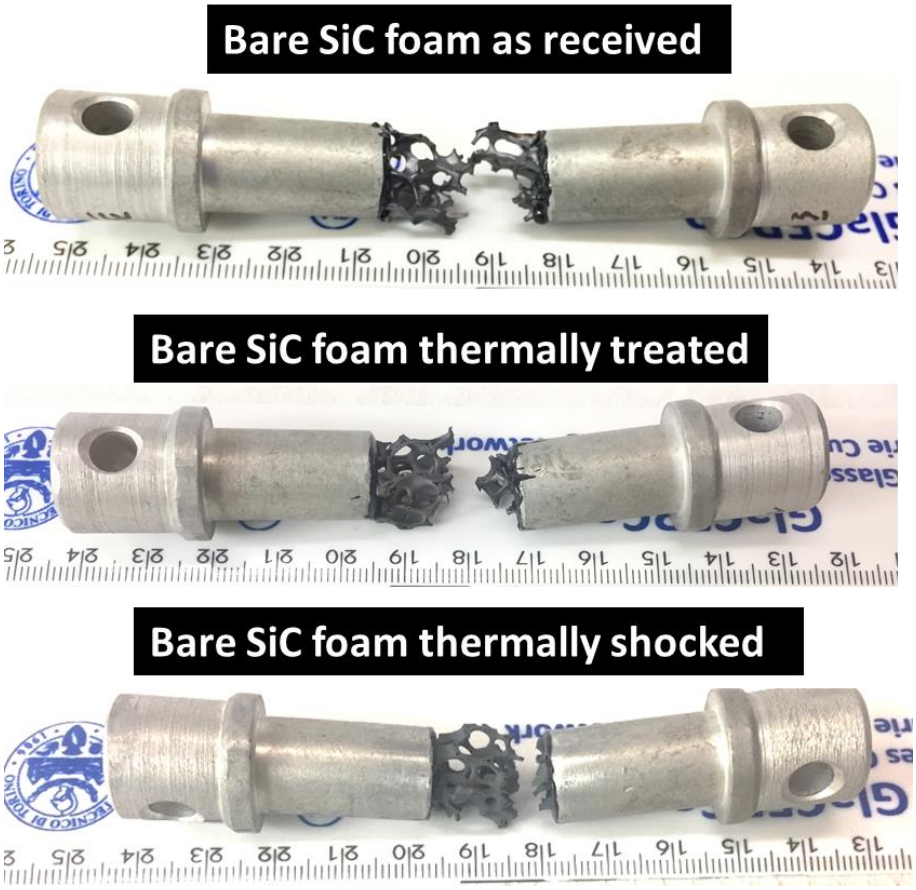


Figure 71 Typical fracture surfaces of bare SiC from tensile tests

Typical fracture surfaces from tensile tests (Figure 72) shows the strong bond of the joining material with both SiC foam and CVD-SiC coated C/SiC skins. The failure occurs inside the SiC foam, and some parts remain attached to the joining material. Figure 73 shows the SEM analysis of the tensile fractured sandwich structures; it shows that the fracture occurs in the foam. As for compression tests, no failure was observed in the joining layer, but foam struts are the first to fail.

Figure 72 Typical fracture surfaces of Sandwiches from tensile tests

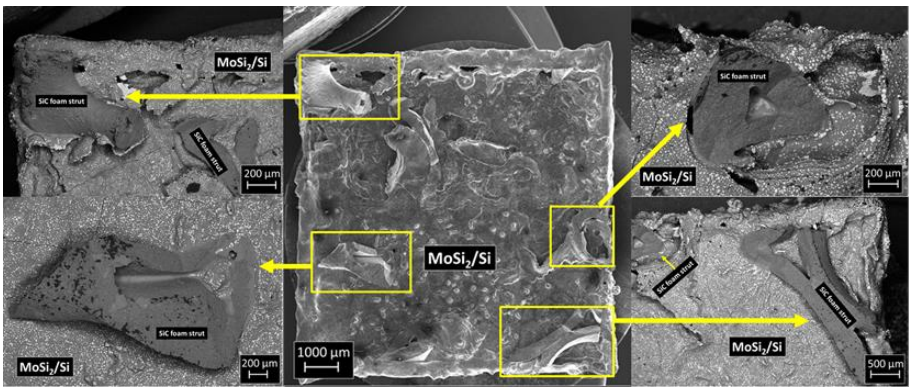


Figure 73 C/SiC-SiC foam-C/SiC sandwich fracture surfaces after tensile test showing SiC foam parts attached to the joining material

## 4.4 Mo-Wrap joining of SiSiC foam to SiSiC Discs

SiC foam was successfully joined to SiSiC discs having a composition of SiC (70-90%) and Si (10-30%), provided by ENGICER, details given in materials chapter 3) by using Mo-Wrap joining (two-step joining, involving silicon coating before Mo-wrap joining) within the European project **NEXTOWER.**

The as-received SiSiC disks and SiSiC foam are shown in Figure 74.

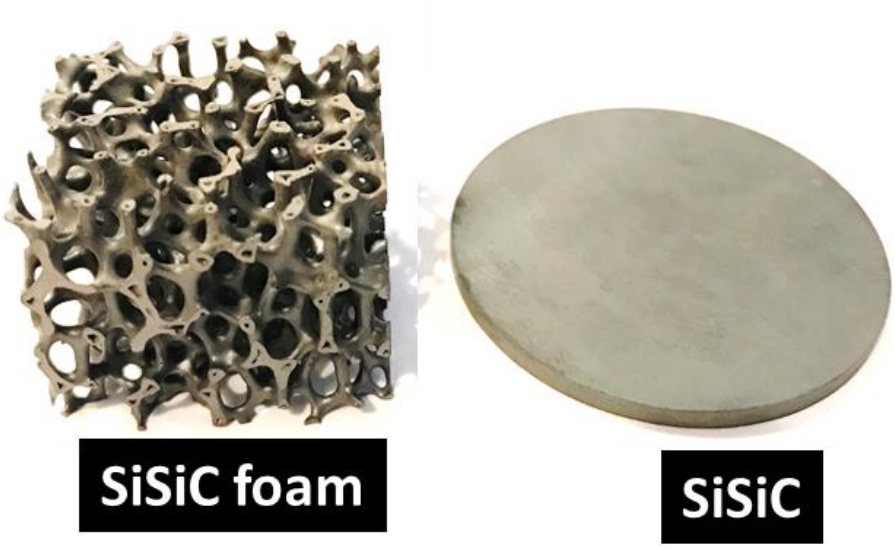


Figure 74 As received SiSiC disks and SiSiC foam

SiSiC disks contain 10-30 % silicon: effects of the joining thermal treatment at 1450 ºC for 5 minutes on SiSiC disk was analyzed to find any significant change in morphological structure. Little sintering effect was observed on SiSiC disk as shown in Figure 75.

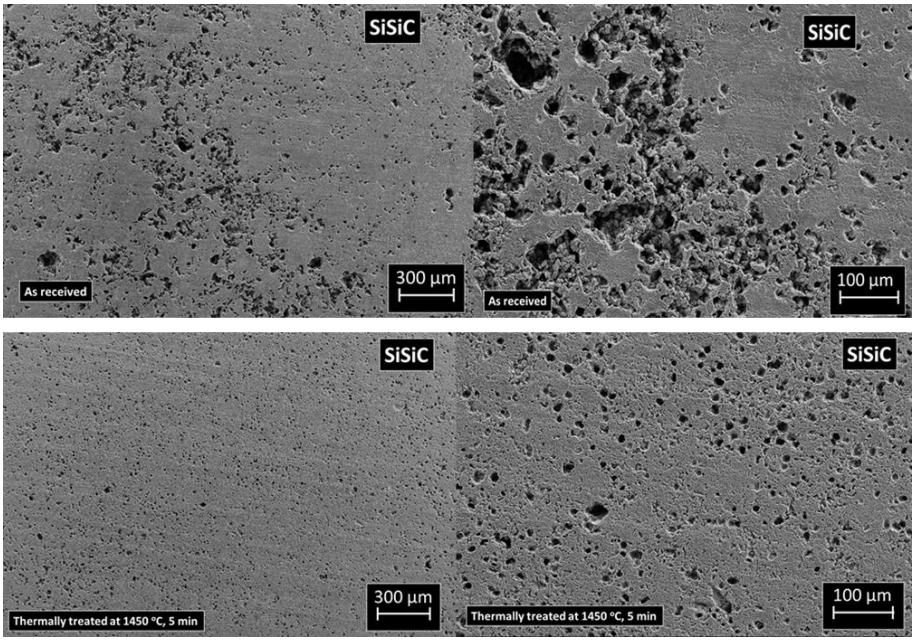


**Figure 75 SiSiC thermally treated at 1450 ºC for 5 min**

Mo-Wrap joining in a single step as for sandwich structures described in 4.3 section was not effective in joining ***SiSiC disk to SiSiC foam*** probably because of reactivity of Mo-wrap with residual silicon of the SiSiC disk (Figure 76).

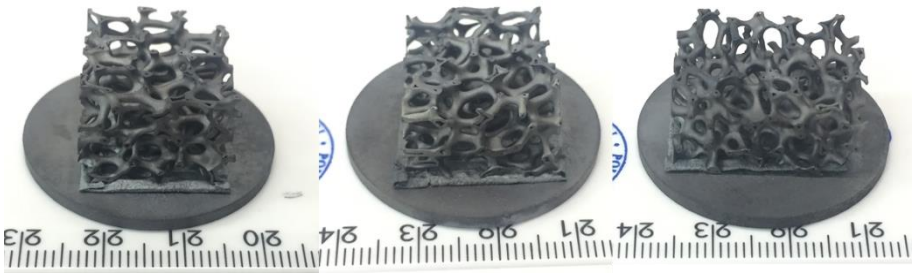

**Figure 76 SiSiC disk to SiSiC foam joined in a single step by Mo-Wrap**

Several experiments were performed by varying the processing parameters (time and temperature). The two step methodology (i) Si coat on SiSiC disk and (ii) Mo-Wrap joining was effective and produced continuous joints.

SiSiC disks were coated with Si for 30 seconds under a inert environment at 1425 $^{o}$C and then joined to the SiSiC foam by Mo-Wrap at 1450 $^{o}$C, 5 min. Joining scheme is shown in Figure 77 and the continuous and robust joint in Figure 78.

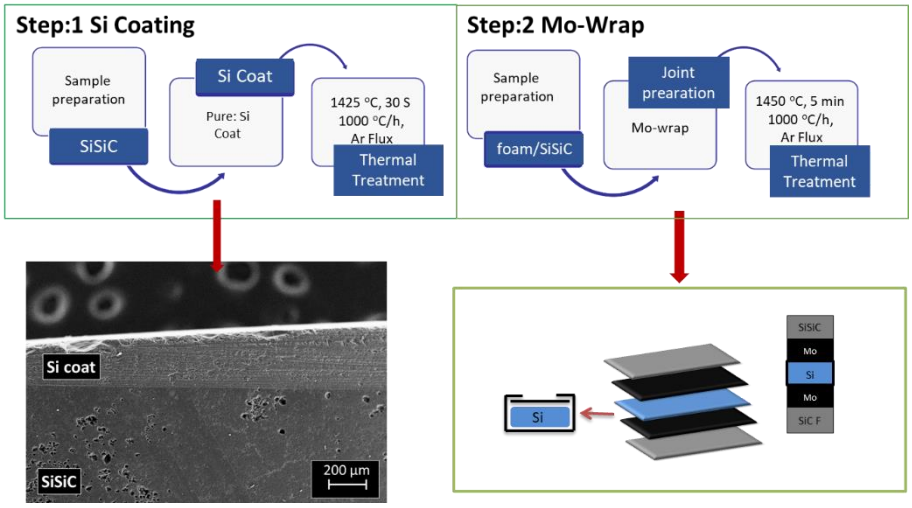


Figure 77 SiSiC disk to SiSiC foam joining scheme (two-steps)

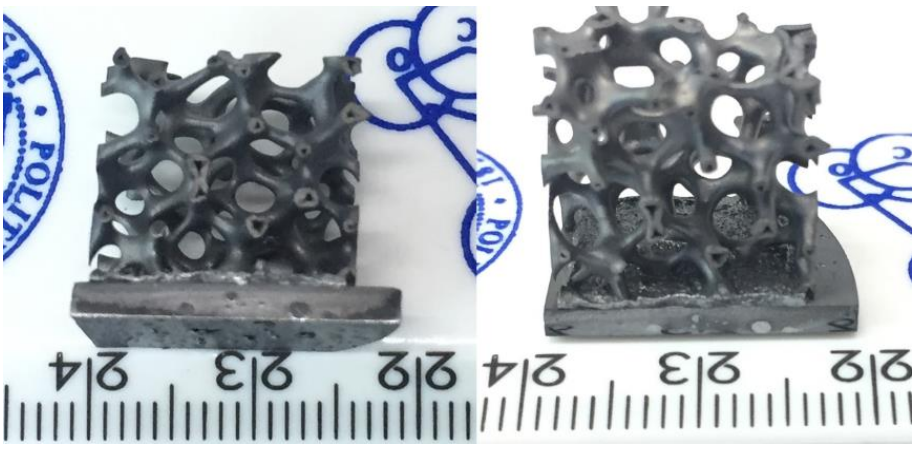

Figure 78 SiSiC disk to SiSiC foam joined by Mo-Wrap (two-step)

### 4.4.1 SiSiC disk to SiSiC foam joints: Morphology (SEM and EDS)

Sandwich structures **SiSiC disk to SiSiC** foam joints have few connecting points, in the joint cross-section, as shown in Figure 79. Joint is uniform, continuous and cracks free having thickness 200-250 µm. The joining conditions are well optimized to avoid any adverse effect on SiSiC which contains unreacted silicon. The continuous joint interface is well evident at higher magnification in Figure 80: both interfaces are continuous and well joined with in-situ formed molybdenum disilicide particles well embedded in the silicon matrix. In some spots (circled in Figure 80) there is a little capillary rise of joining material within SiC foam porosity as previously observed ( Figure 62).

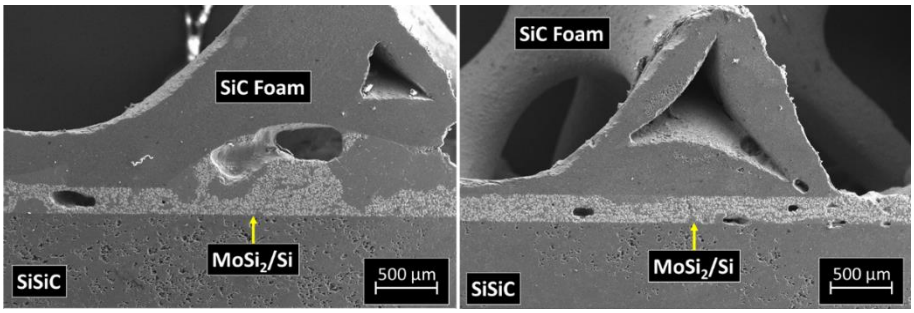


**Figure 79 SiSiC disk - SiSiC foam cross-section (Mo-Wrap, two steps)**

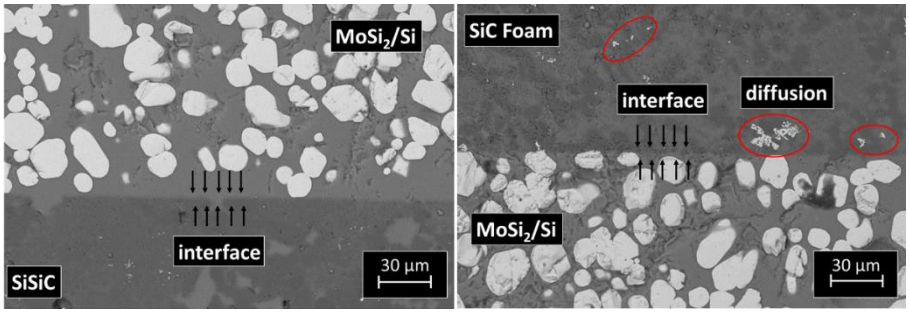


**Figure 80 SiSiC disk - SiSiC foam cross-section: joint interphase at higher magnification (backscattering)**

EDS analysis was done on SiSiC foam, SiSiC disk and joint interphase at different points, as shown in Figure 81.

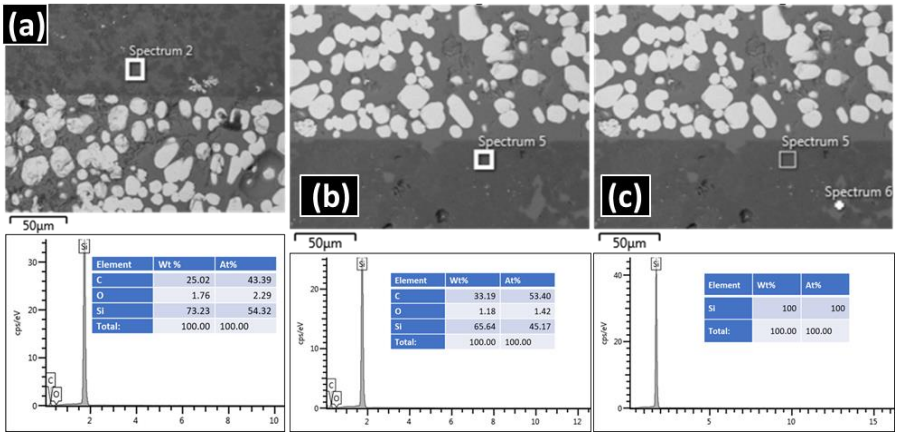


Figure 81 EDS analysis on SiSiC foam and SiSiC disks

The Mo-wrap joint elemental composition is same as detected in all Mo-Wrap joints, as shown in Figure 82.

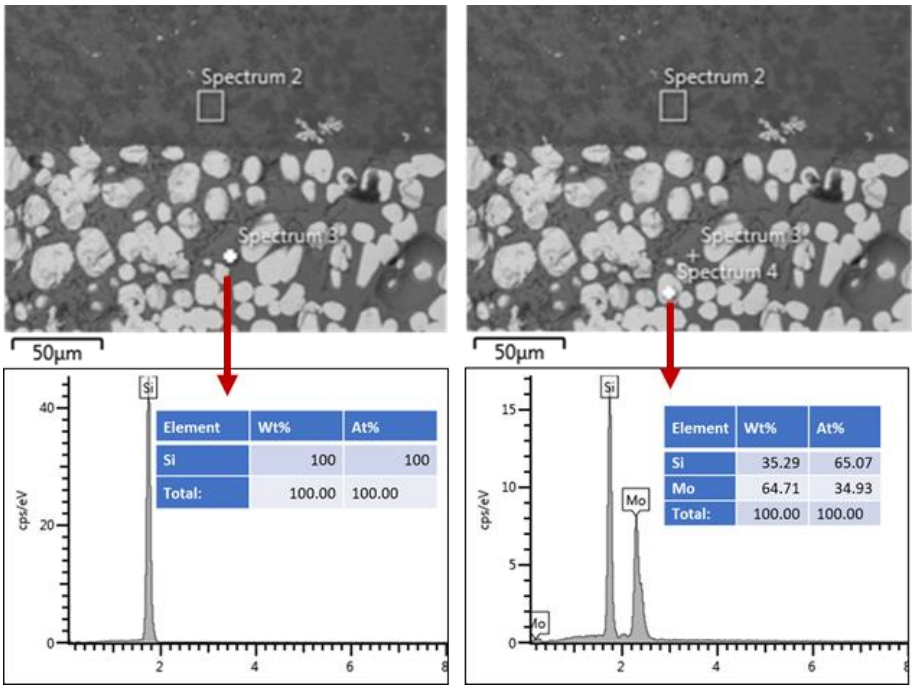


Figure 82 EDS analysis on SiSiC-SiC foam joint interphase

## 4.5 Nb-Wrap: Joining

Nb-Wrap was successfully used for joining uncoated C/SiC with the two step method described before and for monolithic SiC with the single step method, also described before. The development of Nb-Wrap was described in chapter 3.

Joint morphology (SEM), mechanical testing, X-Ray diffraction on fractured surfaces after mechanical tests, thermal/oxidation stability at 1100 $^{o}$C for 6 hours and microhardness are discussed in following sections.

### 4.5.1 Nb-Wrap to join uncoated C/SiC: Morphology (SEM, EDS) and XRD

The two-step (i) Si coat and (ii) Nb-Wrap joining approach was used to join uncoated C/SiC, as described in 4.2.4 for Mo-Wrap.

The surface morphology by SEM and elemental analysis by EDS of uncoated C/SiC composite is described in 4.1.4 and shown in Figure 42. The additional step of Si coat has improved the wettability of the substrate [205]. Joining material obtained by Nb-Wrap is an in-situ formed niobium disilicide ($NbSi_2$) particles embedded in a silicon matrix. EDS confirmed the presence of Nb and Si as elements within the joint interphase, as shown in Figure 84; XRD confirmed the presence of two phases, Si and NbSi2, as shown in Figure 85. Joints (400-450 µm thick) are continuous and $NbSi_2$ particles are well dispersed inside the Si matrix across the joining area, as shown in Figure 83.

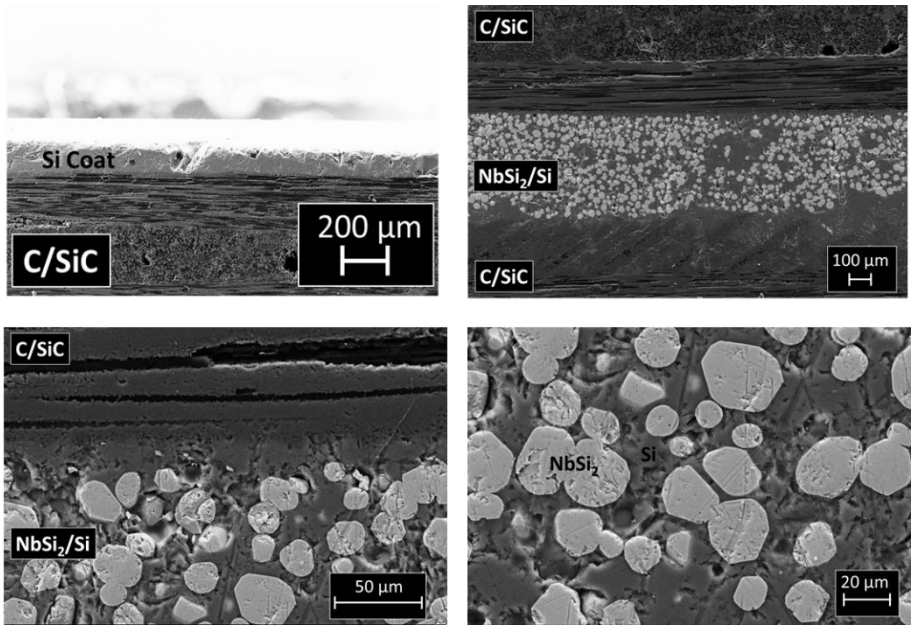


**Figure 83 uncoated C/SiC joined by Nb-Wrap: joint morphology**

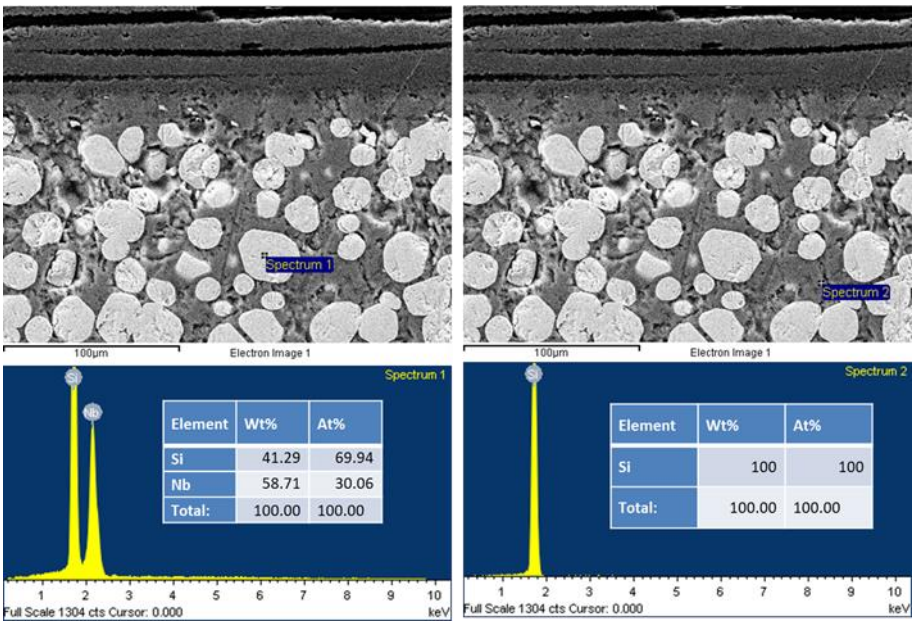


**Figure 84 uncoated C/SiC joined by Nb-Wrap: EDS of the joint**

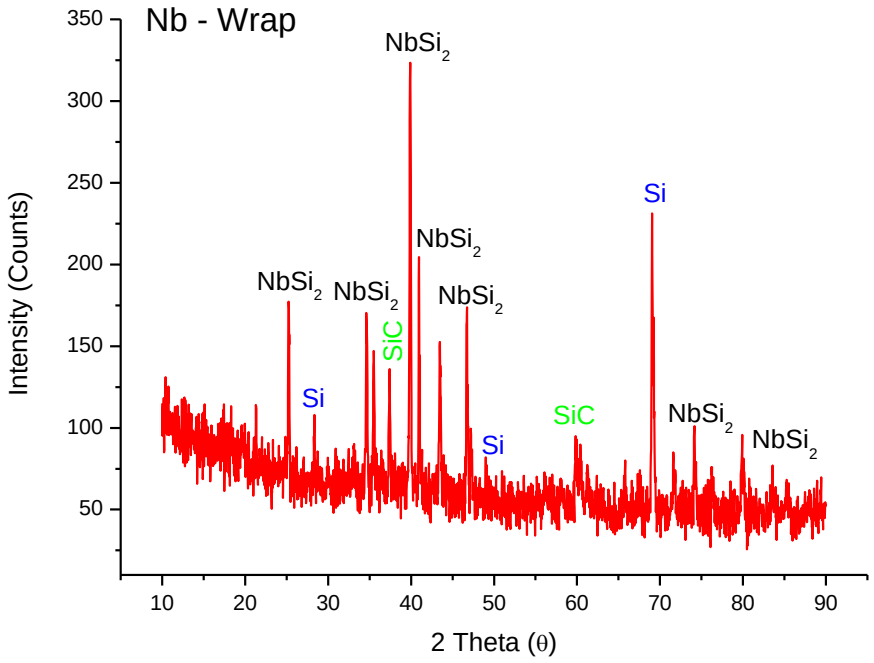


Figure 85 Typical XRD Patterns of Nb-Wrap joint fractured surface

XRD analysis shows the presence of three phases (i) Si (ii) NbSi2 and (iii) SiC, being $NbSi_2$/Si the joining material and SiC peaks are from the joined substrate.

## 4.5.2 Uncoated C/SiC joined by Nb-Wrap: Mechanical Tests (SLO at RT and HT)

Single lap off-set mechanical testing was done on uncoated C/SiC joined by Nb-Wrap at room and high temperature as discussed in 3.10.4.3 of chapter 3 and in section 4.1.5 for Mo-Wrap ones. Joint strength at room temperature was measured 19 MPa and 31 MPa at 1000 ºC; fracture surfaces are shown in Figure 86.

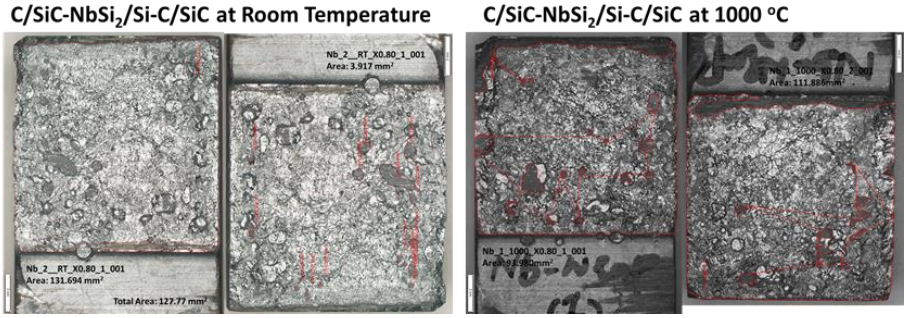


Figure 86 C/SiC-Nb-Wrap-C/SiC joints fractured surfaces tested at RT and HT by SLO

The BTDT temperature of $NbSi_2$ single crystal is reported to be of 400 °C [225]. For $NbSi_2$ polycrystaline structure the temperature dependence of slip morphology and elongation was classified into (i) small plastic strain between 800-1100 °C, (ii) steep slip bend above 1100 °C, and (iii) large elongation at/above 1400 °C [226], which are consistent with the joint strength measure at at room temperature (19 MPa) and at 1000 ºC (31 MPa) in this work.

### 4.5.3 Nb-Wrap to join monolithic SiC: Morphology (SEM)

Nb-Wrap was successfully used also to join monolithic SiC: joint microstructure (interface and interphase) is shown in Figure 87; the joint is well bonded, without any discontinuity, cracks and porosity having thickness of 200-300 µm. The joint is made of in-situ formed $NbSi_2$ particles well dispersed and embedded in a Si matrix. The joint interface exhibited good continuity between the joining material ($NbSi_2$/Si) and SiC.

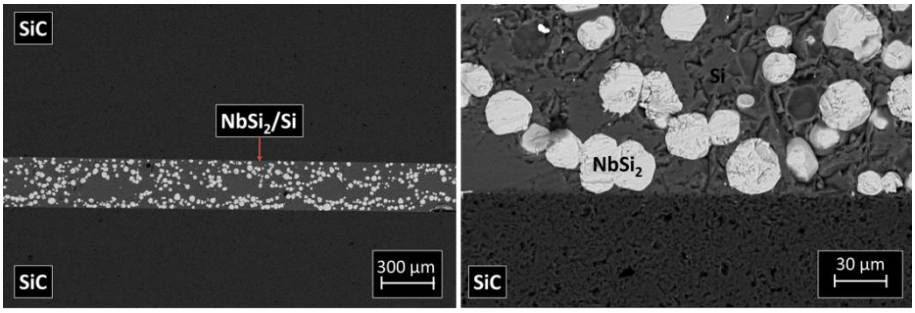


**Figure 87 SiC-Nb-Wrap-SiC joint morphology (backscattering)**

### 4.5.4 Nb-Wrap: Joined Monolithic SiC Oxidation Resistance (SEM)

***SiC-Nb-Wrap-SiC*** were tested at same conditions of Mo-wrap (4.1.3 and 4.2.3) 1100 ºC for 6 hours (with 10 ºC/min heating rate and air cooling). The joint interface after 6 hours thermal treatment at high temperature 1100 ºC is shown in Figure 88: joined samples remains firmly joined and morphologically identical to the untreated samples (Figure 87). Like MoSi2/Si, also $NbSi_2$/Si shows great potential to be used at high temperature.

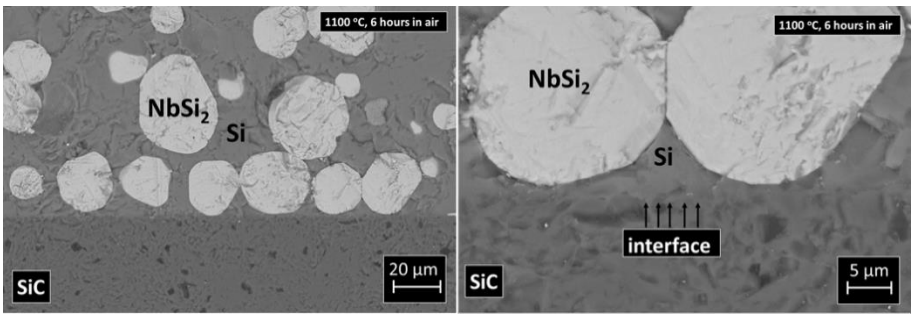


Figure 88 SiC-Nb-Wrap-SiC joint interface/interface after 6 hours at 1100 °C in air

## 4.6.5 $NbSi_2$ Micro-Hardness (Vickers Hardness)

The conventional micro-hardness test was carried out to measure the Vickers-hardness of $NbSi_2$ as described in 3.10.4.6.2 section of chapter 3. Imprints on $NbSi_2$ are shown in Figure 89, and the obtained Vickers-hardness values are presented in Table 16.

Like $MoSi_2$, $NbSi_2$ shows good resistance against deformation: imprints on $NbSi_2$ are small without any crack. Obtained values of micro-hardness at room temperature are in agreement with the as casted $NbSi_2$ (hardness values 1056 ± 48 MPa, reported in [227]).

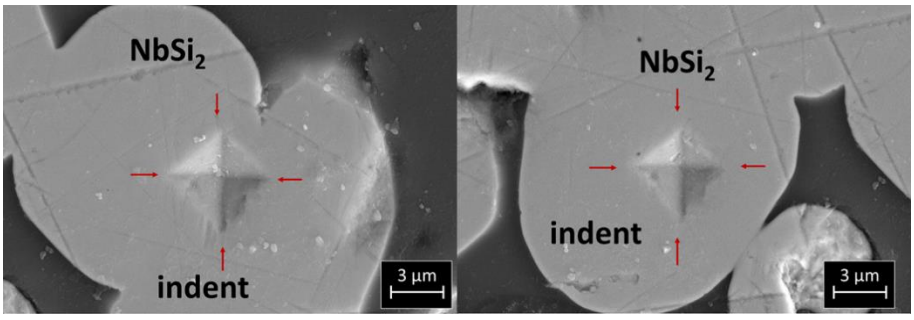


Figure 89 Micro-indentation on NbSi2 (Vickers Hardness)

Table 16 Vickers-hardness values of NbSi2

| Vickers hardness | $NbSi_2$ |
|---|---|
| 1 | 1222 |
| 2 | 1071 |
| 3 | 1091 |
| 4 | 1132 |

| | |
|---|---|
| 5 | 1071 |
| Avg | 1117 |
| MPa | $1.095 \times 10^4$ |

## 4.6 Ta-Wrap: Joining

Ta-Wrap was successfully used for joining uncoated C/SiC (two steps) and monolithic SiC (single step without prior coating). The development of Ta-Wrap is discussed in chapter 3 (Experimental).

Ta-Wrap was used in joining (i) **C/SiC-Ta-Wrap-C/SiC** and (ii) **SiC-Ta-Wrap-SiC.** Joint morphology (SEM), Mechanical testing, X-Ray diffraction (on fractured surfaces after the mechanical test), thermal/oxidation stability (at 1100 $^{o}$C for 6 hours) and microhardness of tantalum disilicide ($TaSi_2$) are discussed in following sections.

### 4.6.1 Ta-Wrap to join uncoated C/SiC: Morphology (SEM, EDS) and XRD

A two-step joining process was also used with Ta-Wrap for joining uncoated C/SiC as described in section 4.2.4 (for Mo-Wrap).

The surface morphology by SEM and elemental analysis by EDS of uncoated C/SiC composite is described in section 4.2.4 and shown in Figure 42.

Joining material obtained by Ta-Wrap is an in-situ formed tantalum disilicide ($TaSi_2$) particles embedded in silicon matrix. EDS confirm the presence of Ta and Si as elements within joint interphase, Figure 90, and XRD confirms the presence of two phases, as shown in Figure 92. Joints are continuous, crack-free (400-550 µm thick) and $TaSi_2$ particles are dispersed in Si matrix across the joining area, as shown in Figure 90.

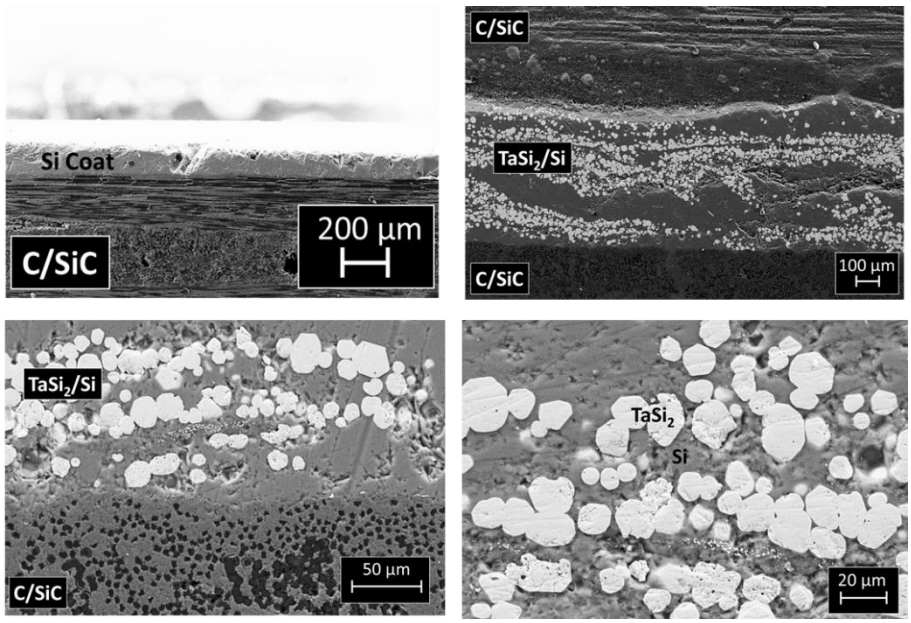


Figure 90 C/SiC-Ta-Wrap-C/SiC joint morphology

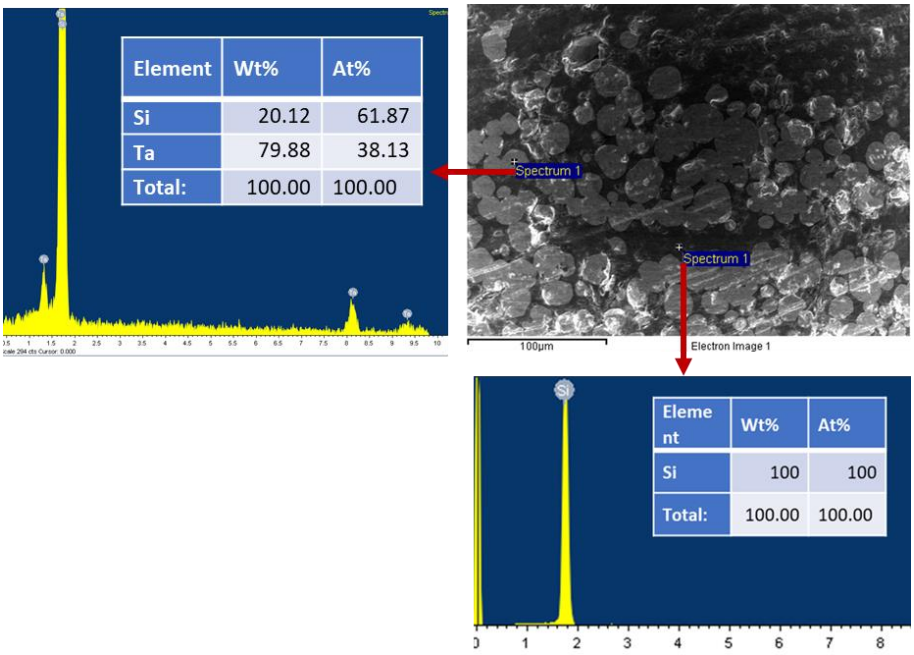


Figure 91 C/SiC-Ta-Wrap-C/SiC joint EDS

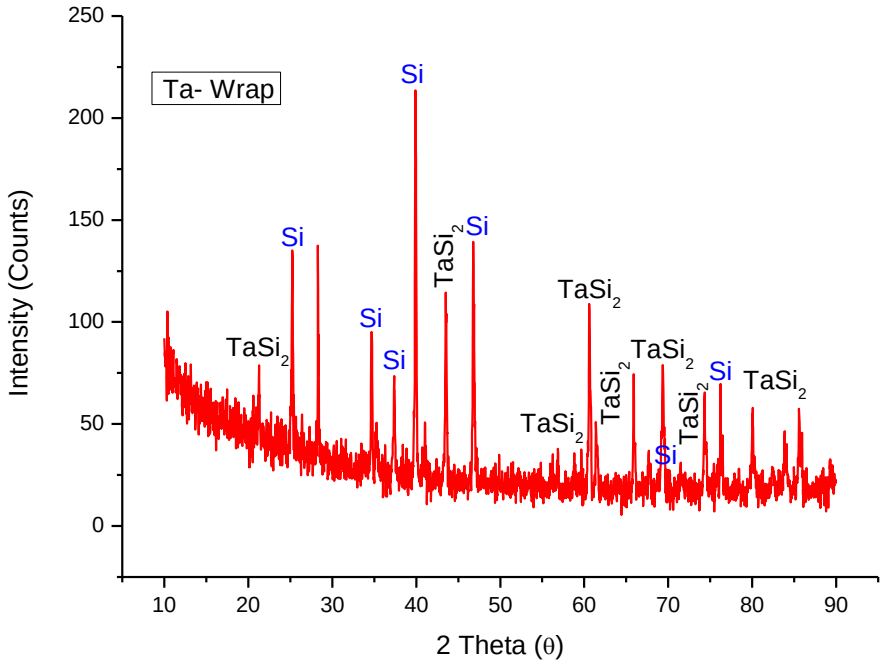


Figure 92 Typical XRD Patterns of Ta-Wrap joint: fractured surface after mechanical test

## 4.6.2 Uncoated C/SiC joined by Ta-Wrap: Mechanical Tests (SLO at RT and HT)

Single lap off-set mechanical tests were done **on Ta-Wrap joined uncoated C/SiC** at room and high temperature as discussed in 3.10.4.3 of chapter 3 and section 4.1.5 (for Mo-Wrap). Joint strength at room temperature was measured 5 MPa and at 17 MPa 1000 ºC; fracture surfaces are shown in Figure 93.

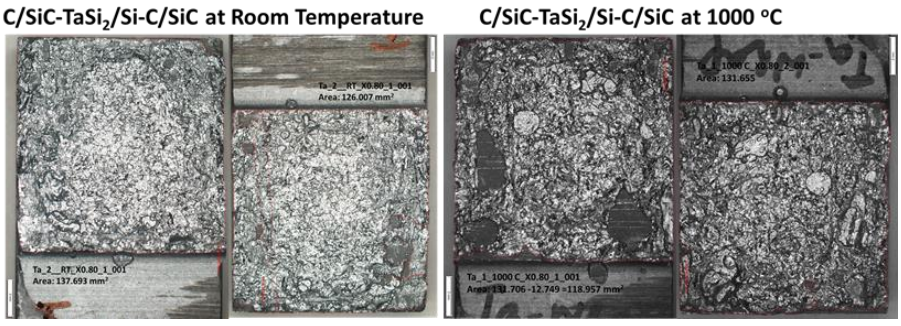


Figure 93 Ta-Wrap joined uncoated C/SiC: fracture surfaces tested at RT and HT by SLO

$TaSi_2$ single crystal had the slip flow above 600 °C and critical resolved shear stress of (basal) slip decrease with increasing temperature and exhibited a moderate peak at 1400 °C [207], which may explain the experimental results of a measure joint strength at room temperature of 5 MPa and of 17 MPa 1000 °C.

### 4.6.3 Ta-Wrap to join SiC: Morphology (SEM)

***SiC-Ta-Wrap-SiC*** joint microstructure is shown in Figure 94: the joint is 400-500 µm thick well bonded, without any discontinuity, cracks and porosity. The joint is made of an in-situ formed $TaSi_2$ particles well dispersed and embedded in Si matrix. The joint interface exhibited good continuity between the joining material ($TaSi_2$/Si) and SiC.

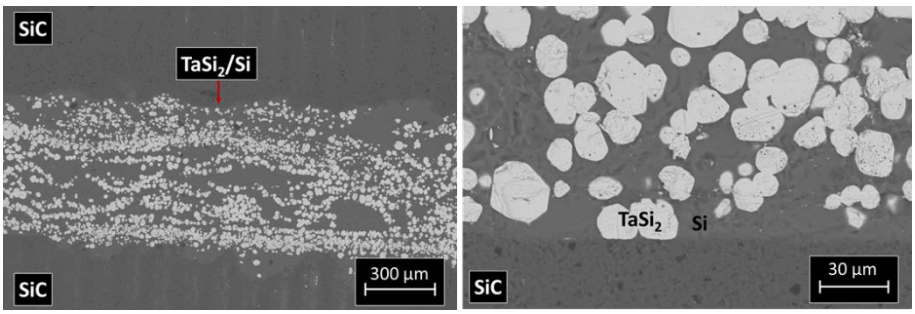


**Figure 94 SiC-Ta-Wrap-SiC joint morphology (backscattering)**

### 4.6.4 Ta-Wrap joined SiC: Oxidation Resistance (SEM)

***SiC-Ta-Wrap-SiC*** (monolithic SiC joints) were tested at same conditions as before (1100 °C for 6 hours). The joint interface after 6 hours is shown in Figure 95: joined samples remain firmly joined and unaffected by the thermal treatment (Figure 94). Like $MoSi_2$/Si and $NbSi_2$/Si, also $TaSi_2$/Si shows great potential to be used at high temperature.

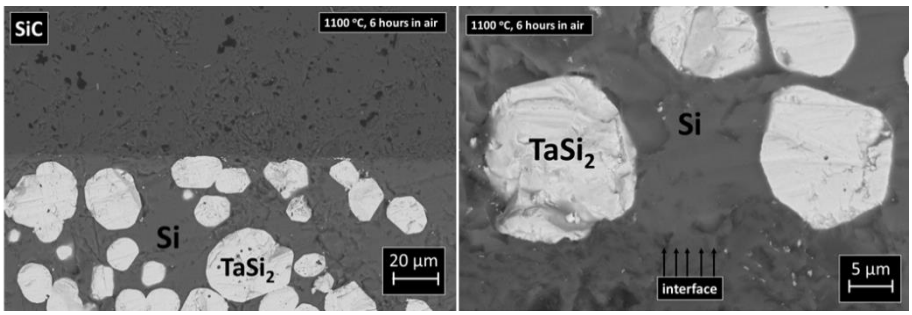


Figure 95 SiC-Ta-Wrap-SiC joint interface after 6 hours at 1100 °C in air

## 4.6.5 $TaSi_2$ Vickers Hardness

The Vickers micro-hardness test was carried out on $TaSi_2$ in-situ grown particles as described in 3.5.4.6.2 section of chapter 3. Imprints on $TaSi_2$ are shown in Figure 96, and the obtained Vickers-hardness values are presented in Table 17.

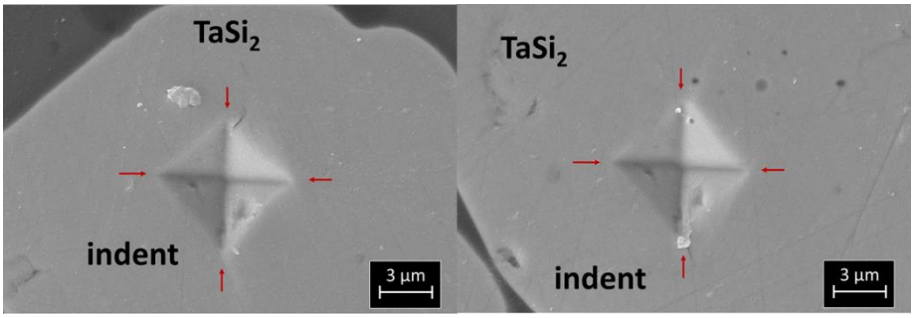


Figure 96 Micro-indentation on TaSi2 (Vickers Hardness)

Like $MoSi_2$ and $NbSi_2$, also $TaSi_2$ particles show the same behavior against the deformation with this load, without any visible crack initiated. The nanoindentation hardness value of some $TaSi_2$ fibers is reported 10.981 GPa [228], much similar to the values obtained in this thesis by micro-hardness testing.

Table 17 Vickers-hardness values of TaSi2

| Vickers hardness (MPa) | $TaSi_2$ |
|---|---|
| 1 | 1176 |
| 2 | 1052 |
| 3 | 1033 |
| 4 | 963 |
| 5 | 1091 |
| Avg | 1063 |
| MPa | $1.042 \times 10^4$ |

## 4.7 W-Wrap to join uncoated C/SiC

W-Wrap was successfully used for joining uncoated C/SiC (Two steps). The development of W-Wrap was described in chapter 3 (Experimental).

### 4.7.1 W-Wrap to join uncoated C/SiC: Morphology (SEM, EDS and XRD)

Joining material obtained by W-Wrap is an in-situ formed tungsten disilicide ($WSi_2$) particles embedded in a silicon matrix. EDS confirmed the presence of W and Si as elements within joint, as shown in Figure 98 and XRD confirms the presence of two phases shown in Figure 99. Sound W-wrap joints are shown in Figure 97, having thickness of 300-400 µm.

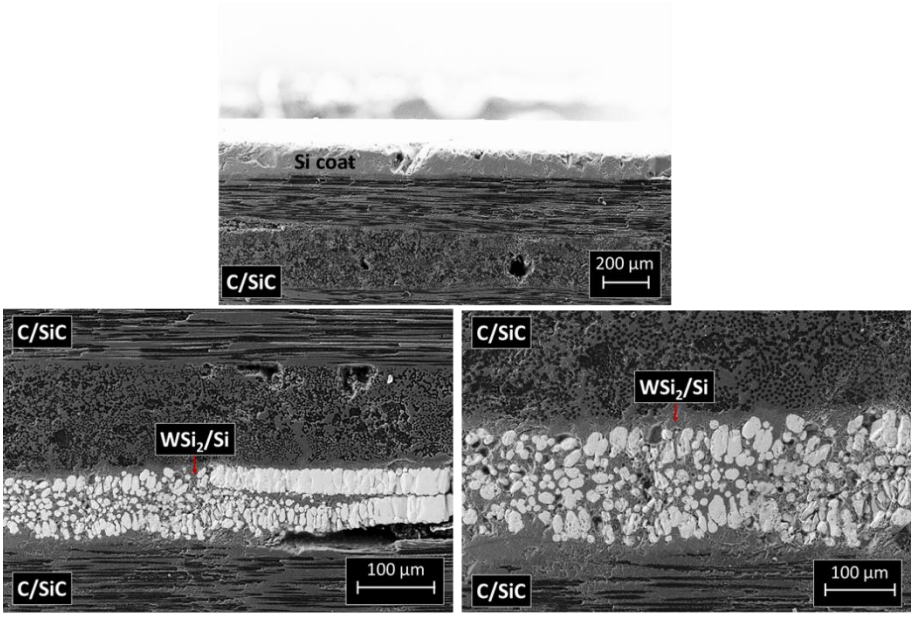


**Figure 97 uncoated C/SiC joined by W-Wrap: joint morphology**

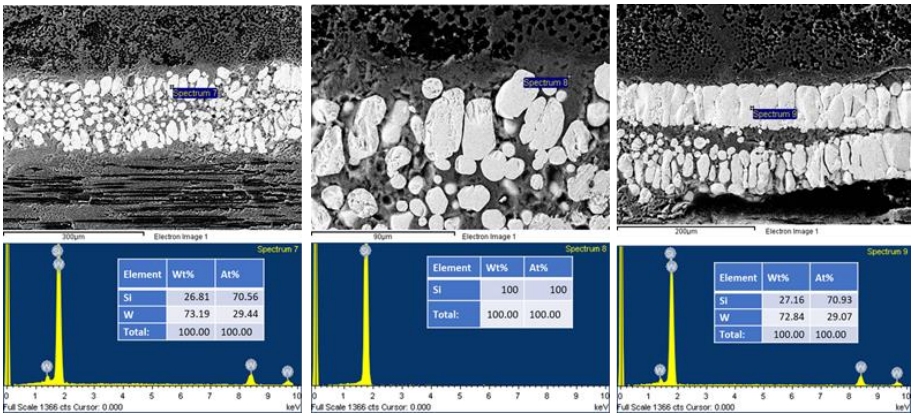


Figure 98 C/SiC-W-Wrap-C/SiC joint EDS

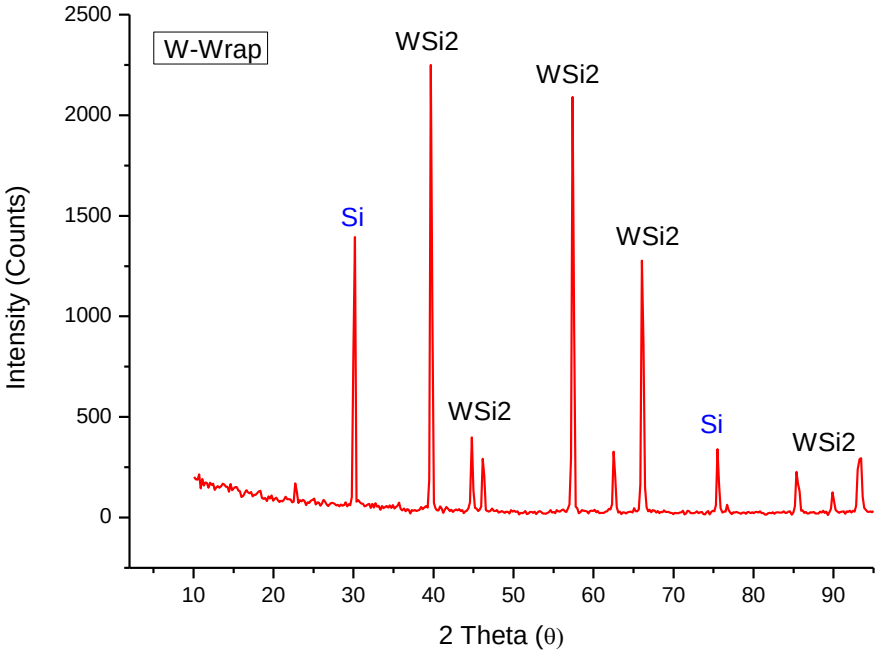


Figure 99 Typical XRD patterns of W-Wrap joints on fractured surface after mechanical test

## 4.8 Combo-Wrap

"Combo-Wraps," a combination of more than one Refractory Metal in a wrap, as described in 3.5 section of chapter 3.

### 4.8.1 MoW-Wrap: Morphology (SEM and EDS)

The two-step approach was adopted for MoW-Wrap for joining uncoated C/SiC as discussed section 4.1.4 (by Mo-Wrap).

Joining material obtained by MoW-Wrap is an in-situ formed tungsten disilicide (WSi2) and molybdenum disilicide ($MoSi_2$) particles well embedded in a silicon matrix having thickness of 350-450 µm. EDS confirm the presence of W, Mo and Si as elements within joint shown in Figure 100. **C/SiC-MoW-Wrap-C/SiC** are well joined, strong enough to be cut by a diamond blade without being previously embedded in resin. $WSi_2$ is easy to distinguish from MoSi2, since W has a higher atomic number than Mo, thus it is much brighter than $MoSi_2$; WSi2 also forms some ribbon-like areas, probably due to a still to be optimized thermal treatment, as shown in Figure 100. EDS analysis showed that the ribbon-like microstructure has a different composition of elements than the particle one, shown in Figure 101.

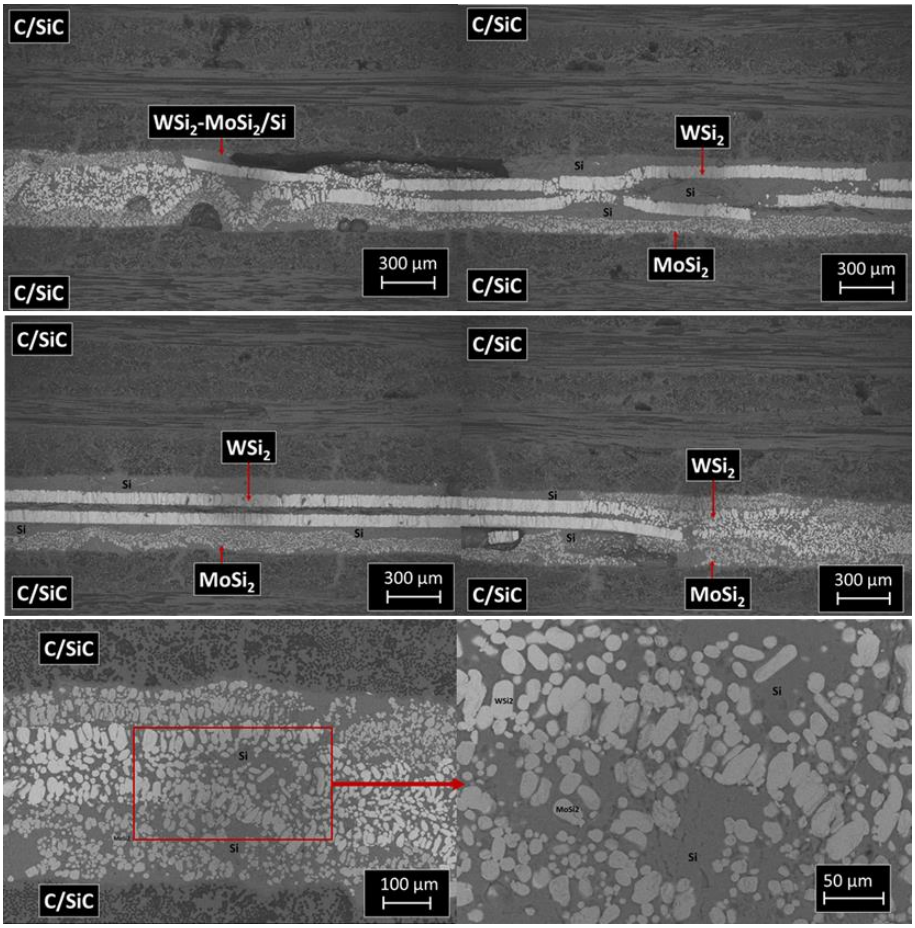


**Figure 100 MoW-Wrap- joint morphology**

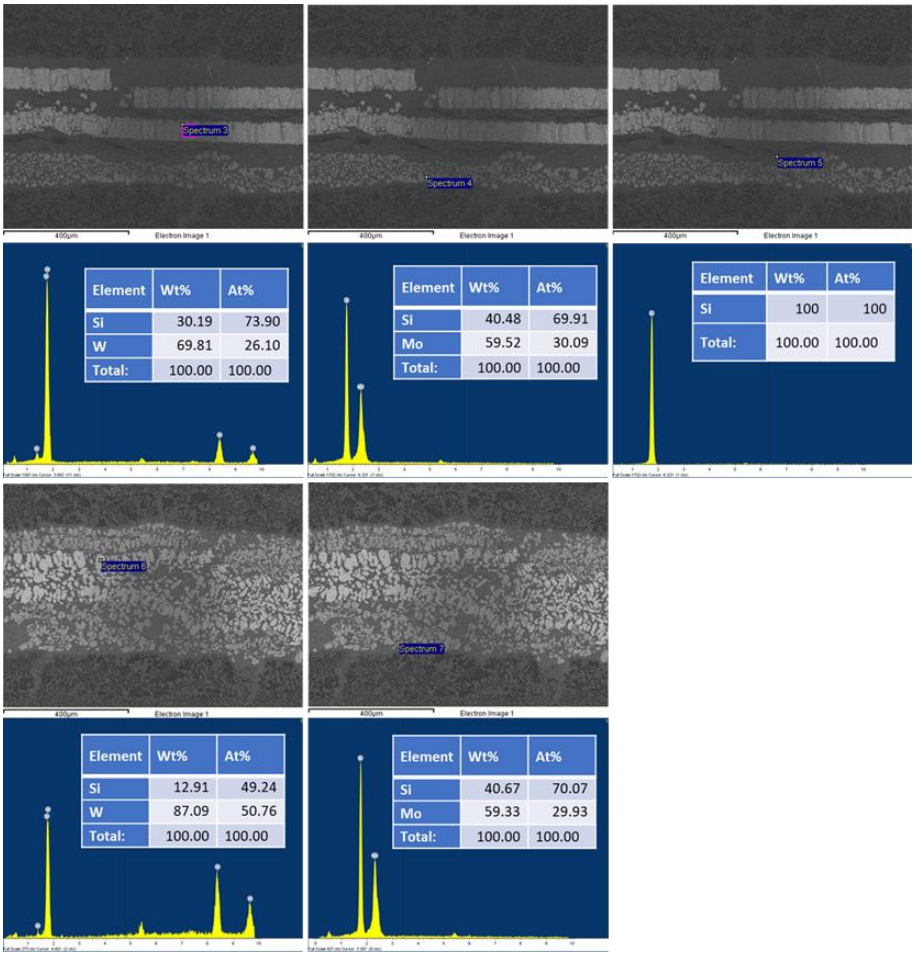


**Figure 101 MoW-Wrap- joint EDS in different regions**

## 4.9 Two Step joining with Cr and Si for uncoated C/SiC: (i) Cr-Coating and (ii) Si-joining

Chromium silicides have been used for joining the C/SiC (uncoated) in two steps (i) Chromium coating and (ii) Si joining, as shown in Figure 102.

Wettability of metals on carbon-based materials can be regarded as (i) reactive, if it forms carbides, (ii) inert, if not [229, 230].

Reactive metals such as (Al, Si, Ti and **Cr**) can form the carbides and improves the surface wettability. Pure Chromium (Cr) and Titanium (Ti) reacts with Carbon and forms chromium and titanium carbides. Several studies report that Cr wets carbon with a contact angle $\theta$ of 30-40 [229].

For this joining procedure, *not based on wraps*, but with the same aim of confining molten silicon, uncoated C/SiC was coated with chromium and then joined with Silicon.

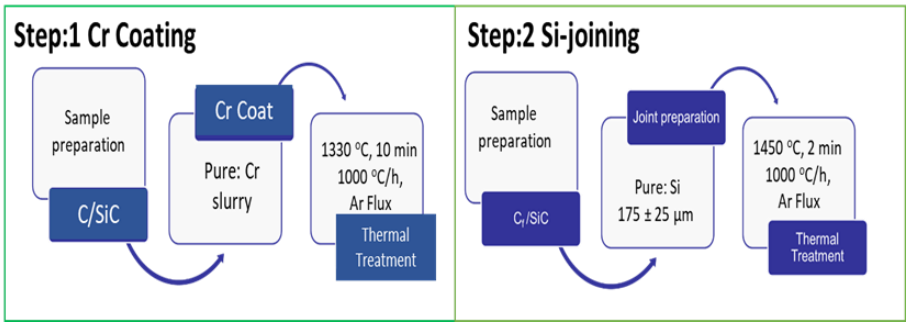


**Figure 102 Two-step joining of uncoated C/SiC (i) Cr-Coat and (ii) Si-joining**

### 4.9.1 Cr/Si joints: Morphology (SEM, EDS and XRD)

Chromium coating forms two layers on the surface (i) Chromium oxide layer (green layer) and (ii) Cr-C-Si layer (silver-like), as shown in Figure 103. The green oxide layer is brittle and can easily be removed by peeling; the silver-like layer (Cr-C-Si layer) is then uncovered. XRD-analysis on both layers were performed (Figure 103), chromium oxide (**$Cr_2O_3$**) was detected in the green layer, chromium carbide (**$Cr_7C_3$**) and chromium silicide (**$Cr_3Si$**) on the silver-like layer. EDS analysis on the silver-like layer confirmed the presence of Cr, C and Si as the only elements, Figure 105.

The morphology of the uncoated C/SiC and after coating with chromium was investigated with SEM. Figure 104 shows the surface morphology of C/SiC after Cr coating at 1330 ºC for 10 minutes under an inert environment. Approximately 10 µm thick layer of Cr-C-Si was measured, after deposition. Roughness and typical morphology of the coating is visible at higher magnification.

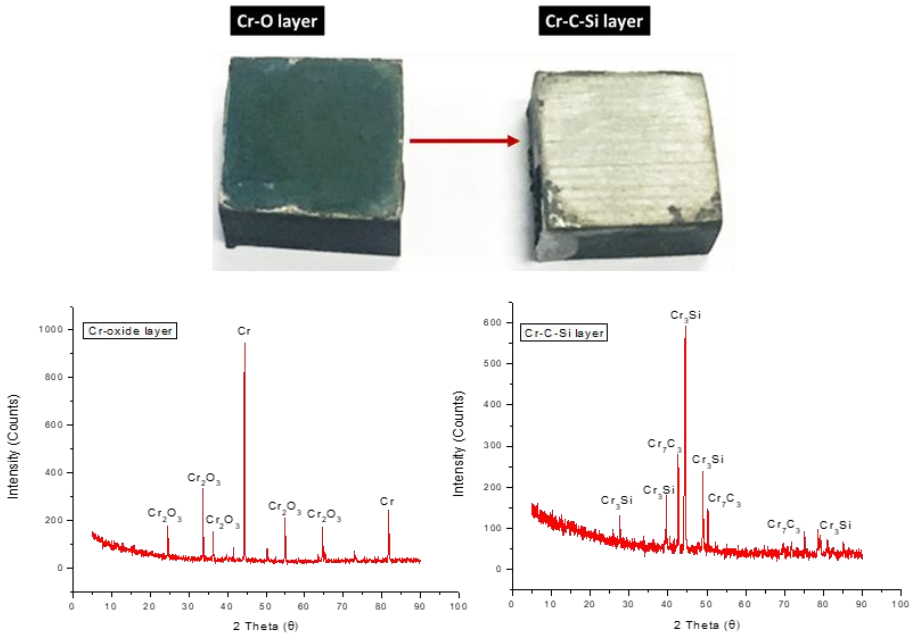


**Figure 103 Chromium coating on C/SiC and XRD-analysis**

The EDS spectrum of the coated C/SiC is composed of Chromium (Cr), carbon (C) and Silicon (Si) peaks, Figure 105, in agreement with XRD analysis of Figure 103.

The joint microstructure is shown in Figure 106: the joint is well bonded, without any discontinuity, cracks and porosity having thickness of 100-150 µm. The joint interface at higher magnification is shown in Figure 107: it is composed of two phases (i) pure Si and (ii) chromium silicides ($CrSi_2$). EDS investigation (Figure 108) on the joint cross-section, line scanning (Figure 109) across the joint and XRD (Figure 110) analysis on the fractured surface after mechanical tests are in agreement: two elements (Cr and Si) and one phase $CrSi_2$ were detected. SiC phase detected in XRD-Patterns are from the substrate (C/SiC).

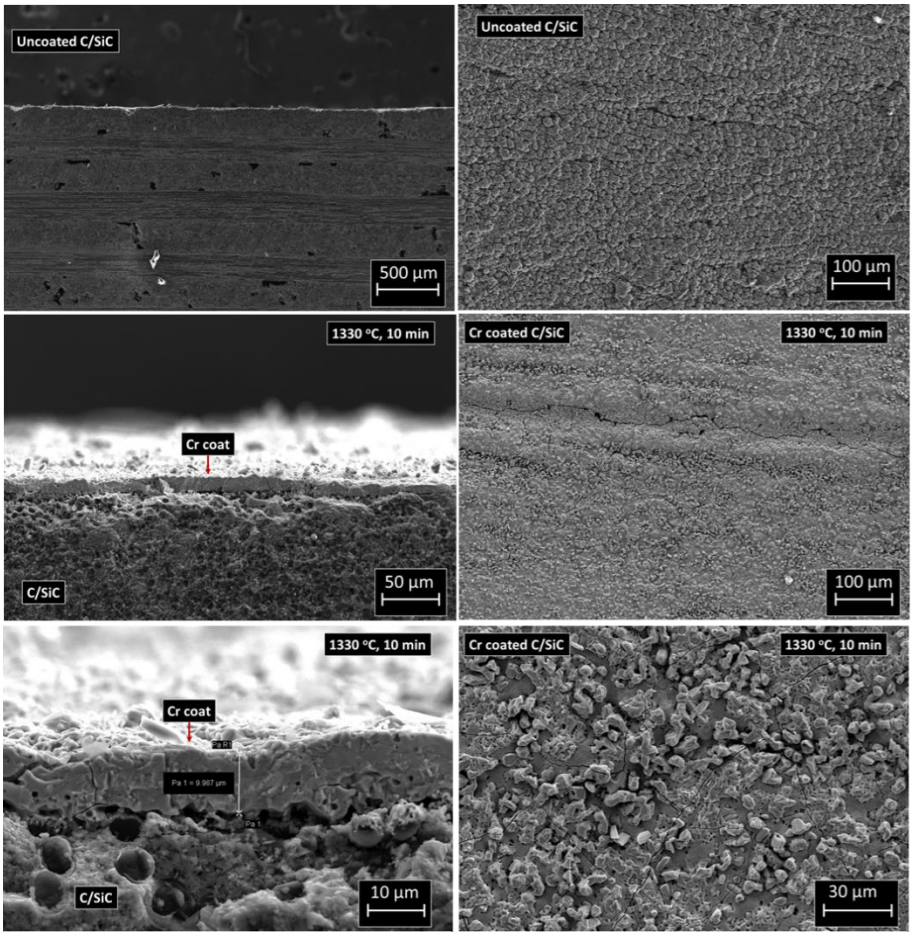


**Figure 104 Morphology of uncoated C/SiC and Cr coated C/SiC**

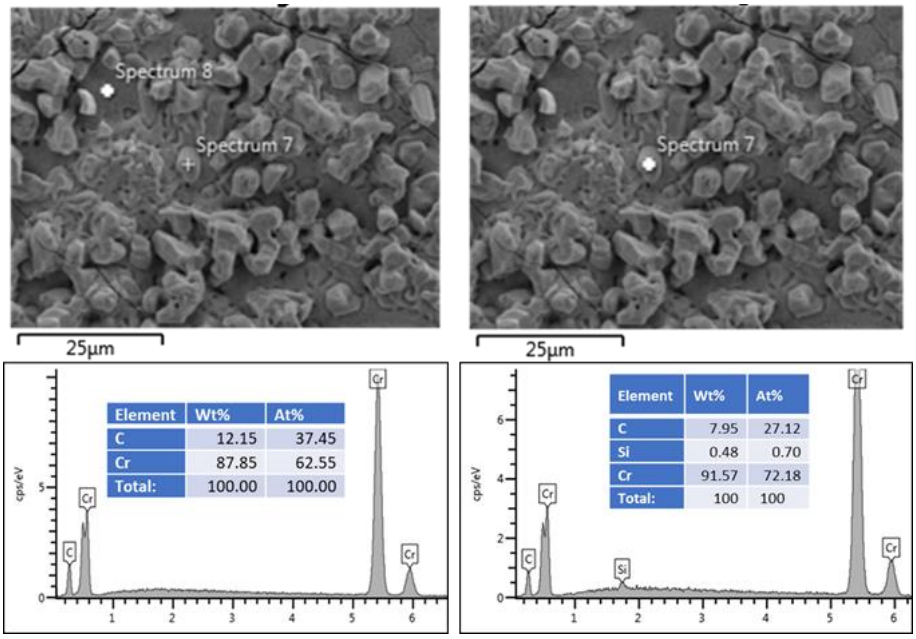


Figure 105 EDS analysis on Cr coated C/SiC

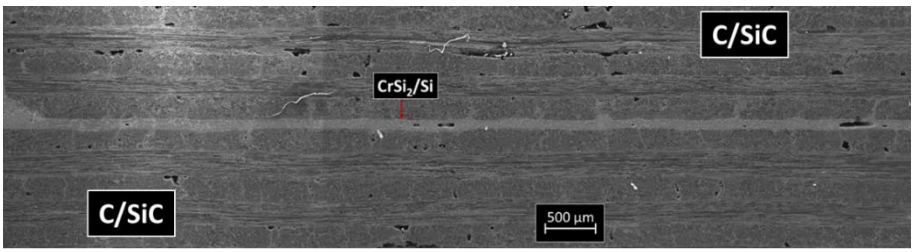


Figure 106 Cr/Si joined uncoated C/SiC: joint morphology

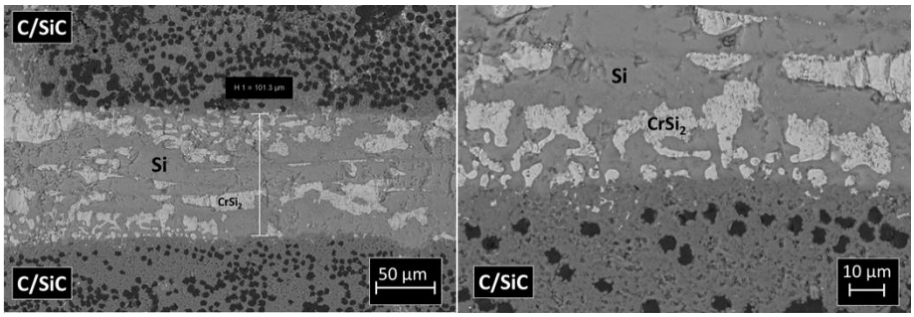


Figure 107 Cr/Si joined uncoated C/SiC: joint morphology (higher magnification)

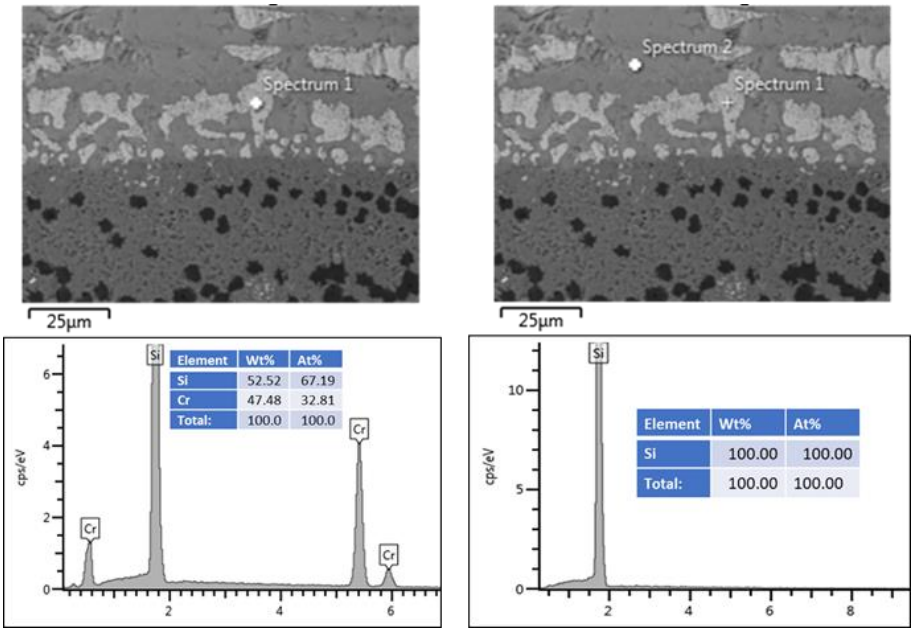


**Figure 108 Cr/Si joined uncoated C/SiC: EDS analysis of the joint**

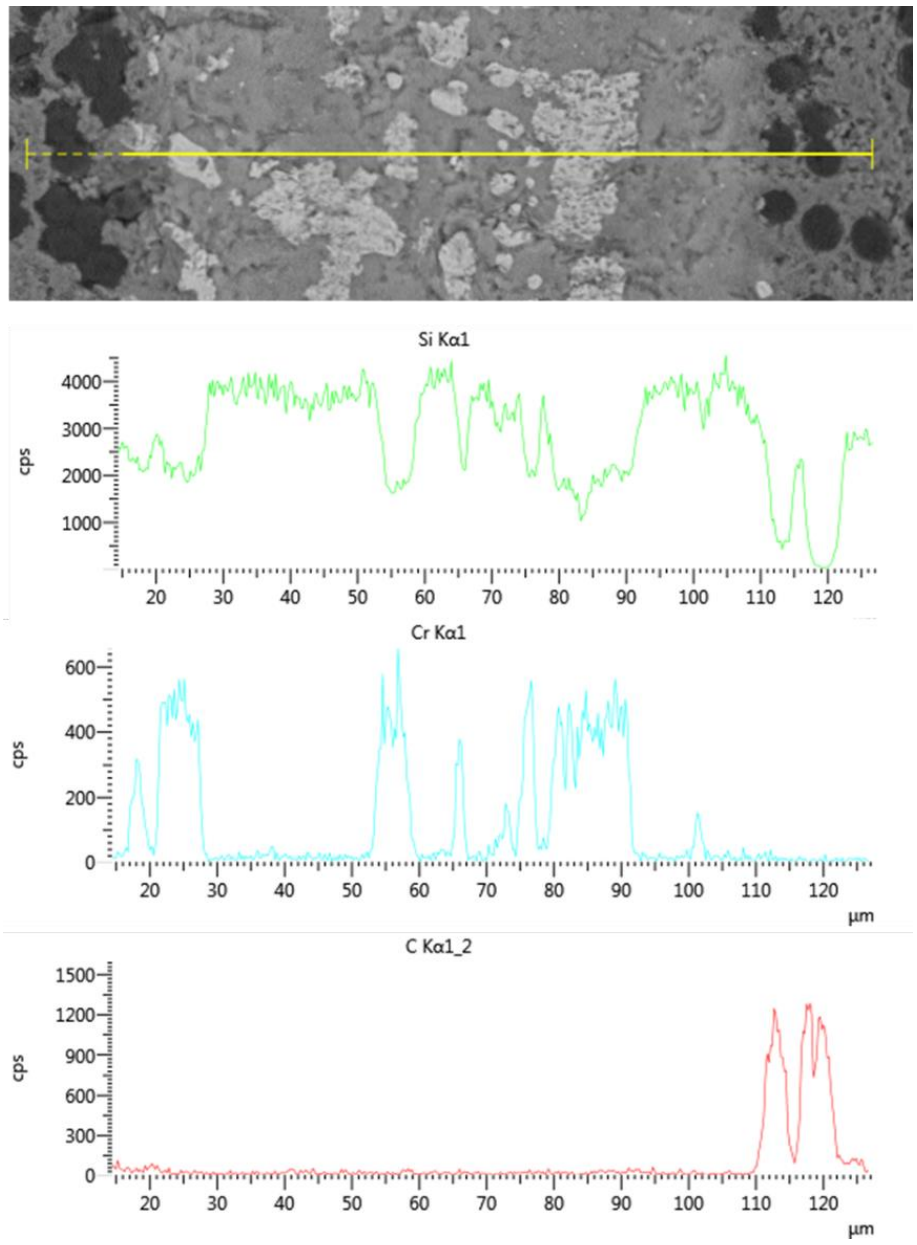


**Figure 109 Cr/Si joined uncoated C/SiC: line scanning analysis on the joint**

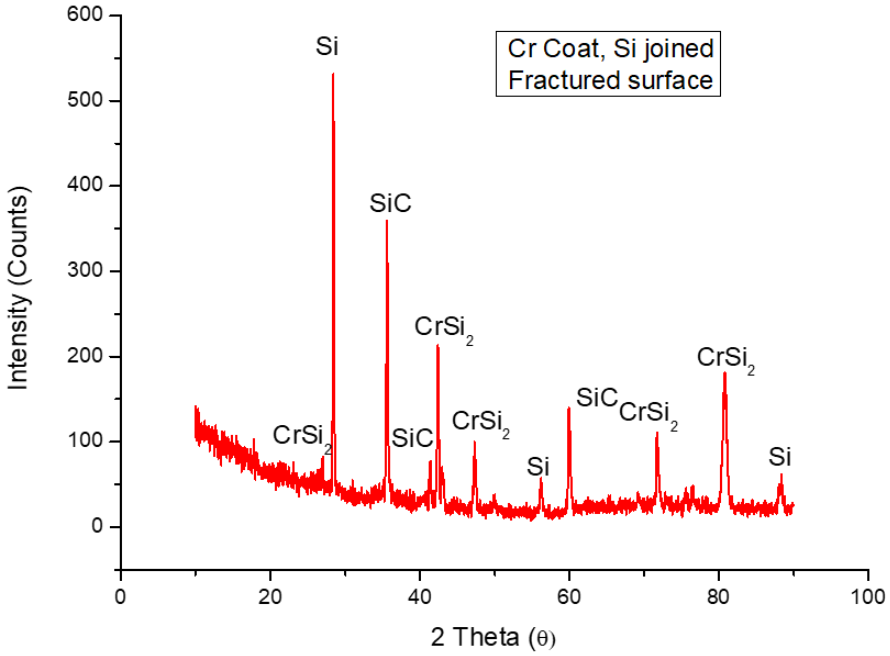


Figure 110 Cr/Si joined uncoated C/SiC: XRD- analysis on fractured surface after mechanical testing

## 4.9.2 Mechanical Testing of Cr-Coat-Si joined C/SiC-CrSi-Cr-C/SiC (SLO-Shear)

Single lap off-set testing as for SiC-Mo-Wrap-SiC joints discussed in 3.10.4.2 section of chapter 3 was used in this case, at room temperature in triplicate. The SLO results are reported in Table 18. Delamination was observed in sample 1 only, as shown in Figure 111.

Table 18 C/SiC-CrSiCr-C/SiC SLO results

| Sample | Maximum force (N) | MPa | Cross-head displacement (mm) at Max. Force | Remark |
|---|---|---|---|---|
| 1 | 963 | 35 | 0.110 | Delamination |
| 2 | 480 | 14.15 | 0.102 | |
| 3 | 674 | 18.72 | 0.179 | |

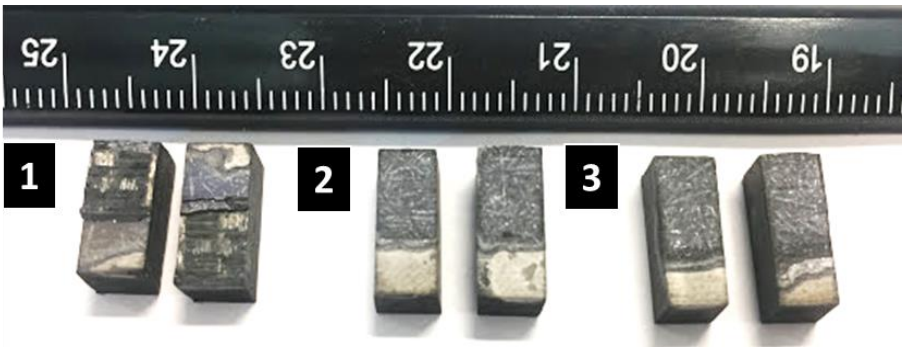


**Figure 111 Cr/Si joined uncoated C/SiC: fractured samples after SLO**

# Conclusion and future insights

The aim of this Ph.D. thesis was to develop a new joining process and material for joining (i) SiC-based ceramics matrix composites, (ii) monolithic ceramics and (iii) SiC foams, for aerospace and energy applications.

A new pressure-less tailorable joining technique named "RM-Wrap" (Refractory metals = RM = Mo, Nb, Ta, W) was developed. RM-Wrap named after the elemental arrangement shown in Figure 112. The wrap is a pressure-less joining technique optimised at 1450 $^{o}$C, with a dwell of 5 minutes, in an inert environment (Argon flux) with a heating rate of 1000 $^{o}$C per hour.

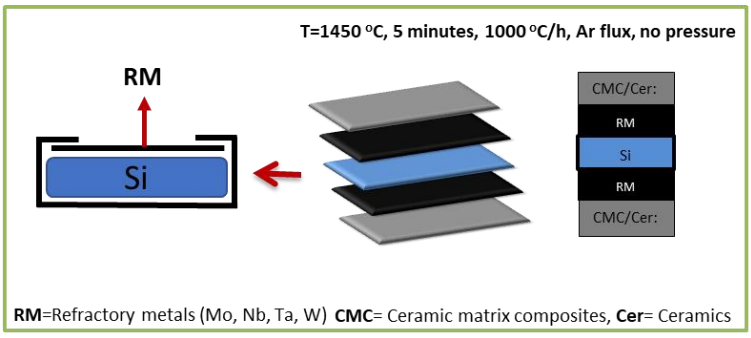


Figure 112 RM-Wrap joining the scheme

The RM-wrap joining technology has successfully worked to join SiC based materials (ceramic matrix composites, foams and monolithic ceramics) and oxide ceramics (alumina and mullite). The joints were characterized for morphology, microstructure, composition, oxidation resistance, thermal shock resistance and mechanical strength.

Morphological analysis by FESEM showed continuous, crack free and well bonded joint interfaces with monolith ceramics and composites irrespective of fibre orientation. Elemental and phase composition of the joining material were investigated in detail using EDS and XRD which showed joint microstructure consists of in-situ formed composite made of a silicon matrix with silicides of molybdenum ($MoSi_2$ in case of Mo-Wrap), niobium ($NbSi_2$ in case of Nb-Wrap), tantalum ($TaSi_2$ in case of Ta-Wrap) and tungsten ($WSi_2$ in case of W-Wrap).

The silicides are oxidation resistive and high temperature stable materials highly demanded in aerospace and energy (solar, nuclear) production applications.

Besides the tailoring capability of RM-Wraps, Combo-wrap has been developed which has more possibilities to develop/tailor the required phases from more than one element according to end user requirements. MoW-Wrap was developed to use $MoSi_2$ and $WSi_2$ together as joining materials. C/SiC was successfully joined using MOW-Wrap.

Thermal and oxidation stability of joints were carried out at 1100 $^oC$ for 30 minutes (for CMC joints) and 6 hours (for monolithic ceramic joints). FESEM analysis before and after thermal ageing showed unaffected joint interfaces and phases.

Sandwich structures (joined with Mo-Wrap) were tested for thermal shock resistance at 1100 $^oC$ in the air. Three cycles on the sandwich structures were performed, resulting in composition unchanged and unaltered joined structure.

Joints were mechanically tested in three different modes (i) compression for CMC, monolithic ceramics and sandwich structures, (ii) tensile for sandwich and (iii) torsion monolithic ceramics. Joint strength was higher than the interlaminar shear strength of composites as the fracture was always observed in composites. In case of SiC a mixed failure (cohesive and adhesive) was found, which may signify that the joint strength is comparable to substrate one; in case of sandwich structures, the SiC foams failed first.

**The key strengths of "RM-Wrap" joining are:**

- It can pressure-less join monolithic ceramics (oxide and non-oxide), ceramic matrix composites (CMC) in a similar (to themselves) and dissimilar configuration.
- It can join oxide (mullite) to non-oxide (SiC) substrates
- It can join highly porous SiC foams to C/SiC composites (sandwich structures) avoiding detrimental infiltration of the joining material
- It can join CVD-SiC coated and uncoated substrates
- RM-Wrap joining has excellent reproducibility
- Short processing route
- Joining material are in-situ formed composites made of a silicon matrix reinforced with silicides of refractory metals
- Excellent oxidation and thermal shock resistance (1100 $^oC$ to RT up to 6 hours)

- Pressureless tailorable joining technique with the quantity of each phase tailored according to end user requirements

For the first time ever, superior properties of refractory metal silicides have been exploited in joining. It can be concluded from the obtained results that RM-Wrap joining offers many attractive advantages and its scope can be further extended to develop the combo-wrap based on MoNb, MoTa and several other possible combinations. Moreover, research may be extended to join other advanced materials such as oxide/oxide composites, borides ($NbB_2$, $TiB_2$, $ZrB_2$, $TaB_2$, $HfB_2$), carbides (NbC, TaC, TiC, ZrC, HfC), and nitrides (NbN, TaN, TiN, ZrN, HfN).

Since the developed joining materials have high melting point and excellent oxidation resistance, other possible research areas could be the joining and coatings by RM-Wrap for (i) hydrothermal corrosion-, (ii) neutron irradiation- and (iii) oxidation-resistant materials for high temperature and high pressure environments.

The silicon matrix of the in-situ formed joining material could be the limitation, considering its melting temperature in comparison with the melting temperature of refractory metal silicides and its behavior in a hydrothermal environment. The silicon matrix can be replaced/changed or alloyed with other material to overcome these shortcomings.

In fact, initial work on some of the above-mentioned future research prospects has already been started and will continue after this dissertation.

# Annex 1

## List of Publications

1. **Pressure-less joining of C/SiC and SiC/SiC by a MoSi2/Si composite**. International Journal of Applied Ceramic Technology, (doi:10.1111/ijac.12631) 2017. **14**(3): p. 305-312

2. **SiC foam sandwich structures obtained by Mo-wrap joinin*g***. Materials Letters, (doi.org/10.1016/j.matlet.2018.03.105) 2018. **221**: p. 240-243.

## List of Conferences

1. **Joining of monolithic ceramics (SiC, Alumina, Mullite) by "RM-Wrap" at** 14th International Conference on Modern Materials and Technologies, Perugia (June 4-8) 2018, Italy.

2. **Coatings on SiC-based components for Light Water Reactors** at 42nd International Conference & Exposition on Advanced Ceramics & Composites**, Daytona Beach, Florida, USA** 21-26 January 2018

3. **Thermal shock performance of Sandwich structures obtained by "Mo-Wrap"** at 42nd International Conference & Exposition on Advanced

Ceramics & Composites**, Daytona Beach, Florida, USA** 21-26 January 2018

4. **"Re-wrap" method (Refractory metals Re=Mo, Nb and Ta) for joining of ceramics and CMC** at 42nd International Conference & Exposition on Advanced Ceramics & Composites**, Daytona Beach, Florida, USA** 21-26 January 2018

5. **Foam sandwich structures obtained by Mo-$Si_2$ joining** at 41st International Conference & Exposition on Advanced Ceramics & Composites**, Daytona Beach, Florida, USA** 22-27 January 2017.

6. **Torsion tests on SiC/SiC joined by "Mo-wrap" method** at 41st International Conference & Exposition on Advanced Ceramics & Composites**, Daytona Beach, Florida, USA** 22-27 January 2017.

7. **Joining of C/SiC for aerospace applications** at 40th International Conference & Exposition on Advanced Ceramics & Composites**, Daytona Beach, Florida, USA** 24-29 January 2016.

8. **Joining of C/SiC Ceramic Composites to themselves and to Ti-6Al-4V for aerospace applications** at the 23rd AIDAA Conference on Aeronautics and Astronautics**, Turin Italy** 17-19 November 2015

9. **Joining of Al-6016 To Al-foam Using Zn-based Alloys to Obtain Aluminum Foam Sandwich (AFS) For Aerospace Applications** at the 23rd AIDAA Conference on Aeronautics and Astronautics**, Turin Italy** 17-19 November 2015

## External Research Activities

**1.** **Activity:** High temperature tests on "RM-Wrap" joined C/SiC **Funding:** 9th Call of KMM-VIN research fellowship**. Host Institute:** Institute of Physics of Materials, Czech Academy of Sciences, Brno, Czech Republic. (August 2017).

# References


1. Bansal, N.P. and J. Lamon, *Ceramic Matrix Composites: Materials, Modeling and Technology*. 2014: John Wiley & Sons.
2. Ferraris, M., *5.11 Joining and Machining of CMCs*, in *Comprehensive Composite Materials II*, P.W.R. Beaumont and C.H. Zweben, Editors. 2018, Elsevier: Oxford. p. 293-307.
3. Singh, M., N. Kondo, and R. Asthana, *Chapter 12 - Manufacturing of Ceramic Components using Robust Integration Technologies*, in *Green and Sustainable Manufacturing of Advanced Material*. 2016, Elsevier: Oxford. p. 295-308.
4. Hald, H., et al. *Development of a nose cap system for X-38*. in *Proceedings of International Symposium Atmospheric Reentry Vehicles and Systems*. 1999.
5. Mühlratzer, A. and M. Leuchs, *Applications of Non-Oxide CMCs.* High temperature ceramic matrix composites, 2001: p. 288-298.
6. Fischer, W.P.P., U. Trabandt, and W. Zeiss, *Concept Studies of a Ceramic Engine Heat Shield for RLV Application*. 2001, SAE International.
7. Katoh, Y., et al., *Current status and recent research achievements in SiC/SiC composites.* Journal of Nuclear Materials, 2014. **455**(1): p. 387-397.
8. Corman, G.S. and K.L. Luthra, *5.13 Development History of GE's Prepreg Melt Infiltrated Ceramic Matrix Composite Material and Applications*, in *Comprehensive Composite Materials II*. 2018, Elsevier: Oxford. p. 325-338.
9. *PW GTF-CFM LEAP market share*. 2012 February 15, 2012; Available from: https://leehamnews.com/2012/02/15/pw-gtf-cfm-leap-market-share/.
10. *CFM: LEAP engine orders exceed 10,000*. 2016 2/8/2016; Available from: https://www.compositesworld.com/news/cfm-leap-engine-orders-exceed-10000.
11. Levy, D. *Ceramic matrix composites take flight in LEAP jet engine*. 2017 January 4, 2017; Available from: https://phys.org/news/2017-01-ceramic-matrix-composites-flight-jet.html.
12. Croft, J. *GE: CMCs may yield 1.5% fuel burn cut in Leap engines*. 2012; Available from: https://www.flightglobal.com/news/articles/ge-cmcs-may-yield-15-fuel-burn-cut-in-leap-engine-374337/.

13. Noda, T., et al., *Effect of nuclear data and impurities on the evaluation of induced activity of CVI SiCf/SiC composites.* Fusion Engineering and Design, 2002. **61-62**(Supplement C): p. 711-716.
14. Prasad, N.E. and R. Wanhill, *Aerospace Materials and Material Technologies*. 2017: Springer.
15. Campbell, F.C., *Joining: understanding the basics*. 2011: ASM International.
16. Singh, M., et al., *Ceramic Integration and Joining Technologies: From Macro to Nanoscale*. Ceramic Integration and Joining Technologies: From Macro to Nanoscale. 2011.
17. Messier Jr, R.W., *Joining of Materials and Structures*. 2004, ElscvierButterworth-Heinemann.
18. Gianchandani, P.K., et al., *Pressure-less joining of C/SiC and SiC/SiC by a MoSi2/Si composite.* International Journal of Applied Ceramic Technology, 2017. **14**(3): p. 305-312.
19. Taylor, A. 26-12-2017]; Available from: https://www.twi-global.com/technical-knowledge/job-knowledge/ceramics-materials-joining-and-applications-054/Alan
20. Casalegno, V., *JOINING OF COMPOSITE MATERIALS FOR NUCLEAR FUSION APPLICATIONS*, in *Material Science and Technology*. 2006, Politecnico Di Torino

Turin, italy. p. 376.
21. Jacobson, D.M. and G. Humpston, *Principles of brazing*. 2005: Asm International.
22. *Mechanical Joining*. 08-02-2018; Available from: https://www.swantec.com/technology/mechanical-joining/.
23. Wang, M., et al., *Silicon Carbide whiskers reinforced polymer-based adhesive for joining C/C composites.* Materials & Design, 2016. **99**: p. 293-302.
24. Wang, X., J. Wang, and H. Wang, *Preparation of high-temperature organic adhesives and their performance for joining SiC ceramic.* Ceramics International, 2013. **39**(2): p. 1365-1370.
25. Wang, X.-z., J. Wang, and H. Wang, *Preparation and performance of a heat-resistant organic adhesive obtained via a liquid SiC precursor.* International Journal of Adhesion and Adhesives, 2012. **35**: p. 17-20.
26. Fernie, J., R. Drew, and K. Knowles, *Joining of engineering ceramics.* International Materials Reviews, 2009. **54**(5): p. 283-331.
27. Ferraris, M., et al., *Glass-ceramic joining and coating of SiC/SiC for fusion applications.* Journal of Nuclear Materials, 1998. **258-263**(PART 2 B): p. 1546-1550.
28. Salvo, M., et al., *Joining of CMCs for thermonuclear fusion applications.* Journal of Nuclear Materials, 1996. **233–237, Part 2**: p. 949-953.

29. Herrmann, M., et al., *Joining technology—A challenge for the use of SiC components in HTRs.* Nuclear Engineering and Design, 2016. **306**: p. 170-176.
30. Ahmad, S., et al., *Application of Nd2O3–Al2O3–SiO2 glass solder for joining of silicon carbide components.* Journal of the European Ceramic Society, 2016. **36**(7): p. 1559-1569.
31. Ferraris, M., et al., *Glass-ceramic joining and coating of SiC/SiC for fusion applications.* Journal of nuclear materials, 1998. **258**: p. 1546-1550.
32. Katoh, Y., et al., *Microstructure and mechanical properties of low-activation glass-ceramic joining and coating for SiC/SiC composites.* Journal of nuclear materials, 2000. **283**: p. 1262-1266.
33. Casalegno, V., et al., *CaO-Al2O3 glass-ceramic as a joining material for SiC based components: A microstructural study of the effect of Si-ion irradiation.* Journal of Nuclear Materials, 2018. **501**: p. 172-180.
34. Gozzelino, L., et al., *He-irradiation effects on glass-ceramics for joining of SiC-based materials.* Journal of Nuclear Materials, 2016. **472**: p. 28-34.
35. Katoh, Y., et al., *Radiation-tolerant joining technologies for silicon carbide ceramics and composites.* Journal of Nuclear Materials, 2014. **448**(1–3): p. 497-511.
36. Ferraris, M., M. Salvo, and F. Smeacetto, *Cordierite–mullite coating for SiCf/SiC composites.* Journal of the European Ceramic Society, 2002. **22**(13): p. 2343-2347.
37. Ferraris, M., et al., *Effects of neutron irradiation on glass ceramics as pressure-less joining materials for SiC based components for nuclear applications.* Journal of Nuclear Materials, 2012. **429**(1-3): p. 166-172.
38. Ferraris, M., et al., *Joining of machined SiC/SiC composites for thermonuclear fusion reactors.* Journal of Nuclear Materials, 2008. **375**(3): p. 410-415.
39. Fu, Q., et al., *A Multi-interlayer LMAS Joint of C/C–SiC Composites and LAS Glass Ceramics.* Journal of Materials Science & Technology, 2015. **31**(5): p. 467-472.
40. Bernardo, E., et al., *Advanced ceramics from preceramic polymers modified at the nano-scale: A review.* Materials, 2014. **7**(3): p. 1927-1956.
41. Lewinsohn, C.A., et al., *Fabrication and Joining of Ceramic Compact Heat Exchangers for Process Integration.* International Journal of Applied Ceramic Technology, 2012. **9**(4): p. 700-711.
42. Khalifa, H.E., et al., *Fabrication and characterization of joined silicon carbide cylindrical components for nuclear applications.* Journal of Nuclear Materials, 2015. **457**: p. 227-240.
43. Triantou, K., et al., *Performance of cork and ceramic matrix composite joints for re-entry thermal protection structures.* Composites Part B: Engineering, 2017. **108**: p. 270-278.

44. Wang, X., J. Wang, and H. Wang, *Joining of SiC ceramics via a novel liquid preceramic polymer (V-PMS).* Ceramics International, 2015. **41**(6): p. 7283-7288.
45. Fan, S., et al., *Progress of ceramic matrix composites brake materials for aircraft application.* Rev. Adv. Mater. Sci, 2016. **44**: p. 313-325.
46. Tong, Q. and L. Cheng, *Liquid Infiltration Joining of 2D C/SiC Composite*, in *Science and Engineering of Composite Materials*. 2006. p. 31.
47. Krenkel, W., T. Henke, and N. Mason. *In-situ joined CMC components*. in *Key Engineering Materials*. 1997. Trans Tech Publ.
48. Renz, R., G. Seifert, and W. Krenkel, *Integration of CMC Brake Disks in Automotive Brake Systems.* International Journal of Applied Ceramic Technology, 2012. **9**(4): p. 712-724.
49. Tong, Q. and L. Cheng, *Liquid infiltration joining of 2D C/SiC composite.* Science and Engineering of Composite Materials, 2006. **13**(1): p. 31-36.
50. Singh, M., *Affordable, Robust Ceramic Joining Technology (ARCJoinT).* 1998.
51. Singh, M. and J. Kiser, *Joining of silicon carbide-based ceramics by reaction forming method.* 1997.
52. Sekulić, D.P., *Advances in brazing: science, technology and applications*. 2013: Elsevier.
53. Kohyama, A., S. Dong, and Y. Katoh, *Development of SiC/SiC Composites by Nano-Infiltration and Transient Eutectoid (NITE) Process*, in *26th Annual Conference on Composites, Advanced Ceramics, Materials, and Structures: A: Ceramic Engineering and Science Proceedings*. 2008, John Wiley & Sons, Inc. p. 311-318.
54. Hinoki, T., et al., *Development of Joining and Coating Technique for SiC and SiC/SiC Composites Utilizing Nite Processing*, in *Mechanical Properties and Performance of Engineering Ceramics and Composites: Ceramic Engineering and Science Proceedings*. 2008, John Wiley & Sons, Inc. p. 399-405.
55. Jung, H.-C., et al., *Development of a shear strength test method for NITE–SiC joining material.* Journal of Nuclear Materials, 2011. **417**(1): p. 383-386.
56. Dong, P., et al., *Understanding the spark plasma sintering from the view of materials joining.* Scripta Materialia, 2016. **123**: p. 118-121.
57. Basu, B. and K. Balani, *Advanced structural ceramics*. 2011: John Wiley & Sons.
58. Dong, H., et al., *Microstructure and mechanical properties of SiC-SiC joints joined by spark plasma sintering.* Ceramics International, 2016. **42**(13): p. 14463-14468.
59. Kopeliovich, D.D. *Spark plasma sintering*. 01/06/2012; Available from: http://www.substech.com/dokuwiki/doku.php?id=spark_plasma_sintering&do=recent&DokuWiki=e579a03e5..

60. Suárez, M., et al., *Challenges and opportunities for spark plasma sintering: a key technology for a new generation of materials*, in *Sintering Applications*. 2013, InTech.
61. Rizzo, S., et al., *Joining of C/SiC composites by spark plasma sintering technique.* Journal of the European Ceramic Society, 2014. **34**(4): p. 903-913.
62. Herrmann, M., et al., *Laser-supported joining of SiC-fiber/SiCN ceramic matrix composites fabricated by precursor infiltration.* Journal of the European Ceramic Society, 2014. **34**(12): p. 2913-2924.
63. Lippmann, W., et al., *Laser joining of silicon carbide—a new technology for ultra-high temperature resistant joints.* Nuclear Engineering and Design, 2004. **231**(2): p. 151-161.
64. Jung, Y.-I., et al., *Microstructures of laser bonded SiC ceramics with Zr interlayers.* Journal of Nuclear Materials, 2014. **455**(1–3): p. 586-590.
65. Shukla, M. and S. Ghosh, *Microwave Joining of Ceramics: An Overview.* 2016.
66. Han, S., et al., *Microwave assisted Self-propagating High-temperature Synthesis for joining SiC ceramics and SiC/SiC composites by Ni-Al system.* Applied Mechanics & Materials, 2014.
67. Bruce, R.W., et al., *Microwave assisted reactive brazing of ceramic materials*. 2006, Google Patents.
68. Wang, W., et al. *Microwave Joining of 95Al2O3 Using Interlayer Containing SiC*. in *Key Engineering Materials*. 2008. Trans Tech Publ.
69. Palaith, D., et al., *Microwave joining of ceramics.* MRS Online Proceedings Library Archive, 1988. **124**.
70. Srinath, M.S., A.K. Sharma, and P. Kumar, *A new approach to joining of bulk copper using microwave energy.* Materials & Design, 2011. **32**(5): p. 2685-2694.
71. Bansal, A., et al., *Characterization of bulk stainless steel joints developed through microwave hybrid heating.* Materials Characterization, 2014. **91**: p. 34-41.
72. Bajpai, P.K., I. Singh, and J. Madaan, *Joining of natural fiber reinforced composites using microwave energy: Experimental and finite element study.* Materials & Design, 2012. **35**: p. 596-602.
73. Meek, T. and R. Blake, *Ceramic—ceramic seals by microwave heating.* Journal of materials science letters, 1986. **5**(3): p. 270-274.
74. Aravindan, S. and R. Krishnamurthy, *Joining of ceramic composites by microwave heating.* Materials Letters, 1999. **38**(4): p. 245-249.
75. Al-Assafi, S. and D.E. Clark, *Microwave joining of ceramics: A study on joining alumina both directly and with alumina gel.* MRS Online Proceedings Library Archive, 1992. **269**.
76. Zhao, Y.N., et al. *Microwave Joining Alumina Ceramics Using Al-Si Alloy Powders at Low Temperature*. in *Advanced Materials Research*. 2013. Trans Tech Publ.

77. Shukla, M., et al., *Fabrication of Reliable Joints of Alumina Ceramics by Microwave-Assisted Reactive Brazing Technique.* MATERIALS TRANSACTIONS, 2016. **57**(3): p. 392-396.
78. Shukla, M., et al., *Microwave-assisted brazing of alumina ceramics for electron tube applications.* Bulletin of Materials Science, 2016. **39**(2): p. 587-591.
79. Suryanarayana, C., J.J. Moore, and R.P. Radtke, *Novel Methods of BRAZING Dissimilar Materials.* Advanced materials & processes, 2001. **159**(3): p. 29-31.
80. Gutmanas, E.Y. and I. Gotman, *Reactive synthesis of ceramic matrix composites under pressure.* Ceramics International, 2000. **26**(7): p. 699-707.
81. Rapp, R.A., A. Ezis, and G.J. Yurek, *Displacement reactions in the solid state.* Metallurgical Transactions, 1973. **4**(5): p. 1283-1292.
82. Cook, G.O. and C.D. Sorensen, *Overview of transient liquid phase and partial transient liquid phase bonding.* Journal of Materials Science, 2011. **46**(16): p. 5305-5323.
83. Gale, W.F. and D.A. Butts, *Transient liquid phase bonding.* Science and Technology of Welding and Joining, 2004. **9**(4): p. 283-300.
84. Saito, N., et al., *Wettability and transient liquid phase bonding of hafnium diboride composite with Ni–Nb alloys.* Journal of Materials Science, 2012. **47**(24): p. 8454-8463.
85. *Active Brazes*. 2018; Available from: http://www.vbcgroup.com/products/brazing/active.
86. M.B, U., et al., *Current Issues and Problems in the Joining of Ceramic to Metal*, in *Joining Technologies*, M. Ishak, Editor. 2016, InTech: Rijeka. p. Ch. 08.
87. Akselsen, O.M., *Advances in brazing of ceramics.* Journal of Materials Science, 1992. **27**(8): p. 1989-2000.
88. Bartolomé, J.F., et al., *Mullite/Mo interfaces formed by intrusion bonding.* Journal of the European Ceramic Society, 2004. **24**(5): p. 785-790.
89. Cockeram, B.V., *Flexural Strength and Shear Strength of Silicon Carbide to Silicon Carbide Joints Fabricated by a Molybdenum Diffusion Bonding Technique.* Journal of the American Ceramic Society, 2005. **88**(7): p. 1892-1899.
90. Martinelli, A.E., et al., *Neutron diffraction and finite-element analysis of thermal residual stresses on diffusion-bonded silicon carbide-molybdenum joints.* Journal of the American Ceramic Society, 1999. **82**(7): p. 1787-1792.
91. Mun, J.D., A.P. Sutton, and B. Derby, *Grain growth and texture changes in a Ni foil during diffusion bonding to ZrO2.* Philosophical Magazine A, 1997. **76**(2): p. 289-305.
92. Mun, J.D., B. Derby, and A.P. Sutton, *Texture change in Ni and Cu foils on diffusion bonding to zirconia.* Scripta Materialia, 1997. **36**(1): p. 1-6.

93. Cockeram, B., *The diffusion bonding of silicon carbide and boron carbide using refractory metals*. 1999, Bettis Atomic Power Lab., West Mifflin, PA (US).
94. Xiong, H.-P., et al., *Joining of Cf/SiC composite with a Cu–Au–Pd–V brazing filler and interfacial reactions.* Journal of the European Ceramic Society, 2014. **34**(6): p. 1481-1486.
95. Xiong, H.-P., et al., *Interfacial reactions and joining characteristics of a Cu–Pd–V system filler alloy with Cf/SiC composite.* Ceramics International, 2014. **40**(6): p. 7857-7863.
96. Halbig, M.C., et al., *Characterization of silicon carbide joints fabricated using SiC particulate-reinforced Ag-Cu-Ti alloys.* Ceramics International, 2013. **39**(4): p. 4151-4162.
97. Liu, Y., Z. Huang, and X. Liu, *Joining of sintered silicon carbide using ternary Ag–Cu–Ti active brazing alloy.* Ceramics International, 2009. **35**(8): p. 3479-3484.
98. Liu, Y., et al., *Microstructure of reaction layer and its effect on the joining strength of SiC/SiC joints brazed using Ag-Cu-In-Ti alloy.* Journal of Advanced Ceramics, 2014. **3**(1): p. 71-75.
99. Tian, W.-B., et al., *Joining of SiC with Si infiltrated tape-cast TiB2–C interlayer: Effect of interlayer composition and thickness on the microstructure and mechanical properties.* Materials Science and Engineering: A, 2011. **530**: p. 580-584.
100. Riccardi, B., et al., *Status of the European R&D activities on SiCf /SiC composites for fusion reactors.* Fusion Engineering and Design, 2000. **51-52**: p. 11-22.
101. Riccardi, B., et al., *Development of homogeneous joining techniques for SiC/SiCf composites*, in *Fusion technology 1998*. 1998.
102. Herrmann, M., W. Lippmann, and A. Hurtado, *High-temperature stability of laser-joined silicon carbide components.* Journal of Nuclear Materials, 2013. **443**(1–3): p. 458-466.
103. Rosa, R., et al., *Microwave assisted combustion synthesis in the system Ti–Si–C for the joining of SiC: Experimental and numerical simulation results.* Journal of the European Ceramic Society, 2013. **33**(10): p. 1707-1719.
104. Jacques, E., et al., *Joining Silicon Carbide Plates by Titanium Disilicide-Based Compound.* Powder Metallurgy and Metal Ceramics, 2014. **52**(9-10): p. 606-611.
105. Chen, X., et al., *Microstructure, mechanical properties, and bonding mechanism of ultrasonic-assisted brazed joints of SiC ceramics with ZnAlMg filler metals in air.* Ceramics International, 2014. **40**(1, Part A): p. 683-689.
106. Jung, Y.-I., et al., *Microstructures of diffusion bonded SiC ceramics using Ti and Mo interlayers.* Journal of Nuclear Materials, 2013. **441**(1–3): p. 510-513.

107. Singh, M., et al., *Microstructure and mechanical properties of joints in sintered SiC fiber-bonded ceramics brazed with Ag-Cu-Ti alloy.* Materials Science and Engineering A, 2012. **557**: p. 69-76.
108. Liu, G.W., et al., *SiC/SiC and SiC/Kovar joining by Ni–Si and Mo interlayers.* Journal of Materials Science, 2010. **45**(16): p. 4299-4307.
109. Luo, Z., et al., *Development of SiC–SiC joint by reaction bonding method using SiC/C tapes as the interlayer.* Journal of the European Ceramic Society, 2012. **32**(14): p. 3819-3824.
110. Dong, H., et al., *Joining of SiC ceramic-based materials with ternary carbide Ti3SiC2.* Materials Science and Engineering: B, 2011. **176**(1): p. 60-64.
111. Greenwood, N.N. and A. Earnshaw, *Chemistry of the Elements*. 2012: Elsevier.
112. Ortiz, M. and T. Herrera, *Molybdenum: Characteristics, production and applications*. Molybdenum: Characteristics, Production and Applications. 2012. 1-266.
113. Okamoto, H., *Mo-Si (Molybdenum-Silicon).* Journal of Phase Equilibria and Diffusion, 2011. **32**(2): p. 176-176.
114. Cherniack, G.B. and A.G. Elliot, *High-Temperature Behavior of MoSi2 and Mo5Si3.* Journal of the American Ceramic Society, 1964. **47**(3): p. 136-141.
115. Vasudévan, A.K. and J.J. Petrovic, *A comparative overview of molybdenum disilicide composites.* Materials Science and Engineering: A, 1992. **155**(1–2): p. 1-17.
116. Zhang, X.L., et al., *In-situ preparation of nano MoSi2SiC composite by melt infiltration of silicon method.* Materials Chemistry and Physics, 2017. **200**(Supplement C): p. 287-294.
117. Dasgupta, T. and A.M. Umarji, *Thermal properties of MoSi2 with minor aluminum substitutions.* Intermetallics, 2007. **15**(2): p. 128-132.
118. Waghmare, U.V., et al., *Microalloying for ductility in molybdenum disilicide.* Materials Science and Engineering: A, 1999. **261**(1): p. 147-157.
119. Zamani, S., et al., *Synthesis and characterization of MoSi2-Mo5Si3 nanocomposite by mechanical alloying and heat treatment.* International Journal of Refractory Metals and Hard Materials, 2012. **31**(Supplement C): p. 236-241.
120. Yen, B.K., T. Aizawa, and J. Kihara, *Synthesis and formation mechanisms of molybdenum silicides by mechanical alloying.* Materials Science and Engineering: A, 1996. **220**(1): p. 8-14.
121. Zhang, S. and Z.A. Munir, *Synthesis of molybdenum silicides by the self-propagating combustion method.* Journal of Materials Science, 1991. **26**(13): p. 3685-3688.

122. Oh, D.Y., et al., *One step synthesis of dense MoSi2–SiC composite by high-frequency induction heated combustion and its mechanical properties.* Journal of Alloys and Compounds, 2005. **395**(1): p. 174-180.
123. Hvizdos, P., et al., *Creep behaviour of MoSi2–SiC and MoSi2–HfO2.* Materials Letters, 2001. **51**(6): p. 485-489.
124. Kim, D.-K., et al., *Consolidation and mechanical properties of nanostructured 2MoSi2–SiC composite synthesized by high-frequency induction heated combustion.* Materials Science and Engineering: A, 2007. **457**(1): p. 368-372.
125. Schwarz, R.B., et al., *Synthesis of molybdenum disilicide by mechanical alloying.* Materials Science and Engineering: A, 1992. **155**(1): p. 75-83.
126. Zakeri, M., et al., *Synthesis of nanocrystalline MoSi2 by mechanical alloying.* Journal of Alloys and Compounds, 2005. **403**(1): p. 258-261.
127. Fei, G.T., et al., *Preparation of nanocrystalline intermetallic compounds WSi2 and MoSi2 by mechanical alloying.* Journal of Alloys and Compounds, 1995. **229**(2): p. 280-282.
128. Kang, P.C., Z. Yin, and O. Celestine, *Effect of milling time on phase transition and grain growth during the annealing process of MA powders.* Materials Science and Engineering: A, 2005. **395**(1): p. 167-172.
129. Laiqi, Z., et al., *THERMODYNAMIC AND KINETIC ANALYSIS OF IN SITU SYNTHESIS OF MoSi_2-SiC COMPOSITE.* Acta Metall, 1998. **34**(11): p. 1205-1209.
130. Kang, P. and Z. Yin, *Phase formation during annealing as-milled powders of molybdenum disilicide.* Materials Letters, 2003. **57**(28): p. 4412-4417.
131. Wiltner, A., et al., *Reaction temperatures within Mo–Si powder mixtures and their influencing factors.* International Journal of Refractory Metals and Hard Materials, 2013. **37**: p. 73-81.
132. Hitoshi, S., et al., *Temperature Dependence of the Viscosity of Molten Silicon Measured by the Oscillating Cup Method.* Japanese Journal of Applied Physics, 1995. **34**(7R): p. 3432.
133. Gianchandani, P.K., et al., *SiC foam sandwich structures obtained by Mo-wrap joining.* Materials Letters, 2018. **221**: p. 240-243.
134. Bewlay, B.P., et al., *Ultrahigh-Temperature Nb-Silicide-Based Composites.* MRS Bulletin, 2011. **28**(9): p. 646-653.
135. Mitra, R., *Structural intermetallics and intermetallic matrix composites*. Vol. 6. 2015: CRC Press.
136. Schlesinger, M.E., et al., *The Nb-Si (Niobium-Silicon) system.* Journal of Phase Equilibria, 1993. **14**(4): p. 502-509.
137. Sankar, M., et al., *Microstructure, oxidation resistance and tensile properties of silicide coated Nb-alloy C-103.* Materials Science and Engineering: A, 2015. **645**(Supplement C): p. 339-346.
138. Suzuki, R.O., M. Ishikawa, and K. Ono, *NbSi2 coating on niobium using molten salt.* Journal of Alloys and Compounds, 2002. **336**(1): p. 280-285.

139. Sun, J., et al., *Silicide coating fabricated by HAPC/SAPS combination to protect niobium alloy from oxidation.* ACS applied materials & interfaces, 2016. **8**(24): p. 15838-15847.
140. Pan, Y., et al., *Relationship between Si concentration and mechanical properties ofNb–Si compounds: A first-principles study.* Materials & Design, 2016. **89**(Supplement C): p. 676-683.
141. Pan, Y., et al., *Influence of vacancy on structural and elastic properties of NbSi2 from first-principles calculations.* Materials & Design, 2016. **108**(Supplement C): p. 13-18.
142. Todai, M., et al., *Microstructure and fracture toughness in boron added NbSi2(C40)/MoSi2(C11b) duplex crystals.* Scripta Materialia, 2016. **113**(Supplement C): p. 236-240.
143. Yeh, C.L. and H.J. Wang, *A comparative study on combustion synthesis of Ta–Si compounds.* Intermetallics, 2007. **15**(10): p. 1277-1284.
144. Stoloff, N.S., *An overview of powder processing of silicides and their composites.* Materials Science and Engineering: A, 1999. **261**(1): p. 169-180.
145. Niu, Y., et al., *Microstructure and thermal stability of TaSi2 coating fabricated by vacuum plasma spray.* Surface and Coatings Technology, 2015. **279**(Supplement C): p. 1-8.
146. Schlesinger, M.E., *The Si-Ta (silicon-tantalum) system.* Journal of Phase Equilibria, 1994. **15**(1): p. 90-95.
147. Vahlas, C., P.Y. Chevalier, and E. Blanquet, *A thermodynamic evaluation of four Si-M (M = Mo, Ta, Ti, W) binary systems.* Calphad, 1989. **13**(3): p. 273-292.
148. Zhang, S. and D. Zhao, *Aerospace materials handbook*. 2012: CRC Press.
149. Shon, I.J., et al., *Dense WSi2 and WSi2–20 vol.% ZrO2 composite synthesized by pressure-assisted field-activated combustion.* Journal of Alloys and Compounds, 2001. **322**(1): p. 120-126.
150. Yen, B.K., et al., *Reaction synthesis of refractory disilicides by mechanical alloying and shock reactive synthesis techniques.* Materials Science and Engineering: A, 1997. **239-240**(Supplement C): p. 515-521.
151. Chen, F., et al., *In situ reactive spark plasma sintering of WSi2/MoSi2 composites.* Ceramics International, 2016. **42**(9): p. 11165-11169.
152. Morris, D.G., M. Leboeuf, and M.A. Morris, *Hardness and toughness of MoSi2 and MoSi2–SiC composite prepared by reactive sintering of powders.* Materials Science and Engineering: A, 1998. **251**(1): p. 262-268.
153. English, J., *Binary and ternary phase diagrams of columbium, molybdenum, tantalum, and tungsten*. 1961, BATTELLE MEMORIAL INST COLUMBUS OH DEFENSE METALS INFORMATION CENTER.
154. Riccardi, B., et al., *Joining of SiC based ceramics and composites with Si-16Ti and Si-18Cr eutectic alloys.* International Journal of Materials and Product Technology, 2004. **20**(5-6): p. 440-451.

155. Raj, S.V., *A preliminary assessment of the properties of a chromium silicide alloy for aerospace applications.* Materials Science and Engineering: A, 1995. **192**(Part 2): p. 583-589.
156. Du, B., et al., *Oxidative protection of a carbon-bonded carbon fiber composite with double-layer coating of MoSi2-SiC whisker and TaSi2-MoSi2-SiC whisker by slurry method.* Ceramics International, 2017. **43**(12): p. 9531-9537.
157. Okamoto, H., *Phase diagrams for binary alloys.* ASM International, 2000. **314**.
158. Yeh, C.L. and J.Z. Lin, *Combustion synthesis of Cr–Al and Cr–Si intermetallics with Al2O3 additions from Cr2O3–Al and Cr2O3–Al–Si reaction systems.* Intermetallics, 2013. **33**(Supplement C): p. 126-133.
159. Zhang, D.L., *The sequence of phase formation during mechanical alloying of chromium and silicon powders.* Journal of Materials Science, 1996. **31**(4): p. 895-899.
160. Filonenko, O., *Structural investigations of thin chromium disilicide films on silicon.* 2005.
161. Auerkari, P., *Mechanical and physical properties of engineering alumina ceramics*. 1996: Technical Research Centre of Finland Espoo.
162. http://www.morgantechnicalceramics.com/en-gb/materials/alumina/.
163. http://accuratus.com/alumox.html.
164. Medvedovski, E., *Alumina–mullite ceramics for structural applications.* Ceramics International, 2006. **32**(4): p. 369-375.
165. Boch, P. and J.-C. Niepce, *Ceramic Materials: Processes, Properties, and Applications*. Vol. 98. 2010: John Wiley & Sons.
166. https://www.ceramtec.com/ceramic-materials/silicon-carbide/.
167. Zhang, Z.-H., et al., *Processing and characterization of fine-grained monolithic SiC ceramic synthesized by spark plasma sintering.* Materials Science and Engineering: A, 2010. **527**(7): p. 2099-2103.
168. Hurwitz, F.I., *Thermal Protection Systems (TPSs.* Encyclopedia of Aerospace Engineering, 2010.
169. Smyth, R. *The use of high temperature heat exchangers to increase power plant thermal efficiency*. in *Energy Conversion Engineering Conference, 1997. IECEC-97., Proceedings of the 32nd Intersociety*. 1997. IEEE.
170. Sommers, A., et al., *Ceramics and ceramic matrix composites for heat exchangers in advanced thermal systems—A review.* Applied Thermal Engineering, 2010. **30**(11–12): p. 1277-1291.
171. Scheffler, M. and P. Colombo, *Cellular ceramics: structure, manufacturing, properties and applications*. 2006: John Wiley & Sons.
172. Eom, J.-H., Y.-W. Kim, and S. Raju, *Processing and properties of macroporous silicon carbide ceramics: A review.* Journal of Asian Ceramic Societies, 2013. **1**(3): p. 220-242.

173. Twigg, M.V. and J.T. Richardson, *Fundamentals and Applications of Structured Ceramic Foam Catalysts.* Industrial & Engineering Chemistry Research, 2007. **46**(12): p. 4166-4177.
174. Studart, A.R., et al., *Processing Routes to Macroporous Ceramics: A Review.* Journal of the American Ceramic Society, 2006. **89**(6): p. 1771-1789.
175. Rezaei, E., et al., *On the nonlinear mechanical behavior of macroporous cellular ceramics under bending.* Journal of the European Ceramic Society, 2014. **34**(10): p. 2133-2141.
176. Karl, S. and A.V. Somers, *Method of making porous ceramic articles*. 1963, Google Patents.
177. Campbell, F.C., *Structural composite materials*. 2010: ASM international.
178. Chawla, K.K., *Ceramic Matrix Composites*. 1st edition. 1993.
179. Chawla, K.K., *Composite materials: science and engineering*. 2012: Springer Science & Business Media.
180. Low, I.-M., *Ceramic-matrix composites: microstructure, properties and applications*. 2006: Woodhead Publishing.
181. Krenkel, W., *Ceramic matrix composites: fiber reinforced ceramics and their applications*. 2008: John Wiley & Sons.
182. Bansal, N.P., *Handbook of ceramic composites*. Vol. 200. 2006: Springer Science & Business Media.
183. Krenkel, W., *Carbon Fibre Reinforced Silicon Carbide Composites (C/SiC, C/C-SiC)*, in *Handbook of Ceramic Composites*, N.P. Bansal, Editor. 2005, Springer US: Boston, MA. p. 117-148.
184. Handrick, K.E., *Ceramic Matrix Composites (CMC) for demanding Aerospace and Terrestrial Applications*, in *XXI Congress AIV*. 2013: catania.
185. Ortona, A., S. Pusterla, and S. Gianella, *An integrated assembly method of sandwich structured ceramic matrix composites.* Journal of the European Ceramic Society, 2011. **31**(9): p. 1821-1826.
186. Ortona, A., et al., *Aging of reticulated Si-SiC foams in porous burners.* Advances in Applied Ceramics, 2010. **109**(4): p. 246-251.
187. Ferrari, L., et al., *Sandwich structured ceramic matrix composites with periodic cellular ceramic cores: an active cooled thermal protection for space vehicles.* Composite Structures, 2016. **154**: p. 61-68.
188. Despènes, L., et al., *Impact of the material on the thermal behaviour of heat exchangers-reactors.* Chemical Engineering and Processing: Process Intensification, 2012. **52**: p. 102-111.
189. Blosser, M., et al., *Advanced metallic thermal protection system development.* 2002.
190. Ortona, A., et al., *Fabrication of cylindrical SiCf/Si/SiC-based composite by electrophoretic deposition and liquid silicon infiltration.* Journal of the European Ceramic Society, 2014. **34**(5): p. 1131-1138.

191. Triantou, K., et al., *Thermo-mechanical performance of an ablative/ceramic composite hybrid thermal protection structure for re-entry applications.* Composites Part B: Engineering, 2015. **82**: p. 159-165.
192. Wang, Y., et al., *Improved sandwich structured ceramic matrix composites with excellent thermal insulation.* Composites Part B: Engineering, 2017. **129**: p. 180-186.
193. Hurwitz, F.I., *Improved fabrication of ceramic matrix composite/foam core integrated structures.* 2009.
194. Esser, B., et al., *Innovative Thermal Management Concepts and Material Solutions for Future Space Vehicles.* Journal of Spacecraft and Rockets, 2016: p. 1-10.
195. Gianella, S., D. Gaia, and A. Ortona, *High temperature applications of Si-SiC cellular ceramics.* Advanced Engineering Materials, 2012. **14**(12): p. 1074-1081.
196. ; Available from: https://www.nikonmetrology.com/en-gb/product/mct225.
197. Ferraris, M., et al., *Torsion tests on AV119 epoxy - Joined SiC.* International Journal of Applied Ceramic Technology, 2012. **9**(4): p. 795-807.
198. Ferraris, M., et al., *Torsional shear strength of silicon carbide components pressurelessly joined by a glass-ceramic.* International Journal of Applied Ceramic Technology, 2012. **9**(4): p. 786-794.
199. Cela Greven, B., et al., *Torsional shear strength of novel glass-ceramic composite sealants for solid oxide fuel cell stacks.* International Journal of Applied Ceramic Technology: p. n/a-n/a.
200. Csanádi, T., et al., *Nanoindentation derived elastic constants of carbon fibres and their nanostructural based predictions.* Carbon, 2017. **119**(Supplement C): p. 314-325.
201. Triantou, K.I., et al., *Thermal shock performance of carbon-bonded carbon fiber composite and ceramic matrix composite joints for thermal protection re-entry applications.* Composites Part B: Engineering, 2017. **111**: p. 270-278.
202. Suzuki, R.O., M. Ishikawa, and K. Ono, *MoSi 2 coating on molybdenum using molten salt.* Journal of Alloys and Compounds, 2000. **306**(1): p. 285-291.
203. Wu, M.L., C.Z. Ren, and H.Z. Xu, *On the wettability diversity of C/SiC surface: Comparison of the ground C/SiC surface and ablated C/SiC surface from three aspects.* Applied Surface Science, 2016. **385**(Supplement C): p. 391-399.
204. Wu, M.L. and C.Z. Ren, *Active control of the anisotropic wettability of the carbon fiber reinforced carbon and silicon carbide dual matrix composites (C/C–SiC).* Applied Surface Science, 2015. **327**(Supplement C): p. 424-431.

205. Li, Z., et al., *Effect of reaction melt infiltration temperature on the ablation properties of 2D C/C–SiC–ZrC composites.* Corrosion Science, 2012. **58**(Supplement C): p. 12-19.
206. Mitra, R., *Mechanical behaviour and oxidation resistance of structural silicides.* International Materials Reviews, 2006. **51**(1): p. 13-64.
207. Inui, H., M. Moriwaki, and M. Yamaguchi, *Plastic deformation of single crystals of VSi2 and TaSi2 with the C40 structure.* Intermetallics, 1998. **6**(7): p. 723-728.
208. Kang, W. and M.T.A. Saif, *In Situ Study of Size and Temperature Dependent Brittle-to-Ductile Transition in Single Crystal Silicon.* Advanced Functional Materials, 2013. **23**(6): p. 713-719.
209. Samuels, J., S.G. Roberts, and P.B. Hirsch, *The brittle-to-ductile transition in silicon.* Materials Science and Engineering: A, 1988. **105-106**(Part 1): p. 39-46.
210. Brede, M., *The brittle-to-ductile transition in silicon.* Acta Metallurgica et Materialia, 1993. **41**(1): p. 211-228.
211. Aikin, R.M., *On the ductile-to-brittle transition temperature in MoSi2.* Scripta Metallurgica et Materialia, 1992. **26**(7): p. 1025-1030.
212. Umakoshi, Y., et al., *High temperature deformation of MoSi2 single crystals with the C11b structure.* Acta Metallurgica et Materialia, 1990. **38**(6): p. 909-915.
213. Ito, K., et al., *Plastic deformation of MoSi2 single crystals.* Philosophical Magazine A, 1995. **72**(4): p. 1075-1097.
214. Ferraris, M., et al., *Torsional shear strength tests for glass-ceramic joined silicon carbide.* International Journal of Applied Ceramic Technology, 2015. **12**(3): p. 693-699.
215. William D. Callister, J., *Materials Science and Engineering*. 2007.
216. Oliver, W.C. and G.M. Pharr, *An improved technique for determining hardness and elastic modulus using load and displacement sensing indentation experiments.* Journal of Materials Research, 2011. **7**(6): p. 1564-1583.
217. Csanádi, T., et al., *Nanoindentation induced deformation anisotropy in β-Si3N4 ceramic crystals.* Journal of the European Ceramic Society, 2016. **36**(12): p. 3059-3066.
218. Oliver, W.C. and G.M. Pharr, *Measurement of hardness and elastic modulus by instrumented indentation: Advances in understanding and refinements to methodology.* Journal of Materials Research, 2011. **19**(1): p. 3-20.
219. Liang, H., et al., *High-pressure sintering of bulk MoSi2: Microstructural, physical properties and mechanical behavior.* Materials Science and Engineering: A, 2018. **711**(Supplement C): p. 389-396.
220. Boldt, P.H., J.D. Embury, and G.C. Weatherly, *Room temperature microindentation of single-crystal MoSi2.* Materials Science and Engineering: A, 1992. **155**(1): p. 251-258.

221. Henžel, M., et al. *Indentation Testing of MoSi2*. in *Key Engineering Materials*. 2005. Trans Tech Publ.
222. Henžel, M., et al., *Micro and nano-indentation of MoSi2.* Journal of Materials Science, 2004. **39**(11): p. 3769-3772.
223. *Silicon*. [cited 2018 06-04-2018]; Available from: https://www.azom.com/properties.aspx?ArticleID=599.
224. Gianchandani, P.K., et al., *Pressure-less joining of C/SiC and SiC/SiC by a MoSi2/Si composite.* International Journal of Applied Ceramic Technology, 2016: p. n/a-n/a.
225. Moriwaki, M., et al., *Plastic deformation of single crystals of NbSi2 with the C40 structure.* Materials Science and Engineering: A, 1997. **239-240**(Supplement C): p. 69-74.
226. Nakano, T., M. Azuma, and Y. Umakoshi, *Tensile deformation and fracture behaviour in NbSi2 and MoSi2 single crystals.* Acta Materialia, 2002. **50**(14): p. 3731-3742.
227. Pitman, S.H. and P. Tsakiropoulos, *Study of The Microstructure and Oxidation of NbSi2 Base Alloys.* MRS Proceedings, 2011. **364**.
228. Cui, C., et al., *Mechanical Properties of the TaSi2 Fibers by Nanoindentation.* Journal of Materials Science & Technology, 2010. **26**(1): p. 65-68.
229. Eustathopoulos, N., M.G. Nicholas, and B. Drevet, *Wettability at high temperatures*. Vol. 3. 1999: Elsevier.
230. Drevet, B., S. Kalogeropoulou, and N. Eustathopoulos, *Wettability and interfacial bonding in Au・Si/SiC system.* Acta metallurgica et materialia, 1993. **41**(11): p. 3119-3126.